DESIGN AND EVALUATION OF CONTROLLERS FOR WAVE ENERGY BASED ELECTRICITY GENERATION SYSTEM

Thesis

Submitted in partial fulfillment of the requirements for the degree of

DOCTOR OF PHILOSOPHY

By

VINATHA U

DEPARTMENT OF ELECTRICAL ENGINEERING

NATIONAL INSTITUTE OF TECHNOLOGY

KARNATAKA, SURATHKAL, MANGALORE -575025

September, 2013

D E C L A R A T I O N

by the Ph.D. Research Scholar

I hereby *declare* that the Research Synopsis entitled **Design and evaluation of controllers for wave energy based electricity generation system** which is being submitted to the **National Institute of Technology Karnataka, Surathkal** in partial fulfillment of the requirements for the award of the Degree of **Doctor of Philosophy** in Electrical Engineering is a *bonafide report of the research work carried out by me*. The material contained in this Research Thesis/Synopsis has not been submitted to any University or Institution for the award of any degree.

050606EE05P03 **Vinatha U**

(Register Number, Name & Signature of the Research Scholar)

Department of Electrical Engineering

Place: NITK-Surathkal
Date: 16 -09-2013

C E R T I F I C A T E

This is to *certify* that the Research Synopsis entitled **Design and evaluation of controllers for wave energy based electricity generation system** submitted by **Vinatha U (Register Number: 050606EE05P03)** as the record of the research work carried out by him/her, is *accepted as the Research Thesis/Synopsis submission* in partial fulfillment of the requirements for the award of degree of **Doctor of Philosophy**.

Research Guide(s)
(Name and Signature with Date and Seal)

Chairman - DRPC
(Signature with Date and Seal)

Acknowledgements

I would like to express profound gratitude to my guide Dr K P Vittal, Professor, Department of E&E, NITK, Surathkal for providing guidance and sharing his vision and experiences throughout the development of this dissertation. Many ideas presented in this thesis are results of several discussions with him. His instructive suggestions and encouragement are deeply acknowledged.

I would like to express my sincere thanks to RPAC members, Dr Muralidhar Kulkarni, Professor, Department of E&C, NITK, Surathkal and Dr Vijay Desai, Professor, Department of Mechanical Engineering, NITK, Surathkal for their timely suggestions throughout the thesis work.

I owe a great deal to NITK Surathkal for permitting to do my research at NITK on part time basis.

I would like to sincerely thank Dr V Jayashankar, Associate Professor, Department of E&E, IIT Chennai for providing the data from the Indian wave energy plant without which the this work would not have been meaningfully completed.

I am grateful to all the faculty and staff of EE department for their help and assistance in several matters.

I am indebted to Professor Subba Rao and Professor Vittal Hegde, Department of Applied Mechanics, NITK Surathkal for extending their help in characterizing the waves.

I would like to express my thanks to Professor H S Y Shastry, Professor P N Sreedhar, Professor Durai Kannu and Professor Udayakumar R Y for their support and encouragement.

I would like to take this opportunity to acknowledge the help extended by undergraduate and post graduate students of NITK Surathkal, Pratulya, Kishore, Ravikiran and Sharath.

I would like to express my thanks to my colleague Girisha Navada for his suggestions and help during the initial stages of research work. I would also like to thank Dr K N Shubhanga and Dr D N Gaonkar for their help. My sincere thanks are due to my colleague Jora Gonda for his help and support during thesis writing.

I have a special appreciation for the advice and encouragement I received from my colleague Dr G S Punekar during my research work.

I would like to acknowledge the exhaustive support and encouragement extended by my parents. Special thanks to my father Professor P K Moily for his well wishes and encouragement.

I would like to thank my friend Dr Varija for spending time in discussions on both academic and non academic matters.

I would also like to thank my daughter Swathi for helping me in editing the thesis.

Last but not the least I appreciate the sacrifice and support given to me by my husband Dr Shivarama K, daughter Swathi and son Gururaj because of which I was able to cross several hurdles faced during the research work.

ABSTRACT

The research work presented in this thesis is an effort to recognize the potential issues associated with harnessing wave energy based on oscillating water column principle.

A model of oscillating water column based on energy balance concept is proposed.

Dynamic model of a wave energy conversion system based on OWC principle consisting of a variable speed Wells turbine driven permanent magnet synchronous generator connected to the grid by means of back to back converters is developed. Results exhibit the randomness in the various quantities like speed of the turbine, torque and powers developed of the turbine and the generators when the input to the system is varying randomly. This demonstrates uncertainty in the wave power due to arbitrariness in the waves and reveals the difficulties in developing an efficient wave harnessing system.

Controllers for the generator side and the grid side converters for a grid connected wave energy conversion system are developed. The overall scheme is evaluated under steady state, dynamic and transient operating conditions. Under different operating conditions it is observed that the control scheme provides a good response in terms of power quality and power control.

An important constituent for developing the wave energy conversion systems is the Wave Turbine Emulator. It offers a controllable test environment that allows the evaluation and improvement of control schemes for electric generators without construction of costly turbine and help in determining the strength and weakness of energy conversion scheme and the related control technologies. In view of this a wave turbine emulator is designed. For the realization of the wave turbine emulator a three phase permanent magnet synchronous motor is used with VSC controller as a drive. Results presented for different wave pattern as input indicates that the speed dynamics of the wave turbine model is exactly followed by wave turbine emulator developed in laboratory. An attempt is also made to study the behavior of the three phase permanent magnet synchronous generator coupled to the emulator developed.

CONTENTS

Chapter 2: Wave Characterization and Modeling of OWC with Wells turbine

Chapter 3: Modeling of WECS connected to grid

Chapter 4: Modeling and design of controllers for a grid connected WECS

Chapter 5: Development of Wave turbine emulator

Chapter 6: Conclusions

List of figures

List of tables

List of symbols

Symbol	Definition	Unit
a	Length of the water column	m
a_r	Annular area of the rotor	m^2
A	Wave amplitude	m
A_1	Area of the OWC	m^2
A_2	Area of the orifice	m^2
A_{duct}	Area of the turbine	m^2
b	Width of the wave	m
b_h	Blade height of the turbine	m
B	Friction coefficient	Kg-m^2/s
C	Velocity of the waves	m/s
Ca	Power coefficient	
C_t	Torque coefficient	
C_k	Link capacitance	F
d	Depth below the still water level	m
dp	Differential pressure within the OWC	Pa
dp_m	Differential pressure within the OWC	Pa
e_v	Error in stator the voltage	V
e_r	Error in the dc link voltage	V
e_d	d- axis current error of generator	A
e_q	q- axis current error of generator	A
E	Emf induced in the stator	V

$E_{density}$	Energy density of the wave	J/m^2
E_d	Energy density at the operating depth	J/m^2
E_{swl}	Energy density of the wave at still water level	J/m^2
E_{wave}	Energy contained in the half wave	J
f	Frequency of the emf induced	Hz
g	Acceleration due to gravity	m/s^2
h	Height of the water level in column	m
h_1	Initial height of the water in OWC	m
h_2	Final height of the water in OWC	m
H	Wave height	m
H_s	Significant wave height	m
i_1	Current through L_1	A
i_c	Current through C_f,	A
$I^s abc$	Three phase Stator current	A
i_{ds}^r	d- axis current of stator in rotor reference frame	A
i_{qs}^r	q- axis current of stator in rotor reference frame	A
i_{fr}	Constant current source representing permanent magnet excitation	A
i_d	Current flowing out of the generator side converter	A
i_g	Grid current	A
i_h	Error in the d axis component of grid current	A
i_j	Error in the q axis component of grid current	A
i_s	Current flowing into the generator side converter	A

i_{dg}	d- axis grid current	A
i_{qg}	q- axis grid current	A
i_v	Current flowing into the grid side converter	A
i_{dc}	DC link current	A
i_{gdref}	d- axis grid reference current	A
i_{gqref}	q- axis of grid reference current	A
I_{qref}	q- axis reference current of generator	A
I_{dref}	d- axis reference current of generator	A
I_{s1} I_{s2},I_{s3}	Inverter switch currents for upper leg devices	A
I_v	Inverter input current	A
I_a,I_b,I_c	Three phase output currents of the inverter	A
J	Moment of inertia of the system	Kg-m^2
k	Wave number	
k_p	Proportional gain of the PI controller	
k_i	Integral gain of the PI controller	
l	Blade chord length	m
L_1	Filter inductor	H
L_2	Filter inductance of grid side including the inductance of grid	H
LCL	Inductance-Capacitance-Inductance	
L_s	Self inductances of the stator winding	H
L_m	Mutual inductance between stator windings and rotor magnets	H

L_q	q- axis inductance of stator winding	H
L_d	d- axis inductance of stator winding	H
m_0	Amount of water displaced	m^3
n	Number of blades of the turbine	
p	Number of pole pairs	
P	Operator	
P_{air}	Pressure at the turbine duct	(Pa)
P_{dc}	DC link power	W
P_e	Electromechanical power	W
$P_{density}$	Energy per wave period	W
P_{dloss}	Grid side converter losses	W
P_{in}	Power flowing into the generator	W
P_{owc}	Power available from the airflow through the OWC outlet	W
$P_{pneumatic}$	Pneumatic power of water column present inside the OWC	W
P_{ref}	Active power reference	W
P_{rloss}	Generator side the converter losses	W
P_s	Active power of the generator	W
P_t	Pneumatic power converted into mechanical power by the turbine	W
P_{wave}	Mean value of wave power	W
$P_{wavefront}$	Power per meter of wave front	W/m
Q_s	Reactive power of the permanent magnet generator	VAr
Q_{ref}	Reactive power reference	VAr

r	Average radius of the turbine	m
R_1	Resistance associated with the filter inductor L_1	Ω
R_2	Resistance associated with the filter inductor L_2	Ω
R_s	Stator winding resistance per phase	Ω
R_d	Direct axis winding resistances	Ω
R_q	Quadrature axis winding resistances	Ω
t	Time	s
T_e	Electromagnetic torque of the generator	N-m
TF	Transfer function	
T_s	Mean wave period	s
T_t	Gross torque produced by the turbine	Nm
T_w	Wave period	s
v	Velocity of air near the water surface in the OWC	m/s
v_x	Velocity near the orifice of the OWC	m/s
V	Volume of air column	m^3
V_{an},V_{bn},V_{cn}	Phase voltage of the inverter	V
V^s_{abc}	Three phase stator voltage	V
V_{qs}^r	q axis component of stator voltage in rotor reference frame	V
V_{ds}^r	d axis component of stator voltage in rotor reference frame	V
V_{dc}	DC input voltage to the inverter	V
V_{ab},V_{bc},V_{ca}	Output line voltages of inverter	V
$V_{cont\_a,b,c}$	Control signals	V
V_{dg}	d axis component of grid voltage	V

V_{qg}	q axis component of grid voltage	V
V_{dcref}	DC link reference voltage	V
V_i	Inverter output voltage	V
V_c	Voltage at the filter capacitor terminal	V
V_g	Grid voltage	V
V_{tri}	Carrier signal	V
λ	Wavelength	m
ρ_w	Density of water	Kg/m^3
ω	Angular frequency of wave	rad/s
ω_0	Peak angular frequency of the wave	rad/s
ρ_{air}	Density of air	Kg/m^3
Δh	Increase in the water level	m
ω_t	Speed of rotation	rad/s
ψ_{pm}	Permanent magnet flux	wb
λ^s_{abc}	Flux linkage	wb
λ^r_{qs}	q axis stator flux linkage in the rotor reference frame	wb
λ^r_{ds}	d axis stator flux linkage in the rotor reference frame	wb
ω_r	Electrical angular velocity	rad/s
ω_m	Mechanical angular velocity	rad/s
λ_{af}	Rotor flux linkages that link the stator	wb

CHAPTER 1

INTRODUCTION

INTRODUCTION

The solutions to today's energy challenges need to be found through increased electricity generation using alternative, renewable and clean energy sources. A huge amount of energy is available to us in the form of solar, wind, ocean and geothermal energy. All these are different manifestations of solar energy. Among all these forms ocean energy shows a lot of promise. An extremely abundant and promising source of energy exists in the world's oceans. It is estimated that if 0.2 percent of the ocean's untapped energy is harnessed it could provide enough power for the entire world. Ocean energy resource can be tapped in three forms namely ocean wave energy, ocean thermal energy and ocean tidal energy. Ocean wave energy is more promising as well as more effective than ocean thermal or tidal energy. Although the technology for extracting energy from the ocean waves is currently not economically competitive with other more mature technologies such as wind energy and solar energy, the interest from the governments and the industries is steadily increasing. Subsequently, generation of electrical energy from the natural motion of waves and the possibility of designing systems which can economically extract the resource yet service severe extremes have become very attractive and challenging. Construction of the plant on the shoreline can solve this problem but with reduction in the average energy available for extraction. The oscillating water column (OWC) based wave energy converter (WEC) is the most successful and most extensively studied shore mounted device (Duckers 1995, Les Duckers 2000, Glendenning 1980).

The work presented in the thesis intends to understand and augment knowledge by investigating the mode of capturing energy from the ocean waves based on OWC principle. Effort in the work basically focuses on the modeling of OWC and studies on the control of grid connected wave energy conversion system (WECS). It also involves the design and hardware implementation of a wave turbine emulator in the laboratory environment.

Ocean Wave Energy

Ocean waves arise from the transfer of energy from the sun to wind and then to water. Solar energy creates wind which blows over the ocean, converting wind energy to wave energy. This wave energy can travel thousands of miles with little energy loss. Most importantly, waves are a regular source of power with an intensity that can be accurately predicted several days before their arrival and is more predictable than wind or solar energy. Figure 1.1 depicts wave power levels in kW/m of wave crest, the typical units for measuring wave energy. There is approximately 8,000-80,000 TWh/year of wave energy in the entire ocean and on an average each wave crest transmits 10-50 kW/m. (Hamish 1999, Childs 1996, Whittaker 1993, Anthony et al. 2005, Muetze et al.2006).

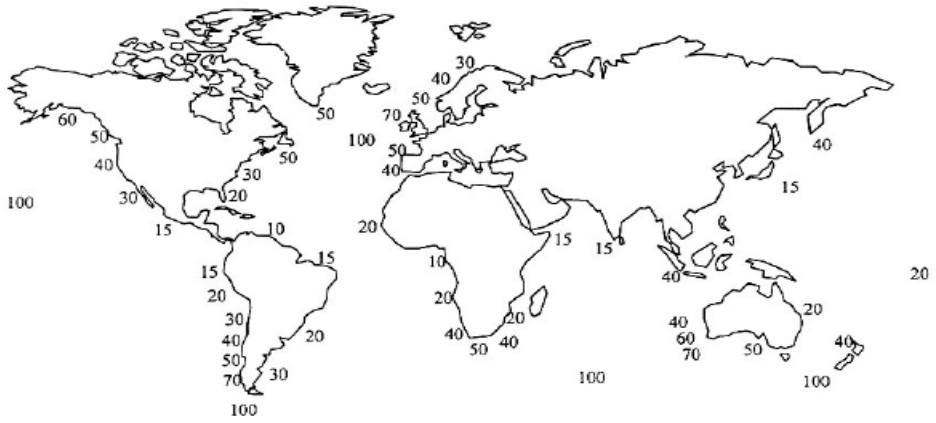

Figure Error! No text of specified style in document.**.1 Approximate global distribution of wave power levels**

In order to assess an area for wave energy development, the wave height and length distributions and total mean water depth should be surveyed. These parameters define the wave climate from which the area's wave power levels can be computed. In general, the waves present on the western edge of the continents contain more energy because of the west-to-east winds. The power carried by waves decreases as they reach the shore due to frictional losses with the coastline (Jones et al. 2002, Gareth et al. 2005).

Wave Characteristics

Wave energy is basically a concentrated form of solar energy. Differential heating of the earth's surface causes the winds to blow. As these winds pass across the sea they transfer some of their energy to the water in the form of waves. The amount of energy transferred depends on the speed of the wind, the length of time for which it blows and the fetch which is the distance over which the wind blows.

The precise mechanisms involved in this transfer are complex and not yet completely understood. Nevertheless, three main processes appear to be operating: Initially, the air flowing over the sea exerts a tangential stress on the water surface, resulting in the formation and growth of waves. Then, turbulent air flow close to the water surface creates rapidly varying shear stresses and pressure fluctuations. Finally, when waves have reached a certain size, the wind can actually exert a stronger force on the upwind face of the wave causing additional wave growth. The process is maximized when the speeds of the wind and the waves are equal. Energy is transferred from the wind to the waves at each of these steps. Waves lying within or close to the areas where they are generated are called storm waves. These waves result in a complex, irregular sea and will continue to travel in the direction of their formation even after the wind dies down.

The mathematical description of periodic progressive waves is complicated. A number of regular wave theories have been developed to describe the water particle kinematics associated with ocean waves of varying complexity. Linear wave theory describes ocean waves as simple sinusoidal waves. Surface waves can be classified into deep water waves ($d/\lambda > 0.25$), traditional water waves ($0.25 \geq d/\lambda > 0.05$) and shallow water waves ($0.05 \geq d/\lambda$), based on the ratio of wave length λ to the water depth d. The part of the wave profile with the maximum elevation above the still water level (SWL) is called the wave crest and the part of the wave profile with the lowest depression is the wave trough. The distance from the SWL to the crest or the trough is the amplitude of the wave and the wave height (H) is defined as the total distance from the trough to the crest. The wavelength of a regular wave at any depth

is the horizontal distance between successive points of equal amplitude (Muetze et al. 2006, Modesto et al. 2001).

Water waves travelling along the surface of the sea with an approximate sinusoidal profile can be characterized in terms of the distance between successive crests (the wavelength, λ) and the time between successive crests (the period, T_w). In deep water these parameters are related as in equation 1.1.

$$\lambda = \frac{gT_w^2}{2\pi} \tag{1 Error! No text of specified style in document.}$$

where g is the acceleration due to gravity.

The velocity of the waves C is related to the wave length and the period as given in equation 1.2.

$$C = \frac{\lambda}{T_w} \tag{1.2}$$

Hence, longer waves travel faster than shorter ones. The energy density of the wave, $E_{density}$ is the mean energy flux crossing a vertical plane parallel to a wave crest as given by the equation 1.3 in terms of the wave height. The energy per wave period is the wave power density, $P_{density}$ and can be found by dividing the energy density by the wave period as in equation 1.4.

$$E_{density} = \frac{\rho_w g H^2}{8} \tag{1.3}$$

$$P_{density} = \frac{E_{density}}{T_w} = \frac{\rho_w g H^2}{8T_w} \tag{1.4}$$

The power per meter of wave front can be calculated by multiplying the energy density by wave front velocity as in equation 1.5.

$$P_{wavefront} = CE_{density} = \frac{\rho_w g^2 T_w H^2}{32\pi} \tag{1.5}$$

where ρ_w is the density of sea water and $P_{wavefront}$ is expressed in watts per unit crest length of the wave (Muetze et al. 2006).

Real sea contains waves which are random in height, period and direction. Statistical parameters must be used in order to describe such sea states and to determine their characteristics which are relevant to wave energy devices. Wave

height and period can be represented by statistical measurements of wave height and energy period. The ones commonly used are the root mean square of wave height H_{rms}, or significant wave height H_s, (~$4H_{rms}$) and the corresponding wave energy period T_s. These can be calculated from the knowledge of the wind climate responsible for the waves.

The variability in wave power levels and direction represents perhaps the most difficult challenge to designers of wave energy devices. It can be seen that, whilst the device has to operate efficiently on average power levels of about 20 kW/m, it also has to withstand sea with power levels above 1,000 kW/m.

To properly size an underwater WEC, the wave power at the operating depth must be known. In general, the wave power below sea level decays exponentially by $-2\pi d/\lambda$ where d is the depth below still water level (SWL) as in the equation 1.6. This property is valid for waves in water with depths greater than $\lambda/2$ (Muetze et al. 2006).

$$E_d = E_{SWL} e^{-2\pi d/\lambda} \tag{1.6}$$

General Aspects in the Utilization of Wave Energy

Development of wave power generation plants face several challenges, the most important of which are:

• Irregularity in wave amplitude, phase and direction; it is difficult to obtain maximum efficiency of a device over the entire range of excitation frequencies.

• The structural loading in the event of extreme weather conditions, such as hurricanes, may be as high as 100 times the average loading.

• The coupling of the irregular, slow motion of a wave to electrical generators requires typically 500 times greater frequency.

The design of a WEC has to be highly sophisticated to be operationally efficient and reliable on the one hand, and economically feasible on the other. As with all renewable energy sources, the available resource and variability at the installation site has to be determined first. The above constraints imply comparably high construction costs and possibly reduced survivability. On the other hand, the advantages of wave energy are obvious, the development of which is in line with sustainable development as it combines crucial economic, environmental and social factors. Wave energy is generally considered to provide a clean source of renewable energy, with limited

negative environmental impacts. In particular, wave power is seen as a large source of energy not involving green house effects (Ted et al. 2009, Raftery et al. 2007, Vining et al. 2007, Fernandes et al. 2009, Dawson et al 1980).

Review of Wave Energy Converters

The idea of converting energy from the ocean surface waves into useful energy forms is not new. There are techniques that were patented as early as 1799. The intensive research and development study of wave energy conversion began after the dramatic increase in the oil prices in 1973. Different European countries with exploitable wave power resources considered wave energy as a possible source of power supply and introduced support measures and related programs for harnessing wave energy. In the last 30 years wave energy has gone through a cyclic process of enthusiasm, disappointment and reconsideration. However the persistent efforts in R&D and the experience accumulated during the past years have constantly improved the performance of wave power techniques and have led wave energy closer to commercial exploitation than before.

There have been a large number of device concepts proposed for the utilization of wave energy over the years. Most of these have been tested in artificial wave tanks rather than at sea. It is technically feasible to construct wave energy converters that will perform efficiently at sea. However, a number of detailed factors that affect the economics are still unknown owing to the lack of operational experience with research prototypes or pilot plants. Tank testing of scaled down model converters have been carried out in a number of countries and mathematical descriptions have been developed. In order to validate these modeling exercises testing of full-size prototypes at sea is necessary. Also reliability and survival of the devices in storm wave conditions has to be determined in full-scale trials (Duckers 2000, Henk Polinder et al 2005).

WEC essentially consist of two major components namely the interface element that is acted on directly by the waves and the power take-off system that damps the interface motion and produces useful work. The interface elements are normally of two main types. These are floats that heave or roll in response to wave action and air chambers within which the pressure varies either by direct contact with the water

surface or indirect contact through a membrane. The power take-off systems can be classified under three main headings namely high pressure hydraulics usually oil, low pressure hydraulics usually using seawater and air turbines.

Other renewable energy technologies like wind, biomass, hydropower or photovoltaic have very few options for the principle of energy conversion. Wave energy conversion, by contrast has infinite number of potential possibilities for realization and after a number of years of research it is still not clear which is the optimum one. However, OWC type wave energy harnessing method is considered as one of the best techniques to convert wave energy into electricity (Amundarain 2010). According to positioning, the wave energy converters are classified into on shore, near to shore and off shore devices.

On shore devices:

On shore devices are usually fixed rigidly to the shore line thus ensuring easier installation, simple maintenance and grid connection and have a modest electrical capacity. These devices can be placed on sea bottom in shallow water, integrated in brake water like structures or fixed to a rocky cliff. Cost of the land intrusion and the possibility of naturally advantageous sites have to be considered in these schemes. Major advantage of shoreline converters lie in easier device installation and reduced maintenance costs. The economic viability of shoreline device depends greatly on the local rock and soil conditions and the presence of wave dissipating rock formations. Basic types of shore line wave power converters are OWC and Tapchan. OWCs are the most popular devices and are usually designed as shore mounted structure having fixed frames of reference. The OWC operates in response to the incoming wave activity and are essentially resonant devices. OWC principle is discussed in detail in section 2.2.

Tapchan:

Tapchan refers to tapered channel. Waves that arrive at the wide end of tapered channel are allowed to propagate towards the narrow end. This causes the wave height to increase until the wave crest spills over the walls and fills the water reservoir. As a result wave energy is gradually transformed into potential energy in the reservoir and is subsequently converted into electricity by allowing the water in the reservoir to

return to sea via a low head Kaplan turbine system. Suitable locations for Tapchan systems must have consistent waves with good average wave energy, a tidal range of less than 1m and convenient and cheap means of constructing the reservoir. A 350 kW prototype built in 1985 in Norway with Kaplan turbine and induction generator delivers electricity into the Norwegian grid. The Tapchan concept is both elegant and simple. With very few moving parts it requires low maintenance and is highly reliable. The storage reservoir also helps to smooth the electrical output (Duckers 2000).

Near shore devices:

These devices are deployed at near shore locations in water depths from 30-100m where they can exploit greater power density of the deeper waves. World's first commercial l2 MW near shore energy device Ospey was launched in 1995 in Scottland. Ospey was a form of OWC and was equipped with dual Wells turbines. This was intended to be the world's first commercial scale near shore wave energy device. Unfortunately it was destroyed by the tail end of hurricane Felix before it could be secured at its chosen location. The Mighty Whale, Japanese floating OWC 50 m long and 30m wide with three chambers fitted with air turbines rated at 50, 30 and 30 kW has been deployed 1.5m from the mouth of Gokasho bay.

Off shore devices:

Floating or submerged devices in deep waters moored to sea floor represent the most promising class of WEC. In order to extract maximum amount of energy from the wave, devices need to be at or near the surface and so usually require flexible moorings and electrical transmission cables. There are several types of off shore devices. Archimedes wave swing (AWS) is a submerged off shore device activated by the fluctuations of static pressure caused by the surface waves thus exploiting only their potential energy. In AWS direct drive energy conversion takes place through a permanent magnet linear synchronous generator. This kind of energy conversion does not allow energy storage. As a result output power exhibits poor quality. This class of device exploits the more powerful wave regimes available in deep water (>40m depth). More recent designs for offshore devices concentrate on small, modular devices, yielding high power output when deployed in arrays. A 2 MW pilot plant

based on AWS has been constructed and is waiting to be deployed off the coast of Portugal. Some of the other promising off shore devices is McCabe wave pump, Floating wave power vessel, Pelamis point absorber, Salter duck and Wave dragon (Duckers 2000).

The Technical Challenge:

Wave energy like many other renewable technologies has high capital costs but low operating cost**.** The high capital costs arise from the need to build and deploy large structures to capture small amounts of energy as the power density of wave environment is low at around 50kW/m. It would be economical if the capital cost is lower. This means the structures must be carefully designed not only to perform their energy conversion tasks at an economic cost but also to be able to withstand the worst wave loadings at the specified location (Tom 2000).The basic reason for the failure of WEC was the challenge of putting something in the sea that would survive and also produce electricity at a competitive price. This is practically a difficult task because of the variation in the wave direction and power levels. The cost of building a structure that can withstand the forces imparted by extreme waves would be extremely expensive. The economics of the wave energy conversion is improved by installation of the onshore devices like OWC, Tapchan. These devices are usually fixed to the shoreline and have a modest electrical capacity.

Technological developments in WECS

In the past decade there has been a worldwide resurgent interest for wave energy especially in European countries such as Ireland, UK, Denmark, Portugal and Spain and also in China, Japan and India. The developments in this sector are comparable to those in wind energy a few decades ago with similar economical potentials. Different technologies to convert ocean wave power into electricity have been used and it still remains unclear what the winning technological approach is. This is reflected by several technical approaches and different methods such as oscillating water columns, hinged contour devices such as the palamis, overtopping devices such as wave dragon and Archimedes wave. However the OWC type wave energy harnessing method is considered to be one of the best techniques to convert wave energy into electricity and has reached the pre-commercial stage. Part of the reason

for this is the fact that standard rotary generators can be deployed in these devices. The standard electrical power generation system used for wave energy harnessing can fundamentally be divided into two categories namely, direct connection power generation system for a fixed speed device and indirect connection systems for variable speed devices. Both of these activities are focused on producing electricity at the lowest possible costs and in an environmental friendly and reliable way (Modesto et al. 2011, Thorpe 1999).

In OWC based WECS, turbines can be designed at speeds consistent with standard off line machines. Hence the machine can be directly coupled to the shaft of the turbine. Therefore study on the suitability of machines can be confined to doubly fed induction generator (DFIG), squirrel cage induction generator (SCIG), permanent magnet synchronous generator (PMSG) and field wound synchronous generator. For fixed speed wave energy conversion system SCIG is directly connected to the utility because of its robustness and cost effectiveness (O'Sullivan et al. 2008, Jennifer et al. 2009). Several research papers have been published on the performance assessment of OWC based wave energy converter with induction generator (Jayashankar et al. 2000, Yagna Narayanan et al. 1996, Ravikiran et al. 2007, Yagna Narayanan et al. 1999, Hodgins et al. 2008, Wang et al. 2010, Mala et al. 2009, Muthukumar et al. 2005, Indiresan et al. 1989). For a variable speed WEC a power electronic interface is required in order to have a constant voltage and constant frequency power supplied to the grid. Several grid power integrating technologies have been proposed for wave power. Challenges and possibilities of the use of different interface configurations and different control strategies specific to various wave energy converting devices have been studied (Martha et al. 2007, Tarek et al. 2010 , Mikel et al. 2010, Marian et al. 2010). Research on the use of linear tubular, synchronous, permanent magnet generators as energy converters enabling the direct coupling of the motion of the buoy to the energy harvesting system is also under progress (Evan et al. 2009, Cancelliere et al. 2005, Adel et al. 2009, Wu et al. 2009, Haojie et al. 2009, Henk Polinder et al. 2005, Muller 2002).

Aim of thesis

The research work presented in this thesis is an effort to recognize the potential issues associated with harnessing wave energy using OWC principle. It basically focuses on the aspects associated with converting the wave energy into pneumatic energy, further into electrical energy and then its control. It also involves the development of a wave turbine emulator which will support studies related with wave energy conversion systems.

Layout of thesis

Fundamentals of capturing wave energy and wave characteristics are discussed in chapter 1. General aspects in the utilization of wave energy are discussed. Basic elements of the WEC are introduced. The classification of WEC based on the positioning of the converter is presented. The technical challenges a WEC has to face are also discussed and a review of technological developments in WECS is presented. Furthermore, the gist of the work and contents of different chapters that follow are summarized.

Chapter 2 deals with the wave characterization based on spectral analysis and modeling of OWC column with the Wells turbine. The concept of OWC for extracting energy from sea waves is discussed. Various prototypes of OWC devices installed world-wide are presented. Modeling aspects of OWC are discussed and modeling based on energy balance concept is presented. The model is tested with the actual wave pattern as input. Results of the simulated model are presented and validity is checked by comparing with the corresponding actual measured quantities obtained from Indian wave energy plant set up at Vizhinjam off Trivandrum coast in India.

Modeling aspects of the grid connected WECS are discussed in Chapter 3. A brief description of the system under study is given. Modeling of the PMSG based on d q axis is presented. The implementation of pulse width modulated (PWM) rectifier and the inverter modeling based on switching function concept, model for the dc link dynamics, filter and the ac grid are presented. Validity of each model is checked. Performance of the generator with constant axial velocity, with varying axial velocity and with actual wave pattern as input to the OWC model is analyzed.

Design of controllers for the generator side converter and the grid side converters for a grid connected wave energy conversion system are explained in Chapter 4. Different control schemes that can be used for the generator side converter are briefly reviewed. The constant stator voltage control scheme for the generator side converter in order to maintain the dc link voltage constant is implemented. The controller for the grid side converter is implemented with the objective of the regulating the magnitude and phase angle of the grid supply current so that the real and the reactive power entering the network can be controlled.

Chapter 5 deals with the hardware implementation of the wave turbine emulator. The design and implementation of a Wave Turbine Emulator (WTE) based on OWC principle in the laboratory environment is presented in this chapter. An attempt is also made to study the behavior of the PMSG coupled to the emulator developed.

Conclusions and recommendations for further work are identified in Chapter 6.

CHAPTER 2
WAVE CHARACTERIZATION AND MODELING OF OWC WITH WELLS TURBINE

INTRODUCTION

In a wave energy plant, the power take-off equipment is required to convert an energy flux that is oscillatory, highly irregular and largely random unless a large energy storage interface follows the waves in the energy conversion chain of the plant. In the basic studies as well as in the design stages of any wave energy plant the knowledge of the statistical characteristics of the local wave climate is essential, no matter whether physical or theoretical/numerical modeling methods are to be employed. This information may result from wave measurements, more or less sophisticated forecast/hind cast models or a combination of both, and usually takes the form of a set of representative sea states, each characterized by its frequency of occurrence and by a spectral distribution.

Wave characterization:

Waves are considered as combination of series of components of different periods or frequencies. A certain amount of power or energy is contributed by each of such components. To describe and represent this power of each component the concept of power and energy spectrum of wave is used. The three parameters that help to differentiate different wave patterns are the significant wave height, time period and spectral energy density (Subba Rao et al. 2006).

Significant wave height is defined as average height of the highest one third waves in a wave spectrum and the corresponding mean of time periods is the time Period T_s. The spectral energy density describes how the energy of a wave is distributed with

frequency. There are several methods used to get the Energy density spectrum. Some of these methods are Scott, Bretschneider and Neumann spectrum.

Scott Spectrum

This has its basis as Derbyshire Spectrum. The spectrum in terms of H_s and ω_o is given in equation 2.1.

$$S(\omega) = 0.214\, H_S^2 \exp\left[-\left\{ (\omega - \omega_0)^2 / 0.065(\omega - \omega_0 + 0.26) \right\}^{1/2} \right] \quad \text{(Error! No text of specified style in document..1)}$$

where ω is the angular frequency, ω_o is the peak angular frequency and H_s is the significant wave height.

Bretschneider Spectrum

This spectrum is given in terms of H_s and ω_o as in equation 2.2.

$$S(\omega) = 5\, (m_0 / \omega_0)\, (\omega / \omega_0)^5 \exp\left[-\left\{ 1.25\, (\omega_0 / \omega)^4 \right\} \right] \quad \text{(Error! No text of specified style in document..2)}$$

Neumann Spectrum

This spectrum is given in terms of H_s and ω_o as in equation 2.3.

$$S(\omega) = 24\, (m_0 / \omega_0)\, (\omega_0 / \omega)^6 \exp\left[-\left\{ 3(\omega_0 / \omega)^2 \right\} \right] \quad \text{(Error! No text of specified style in document..3)}$$

where

$$m_0 = 0.0625\, H_S^2 \quad \text{(Error! No text of specified style in document..4)}$$

$$\omega_0 = 2\pi f_0 \quad \text{(Error! No text of specified style in document..5)}$$

A MATLAB® code is written to calculate the significant wave height (H_s) and time period (T_s) and spectral energy density. For a wave pattern shown in figure 2.1, the spectral energy density curve using the above said methods is shown in figure 2.2. Among the above methods Scott spectrum provides reasonable maximum energy

density and is considered to be the best fit with the measured spectra as concluded by the authors in (Subba Rao et al. 2006).

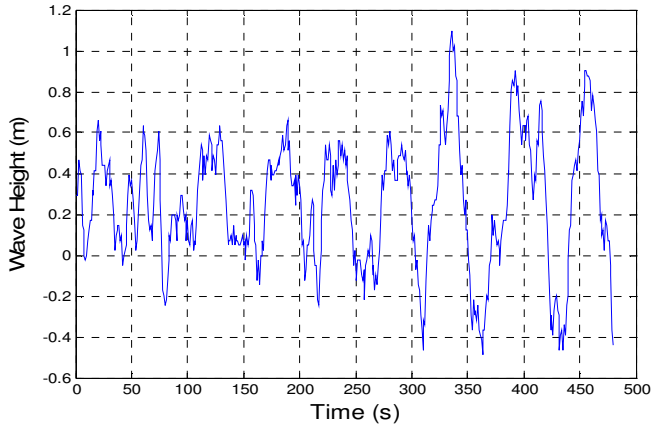

Figure Error! No text of specified style in document.**.2** **Wave pattern**

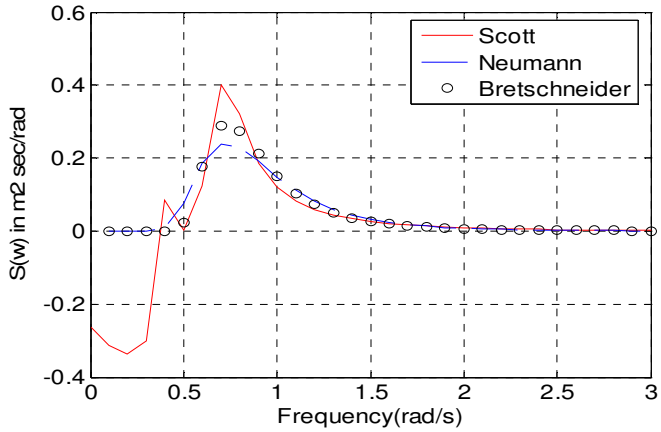

Figure Error! No text of specified style in document.**.3** **Spectral energy density curve**

The spectral energy density curve shown in figure 2.2 is for a wave pattern having significant wave height of 1.552m and wave period of 18.88s. The maximum energy density obtained using Scott spectrum is 0.4m^2s/rad at a peak angular frequency of 0.7306 rad/s.

Table 2.1 lists spectral parameters of wave data with different characteristics. The wave data is obtained from the Indian wave energy plant located at Vizhinjam off Trivandrum coast in India. Wave data is the data of variation in the wave height as a

function of time measured from the plant site. The Indian wave energy plant was set up by Ocean engineering centre, Indian institute of technology, Madras through a sponsored research project funded by the department of ocean development government of India in 1983 (Jayashankar et al. 2000, Yagna Narayanan et al. 1996, Indireshan et al. 1989). Spectral parameters are evaluated for different wave patterns so as to distinguish between the patterns. Wave data 1 is pattern having high significant wave height and large period, wave data 2 is the pattern having high significant wave height with medium period, wave data 3 is the pattern having medium significant height with medium period, wave data 4 is the pattern having medium significant height and high period and wave data 5 is corresponding to the pattern with low significant height and low period. As wave power is a function of wave height and period, the variations in wave height and period symbolize the vagueness in wave power.

Table 2.1 Spectral parameters for different wave data.

Wave Data	H_s (m)	T_s (s)	ω_o (rad/s)
Wave data 1	1.9189	36.48	0.4028
Wave data 2	1.9512	19.025	0.476
Wave data 3	1.552	18.8857	0.7306
Wave data 4	1.336	25.325	0.561
Wave data 5	1.005	16.7333	0.6545

Oscillating Water Columns

The most successful and most extensively studied device for extracting energy from sea waves is the oscillating water column device (OWC). A wave capture chamber set into the rock face of the shoreline is called the caisson. The construction of the caisson is the basic factor which decides the amount of energy to be extracted. Bigger the size of the caisson higher is power that can be extracted and higher is the investment cost. The caisson has an opening at the mouth through which the waves are forced in. Working principle is based on the exchange of energy between the water and the air that is trapped above the water surface by an air chamber which is open at the bottom. An incident wave crest increases the pressure of the water inside

the column, forcing the internal water level to rise and in turn pushing air out from the top of the column. The air turbine is installed in a duct which connects the chamber to the atmosphere thereby extracting energy from the air flow. The air flow reverses to refill the column when the wave trough appears (Jayashankar et al. 2000, Indireshan et al.1989).

OWC based wave energy plant has a three stage energy conversion process the OWC converts the variations in sea surface elevations to pressure, a bidirectional turbine converts pneumatic air power into mechanical shaft power and an electrical generator coupled to the turbine provides electrical power that is exported to the grid. Configuration of an ocean wave energy converter plant, using the OWC device is shown in figure 2.3. The overall plant efficiency is the product of the efficiencies of each of these power conversion stages.

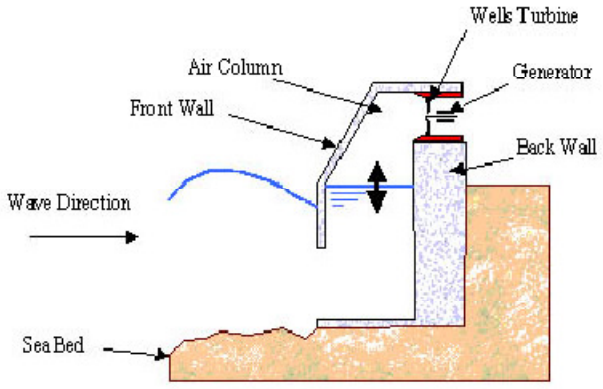

Figure Error! No text of specified style in document..**4 Diagrammatical illustration of an OWC**

The wave-to-pneumatic energy conversion may be studied theoretically/numerically, or by testing a physical model in a wave basin or wave flume. The OWC class of WEC operates much like a wind turbine according to the principle of wave-induced air pressurization. The power available from the airflow through the OWC outlet depends on the airflow speed at the turbine v_x, the area of the turbine A_{duct} , the pressure at the turbine duct P_{air} and the air density ρ_{air}. This power as given in equation 2.6 is comprised of two terms: (i) the air flow kinetic energy

term, $v_x^3 A_{duct} \rho_{air}/2$, which is common to wind turbine analysis, and (ii) the air pressure term, $P_{air} v_x A_{duct}$, that is unique to this application.

$$P_{OWC} = \left(P_{air} + \rho_{air} v_x^2 / 2\right) v_x A_{duct}$$ (Error! No text of specified style in document.**.6).**

Modeling of OWC

The OWC is the most highly developed type of wave energy converter and one of the very few to have reached the stage of full-sized prototype. Design optimization of OWC plants, especially of their power take-off equipment is very important. Several approaches have been used in the past to model and optimize OWC and WEC in general. The simple theoretical model assumes the incident wave to be regular or monochromatic, which allows the analysis to be performed in the frequency domain, provided the air turbine characteristic is approximately linear. In this case the hydrodynamic coefficients of radiation and diffraction are required for the wave frequency under consideration, which can be obtained analytically for simple geometries or experimentally evaluated. Mechanical model for OWC with compressibility is presented by Szumko in which certain aspects of modeling OWC wave power device, with particular reference to its behavior at representative off-resonant frequencies is discussed (Szumko 1989). A stochastic model was applied to devise an optimal algorithm for the rotational speed control of an OWC wave power plant equipped with a Wells turbine to evaluate the average power output of the plant in (Falcao 2002). Experimental measurements on scaled down models of OWC, are discussed in the literature (Thiruvenkatasamy et al. 2005, David et al. 2010).

In the work presented, modeling of OWC is done based on the energy concept which avoids the necessity of conducting tests on scaled down physical models and experimental facilities. For the model proposed, input is the real wave pattern which is the variation of wave height with time. This avoids the modeling of wave. Measured wave data from the Indian wave energy plant are applied to this model. Dimensions of the OWC of the Indian wave plant are used in the model. Output of the model is the axial velocity of air within the water column which can be used to find the differential pressure within the column. Though the compressibility of air is not

taken into consideration in modeling, output of the model are in qualitative agreement with the experimental output from the Indian wave energy plant.

OWC devices are shore-mounted structures having fixed frames of reference which operate in response to the incoming sea waves. Figure 2.4 indicates the dimensions of the OWC where *a* is length of the water column, *b* is the width of the chamber and h is the height of the water level within the OWC.

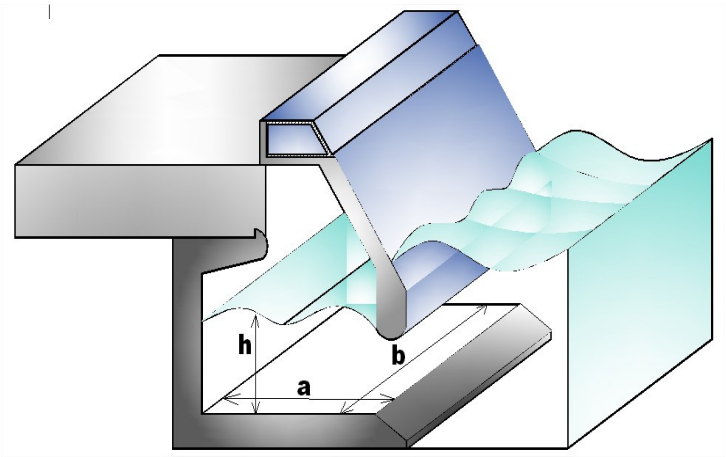

Figure Error! No text of specified style in document.**.5 Figure showing the dimensions of the OWC**

When sea wave enters the OWC the water level in the column increases for the wave crest as shown in figure 2.5 and decreases for the wave trough as shown in the figure 2.6. When the wave crest enters the OWC, water level increases. During a wave crest, if h_1 was the initial height of the water in OWC and h_2 is the final height of the water in OWC, then increase in the water level is given by equation 2.7.

$$\Delta h = h_2 - h_1 \qquad \text{(Error! No text of specified style in document.7)}$$

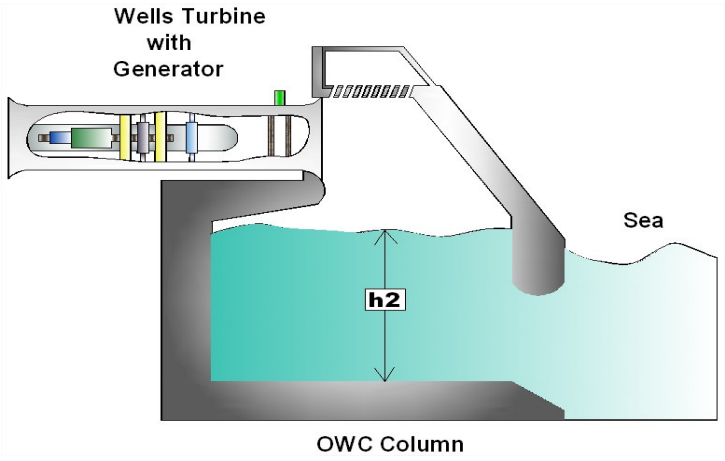

Figure Error! No text of specified style in document.**.6 Increase in the water level in OWC for the wave crest.**

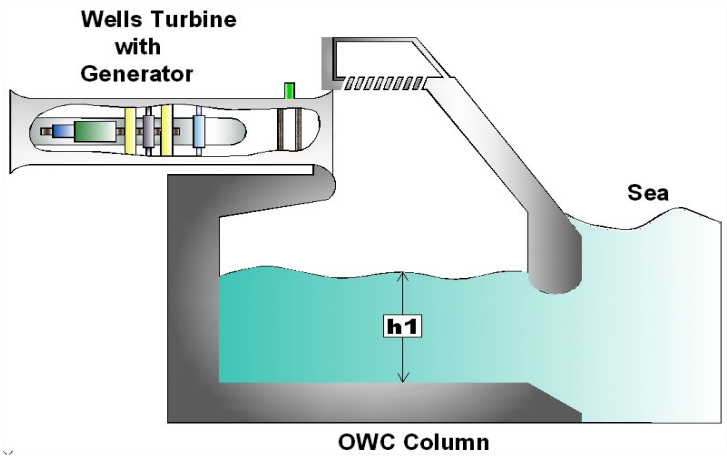

Figure Error! No text of specified style in document.**.7 Decrease in the water level in OWC for the wave trough.**

If the rise in the height of water in OWC is considered as a movement of a water slab from height h_1 to h_2, then the amount of water displaced m_0 can be expressed as in equation 2.8.

$$m_0 = \rho_w ab(h_2 - h_1) \quad \text{(Error! No text of specified style in document.8)}$$

b is the width of the wave which is assumed equal to the width of the chamber and ρ_w is the density of water.

Energy contained in the half wave in terms of wave amplitude and wave length is given by the equation 2.9.

$$E_{wave} = b \rho_w A^2 \lambda / 8$$ (Error! No text of specified style in document..**9**)

where, A is the wave amplitude and λ is wave length in meters. E_{wave} is the energy transferred to the water slab in Joules. This energy is responsible for rise in potential energy of water slab as well as the gain in kinetic energy of air in OWC. Using the principle of energy balance E_{wave} can be equated to the sum of increase in potential energy of water and kinetic energy of air as in equation 2.10.

$$E_{wave} = m_0 g \Delta h + V\left(\rho_{air} v^2\right)/2$$ (Error! No text of specified style in document..**10**)

where, V is the volume of air column, ρ_{air} is the density of air, g is the acceleration due to gravity and v is the velocity of air near the water surface. Assuming sinusoidal waves and neglecting superposition of waves entering into the water column, wave can be expressed as in equation 2.11.

$$y = y(x,t) = A \sin(kx - \omega t)$$ (Error! No text of specified style in document..**11**)

Where, k is the wave number given by equation 2.12 shown below and ω is the angular frequency in rad/s given by equation 2.13.

$$k = 2 * \pi / \lambda$$ (Error! No text of specified style in document..**12**)

$$\omega = 2 * \pi / T_w$$ (Error! No text of specified style in document..**13**)

T_w is the wave period. Increase in the height of water level is a function of the wave entering, hence can be related as shown in equation 2.14 using mass conservation,

$$ab\Delta h = b \int_0^{\lambda/2} A \sin(kx - \omega t)$$ (Error! No text of specified style in document..**14**)

Hence increase in the water level Δh is given by equation 2.15.

$$\Delta h = A \lambda \cos(\omega t) / a$$ (Error! No text of specified style in document..**15**)

Using equations 2.7- 2.15 the velocity of air near the water surface in the OWC can be found as in equation 2.16.

$$v = \sqrt{\left(2\rho_w g\left(\left(bA^2\lambda/8\right) - \left(ab\,\Delta h^2\right)\right)/\left(V\,\rho_{air}\right)\right)} \quad \text{(Error! No text of specified style in document..16)}$$

Then the velocity near the orifice of the OWC can found from the equation of continuity, assuming incompressible flow of air as shown in equation 2.17.

$$v_x = \left(A_1/A_2\right)\left\{\sqrt{\left(2\rho_w g\right)}\left(\left(bA^2\lambda/8\right) - \left(ab\,\Delta h^2\right)\right)/V\rho_{air}\right\} \quad \text{(Error! No text of specified style in document..17)}$$

where A_1 and A_2 are area of the OWC and the area of the orifice respectively and v_x is the axial velocity of air in the OWC near the orifice.

When wave enters into the OWC, it causes change in pneumatic power of water column within the OWC. Pneumatic power is related to the axial velocity of air within the OWC as shown in the equation 2.18.

$$P_{pneumatic\ power} = \left(dP\right)v_x\,ab \quad \text{(Error! No text of specified style in document..18)}$$

where dP is differential pressure within the oscillating column.

Historical development of the air turbine

The air turbine is the most critical element of the energy conversion chain and is where a major fraction of the energy losses occur. A large part of the R&D on OWC plants has been devoted to turbine aerodynamics. The air turbine of an OWC is subject to much more demanding conditions than the turbines in any other application, including wind turbines. The flow through the turbine is reciprocating and is random and highly variable over several time scales, ranging from a few seconds to seasonal variations. The time-average efficiency of an air turbine in an OWC is substantially lower than that of a water, steam, gas, wind turbine working in nearly steady conditions. Several types of air turbines have been proposed for wave energy conversion. Performance prediction of turbines under real sea conditions and

control of their speed for ocean energy conversion system have been discussed in the literature (Tindall et al. 1996, Anand et al. 2006).

The Wells turbine was invented, about 25 year ago by Dr. Allan Wells Professor at Queen's University of Belfast. It is an axial-flow turbine that is self-rectifying, which means its torque is not sensitive to the direction of the air flow, schematic diagram of which is shown in figure 2.7. Several versions have been studied since then namely, a single rotor without or with guide vanes, twin rotors in series, two counter-rotating rotors (Jayaraj Joseph et al. 2009, Mala et al. 2009 , Setoguchi et al. 2003).

The variable-pitch-rotor-blade turbine is a much more sophisticated version and allows phase control. All these versions have been objects of considerable theoretical and/or experimental R&D, especially in Europe (UK, Portugal and Ireland), Japan, India and China (Tease 2002, Anand et al. 2006, David et al. 2010).

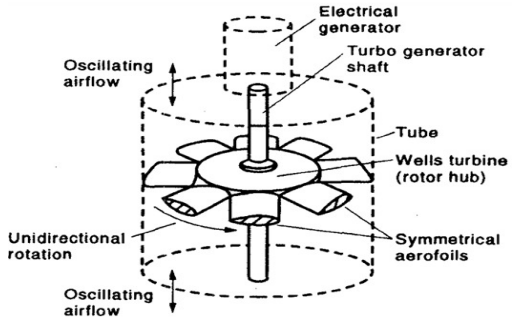

Figure Error! No text of specified style in document.**.8 Schematic of Wells Turbine**

The impulse turbine is the most popular alternative to the Wells turbine. This also belongs to the class of self rectifying turbines. Most of the R&D on this type of turbine has been done in Japan and to a lesser extent in India, China, UK and Ireland in the last decade. The advantages and disadvantages of the self-rectifying impulse turbine as compared with the Wells turbine are not yet very clear. In general, one can say that the Wells turbine is characterized by a considerably higher rotational speed than the impulse turbine, which enhances the storage of energy by fly-wheel effect and hence resulting in smoothing effect upon power delivered to the grid. Both wells turbine and impulse turbine are currently in operation in different power plants in Europe and Asia on experimental basis. Currently research around the world is focused on improving the performance of these turbines under different operating

conditions (Watterson et al. 1996, Thakker et al. 2002, Ajit et al. 2003, Ajit et al. 2004).

Modeling of the Wells turbine

The Wells turbine is the most frequently proposed and used air turbine to equip OWC plants. Its favorable features include high blade to air flow ratio. This means that relatively high rotational speed about 100-2000 rpm may be achieved for a low velocity of air flowing through the turbine. A high rotational speed allows a cheaper generator to be used, and also enhances the possibility of storing energy by flywheel. It is relatively cheap to construct and a fairly good peak efficiency of 0.7- 0.8 can be obtained for a full sized turbine. Weak points of the Wells turbine are low or even negative torque at relatively small flow rates and drop in power output due to aerodynamic losses at flow rates exceeding the stall free critical value. Recent research work indicates that this can be improved by suitable geometry of the rotor blades. By using variable pitch turbine, blade stalling can be avoided, or greatly reduced over a large range of flow rates, therefore allowing a substantially better time- averaged aerodynamic performance (Tease 2002).

Mathematical equations used for the modeling of the Wells turbine are as given by equation 2.19 and 2.20 (Jayashankar et al. 2000, Muthukumar et al. 2005, Yagna Narayanan et al. 1996).

$$dp = C_a \rho_{air} b_h l \ (n/2) \ (1/a_r) \ \left(v_x^2 + r\omega_t^2\right) \quad \text{(Error! No text of specified style in document..19)}$$

$$T_t = C_t \rho_{air} b_h l \ (n/2) \ r \ \left(v_x^2 + r\omega_t^2\right) \quad \text{(Error! No text of specified style in document..20)}$$

where dP is the differential pressure in Pascal, T_t is the gross torque produced by the turbine in Nm, ρ_{air} is the mass density of air in Kg/m^3, b_h is the blade height of the turbine in m, l the blade chord length in m, n is the number of blades of the turbine, r is the average radius of the turbine in m, a_r the annular area of the rotor in m^2, ω_t is the speed of rotation in rad/s, v_x is the axial velocity of air within the OWC in m/s, C_a is the power (Input) coefficient and C_t is the torque coefficient. The power coefficient and the torque coefficient are the two important characteristic parameters of the

turbine needed for the modeling of the turbine. The experimentally obtained plot of these two parameters as a function of the flow coefficient is given in figures 2.8 and 2.9. These characteristic curves have been obtained from the Indian wave energy plant (Jayashankar et al. 2000).

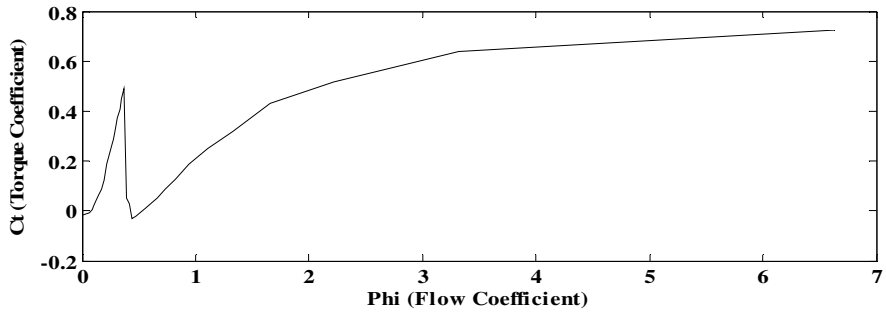

Figure Error! No text of specified style in document..**9** **Toque coefficient vs. flow coefficient Characteristic of Wells turbine**

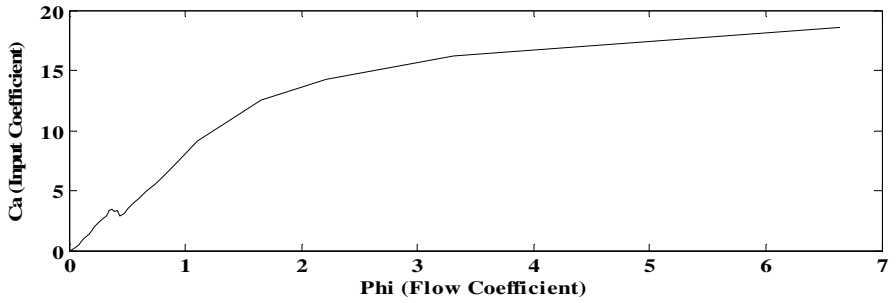

Figure Error! No text of specified style in document..**10** **Power coefficient vs. flow coefficient Characteristic of Wells turbine**

The flow coefficient φ_t is defined as in the equation 2.21.

$$\phi_t = v_x / (r\,\omega_t) \qquad \text{(Error! No text of specified style in document..21)}$$

The pneumatic power converted into mechanical power P_t by the Wells turbine is given by equation 2.22.

$$P_t = \omega_t T_t \qquad \text{(Error! No text of specified style in document..22)}$$

Results and discussion

OWC model with Wells turbine is tested with the actual wave pattern as input. The wave pattern has been obtained from the Indian wave energy plant which is the actual wave height measurement for a time length of 500s. Figure 2.10 shows a wave pattern corresponding to group of wave data 5 for 500s which has a significant wave height of 1.55m and wave period of 18.57s. From the spectral energy density curve it is observed that, the peak frequency corresponding to maximum energy density is 0.65rad/s and the wave power calculated in terms of the significant wave height and period is 143.23 kW. For this wave pattern the absolute axial velocity of air in OWC is shown in figure 2.11. Axial velocity has a maximum value of 11.44m/s and a mean value of 5.77 m/s.

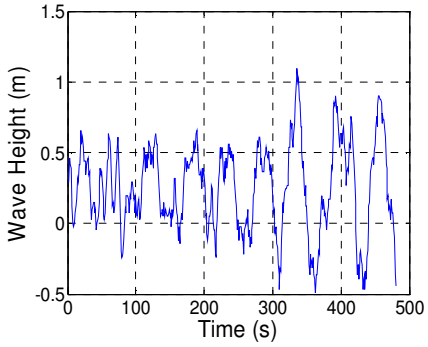

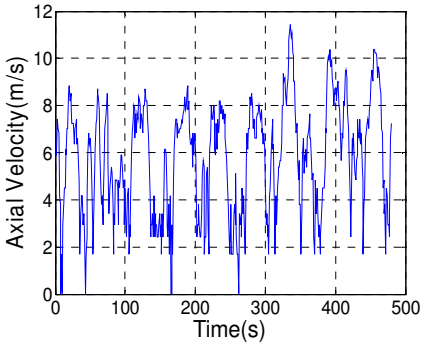

Figure Error! No text of specified style in document.**.11 Wave Pattern**

Figure Error! No text of specified style in document.**.12 Absolute Axial Velocity**

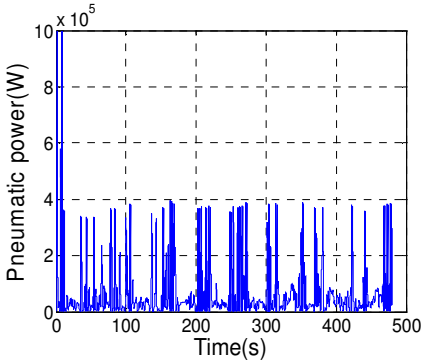

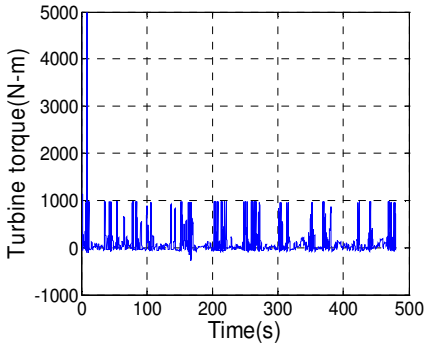

Figure Error! No text of specified style in document.**.13 Pneumatic power**

Figure Error! No text of specified style in document.**.14 Turbine torque**

It is observed that the absolute axial velocity of air in the OWC varies in accordance with the variations in the input wave data pattern. The pneumatic power within the OWC for the wave pattern considered is as shown in figure 2.12. Turbine torque and power are shown in figures 2.13 and 2.14 respectively. Figure 2.15 shows the variation of the turbine speed with time. Figures 2.16 and 2.17 show the plot of variations of differential pressure with time from the OWC model, and the plot of measured differential pressure from the Indian wave energy plant respectively.

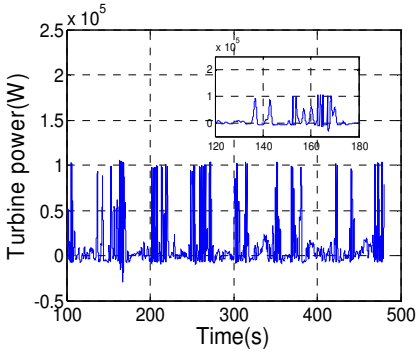

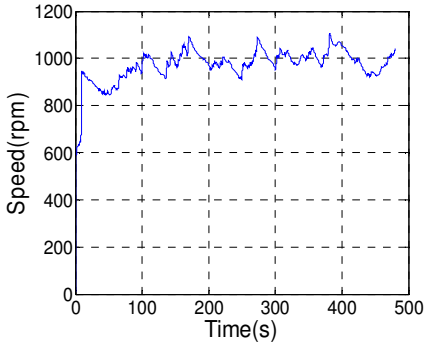

Figure Error! No text of specified style in document.**.15** **Turbine power**

Figure Error! No text of specified style in document.**.16** **Turbine speed**

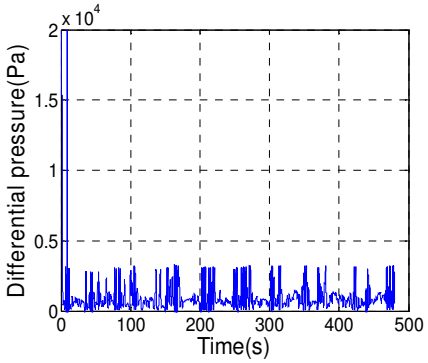

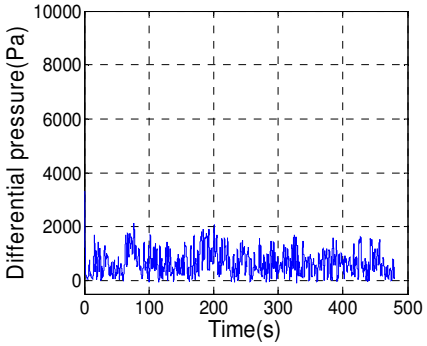

Figure Error! No text of specified style in document.**.17** **Differential pressure**

Figure Error! No text of specified style in document.**.18** **Differential pressure measured.**

The simulated model is applied with different wave patterns. The significant wave height H_s, period T_s, mean values of wave power P_{wave}, axial velocity v_x, pneumatic power within the oscillating water column P_{num}, turbine power P_t, differential pressure

within the oscillating water column 'dP_m' are evaluated and presented in the table 2.2. Also the differential pressure measured from the Indian wave energy plant for the corresponding input wave patterns is given as dP. The results got from the model are compared with the measured values from the Indian wave energy plant and it is observed that the output of model is in close agreement with the actual measured site data.

Table 2.2 Response of the OWC-turbine model for different wave patterns

wave data	H_s(m)	T_s(s)	P_{wave}(kW)	v_x(m/s)	P_{num}(kW)	P_t(kW)	dP_m(Pa)	dP(Pa)
Wave data1	1.9189	36.48	729	6.635	49.56	7.98	1075	982.5
Wave data 2	1.9562	19.025	400.4	5.879	46.95	7.63	1006	968.3
Wave data 3	1.7552	18.88	319.82	5.772	39.78	6.588	904.4	874.0
Wave data 4	1.3367	25.325	248	5.1	36.78	6.424	815.7	745.8
Wave data 5	1.005	16.7333	92.95	4.95	31.25	5.959	787.3	696.4

From the results it is seen that the Pneumatic power, turbine torque, turbine power fluctuate in accordance with the variations in the input wave data pattern. Since the waves are irregular, the air flow generated by the oscillating water column is irregular and hence the power and torque of the turbine is also irregular. For the wave patterns considered the significant wave height is varying in the range 1 to 2 m with wave period varying in the range 16 to 36s. It is observed that the though the range of variation of the mean axial velocity is less 4.9 to 6.63m/s, the maximum value goes up to 12m/s. The mean wave power variation range for the cases considered is 93 to 729 kW which is quite large, also the maximum pneumatic power shoots up to a value about three to four times the average value depending upon how the wave height and period are varying. This demonstrates the uncertainty in the wave power due to arbitrariness in the waves and reveals the difficulties in developing an efficient wave harnessing system. In the next chapter modeling of WECS connected to the grid is presented.

CHAPTER 3

MODELING OF WECS CONNECTED TO GRID

INTRODUCTION

The critical issue for the design of the generator and electrical equipment is the choice between constant and variable rotational speed. A fixed speed generator will extract smaller fraction of available power compared to a variable speed generator. During gust or swell conditions a fixed speed generator will experience severe shock whereas if the speed is allowed to change the inertia will absorb some of the extra

power input. Constant speed allows a cheaper generator to be used and does not require sophisticated power electronics. However one of the shortcomings of fixed speed system is that the rotational speed of the turbine cannot be adjusted to match the variations in the wave and hence storing and releasing energy by flywheel effect is not possible. This implies that the large power fluctuations resulting from the wavy nature of the energy resource are transmitted to the electrical grid without attenuation. This is not tolerable in small grids (Muthukumar et al. 2005).

On the other hand variable speed power generation enables the turbine to capture larger amount of energy, resulting in higher overall efficiency of the system. It keeps the turbine at its ideal speed for best efficiency and reduces peak structural stresses. Variable rotational speed necessitates sophisticated power electronics thereby increasing the overall cost of the system. In recent years advancements in the development of high power switching devices has led to the adoption of fully variable speed controlled generators. Such equipment is now becoming readily available in the market at reasonable prices. These variable speed generators are either gear coupled doubly fed induction generators with power electronics control of the rotor voltage and frequency or direct coupled synchronous generator with power electronics control of the stator voltage and frequency with permanent magnet excitation (Sullivan et al. 2008). Power electronic converter used for grid connection produces harmonics. Therefore filtering becomes necessary. Voltage jumps may be produced due to combination of many high frequency harmonics. All these issues have to be addressed in the control methodology. (Marian et al. 2010, Vining et al. 2007).

Electrical machines in wave energy conversion systems

In a WECS based on OWC principle, energy conversion takes place in three steps. In the first step variations in state of sea are converted into pressure difference within the OWC. Then the pressure variations are converted into the mechanical power by means of air turbine. Finally the mechanical power is converted into electrical power by means of a generator. As OWC is a linear device, variations in state of sea are reflected in the differential pressure within the OWC, and hence in the electrical power generated. The electrical generator can be connected to the power grid or to an isolated load. The standalone generation unit is difficult to control since the system

inertia is not large enough to maintain the system frequency. Hence an isolated system requires extensive control system in order to balance the input. In case of grid connected scheme, the grid acts like a fly wheel and absorbs the power fluctuations. At the same time it introduces some stability problems. In the past decade, wind energy conversion has been developed to a stage of maturity where the electrical system configuration is converging to a small number of options. Wave energy can profit from this knowledge because of the similarities between wind and wave energy.

With variable speed system possible options of ac generators are Induction generator, DFIG, wound field synchronous generator and PMSG. Induction generator can provide small range of speed variation with minimal control requirements. But it depends on an external voltage source to produce magnetic field in the stator. If variable speed is adopted with slip ring induction generator, the peak to average power fed to the grid is reduced at the expense of increased losses (Ravi Kiran et al. 2007). With variable speed operation, the synchronous generator will produce a variable frequency output and therefore requires an additional frequency converter before it can be connected to the grid. It also requires variable dc current for the field excitation and since the field current has to be supplied through the brushes and slip rings it necessitates regular maintenance. On the other hand, PMSG in which the electromagnets of conventional synchronous machine are replaced by permanent magnets neither requires dc power to create magnetic field as in conventional synchronous generator, nor ac power as in induction generator. On examination of the technology employed by the wind energy system, DFIG represents the state of the art with direct coupled PMSG representing a more recent trend. With DFIG the system cost, size and the power efficiency is optimum for a variable speed operation. This is due to the fact that power electronics ought to be rated for only 30-50% of the system rated power. But DFIG has the danger of being influenced by grid faults and failures since its stator is directly connected to the grid. Both DFIG and the brushed synchronous machine require regular maintenance and replacement of the brushes. In case of PMSG the initial cost is significantly more due the high cost of permanent magnets and 100% rating of the power electronics. However the major advantage of PMSG is increased reliability and reduced maintenance. This is due to the lack of brushes. In OWC based WEC, gearing is typically not an issue since the turbine can

be designed to rotate at speeds consistent with standard offline machines such as, 750/1000/1500/3000 rpm (O'Sullivan et al. 2008, Indiresan et al. 1989, Muthukumar et al. 2005, Yagnanarayanan et al. 1996, Wang et al. 2010, Yagnanarayanan et al. 1999).

Based on the research on the suitability of electrical generators for wave energy harnessing it appears that the induction generator and permanent magnet synchronous generator are the strong contenders. In the past induction generators were used as they were cheap, robust and easy to control. However PMSG has fewer loss mechanisms and therefore may be a better option due to its improved energy yield, weight and controllability (O'Sullivan et al. 2008, Hodgins et al. 2008).

Power electronic interface technologies

With variable speed operation both voltage and frequency at the output of the generator vary depending on the change in the axial velocity of air in OWC. This requires a power electronic interface between the generator and the grid or local load. Several interface systems have been discussed in the literature especially for wind power conversion. Several converter topologies for wind turbines both for fixed speed and variable speed have been proposed, implemented and investigated. Control solutions contributing to grid control using active and reactive power control enabled by power electronics have been widely discussed in the literature (Juan Manuel et al. 2006, Chen 1998, Fotios et al. 2006, Chen et al. 2001, Martha et al. 2005).

The standard electrical power generation system of the power take off of wave energy conversion device can be fundamentally divided into two categories. One is a direct connection of power generation system for a fixed speed operation and the other an indirect connection of power generation system for a variable speed. For fixed speed system a squirrel cage induction generator is directly connected to the utility as shown in Figure 3.1 (Tarek and Zobaa 2009). Output voltage of the induction generator is stepped up using a step up transformer and the reactive power requirement of the induction generator is supplied from either the grid or switched capacitors connected to the machine terminals. For variable speed wave energy device a PMSG can be used with full scale power electronics as shown in Figure 3.2 (Tarek and Zobaa 2009) converting the variable voltage, variable frequency output.

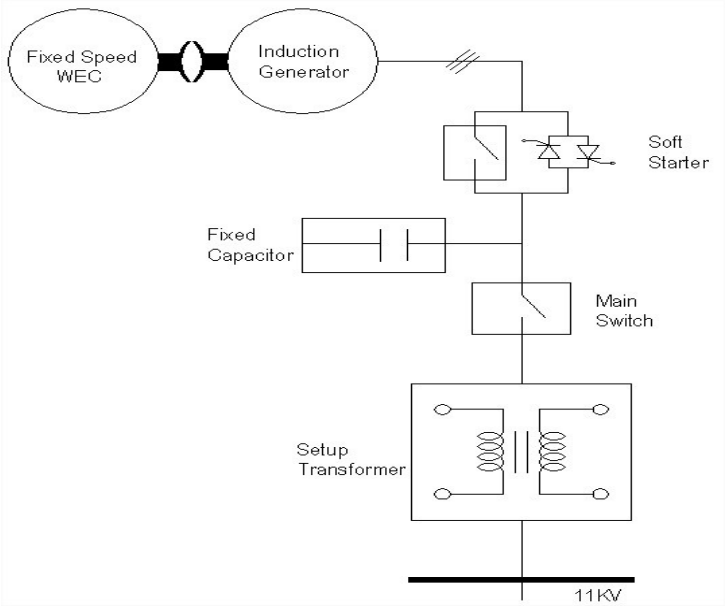

Figure Error! No text of specified style in document.**.19 Fixed speed generating system**

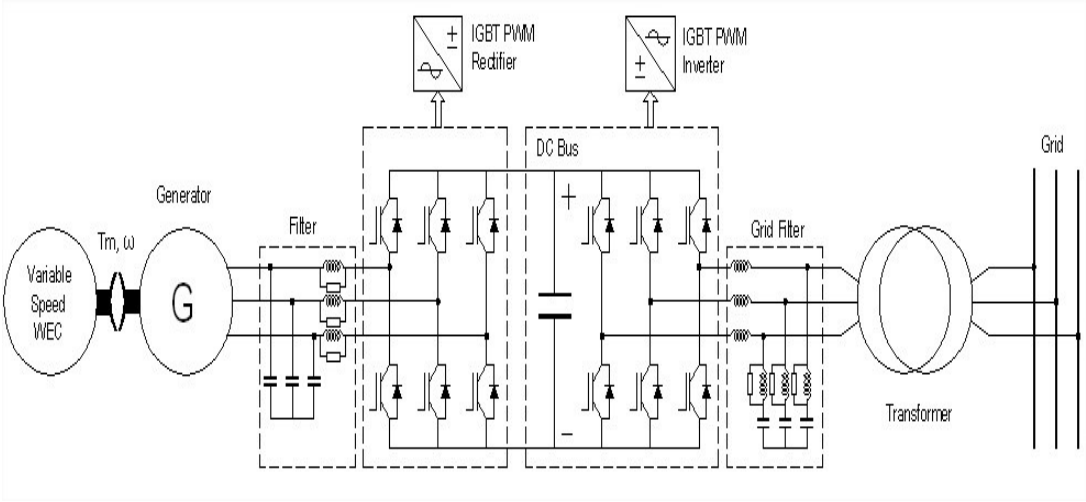

Figure Error! No text of specified style in document.**.20 Variable speed generating system with full scale power electronics**

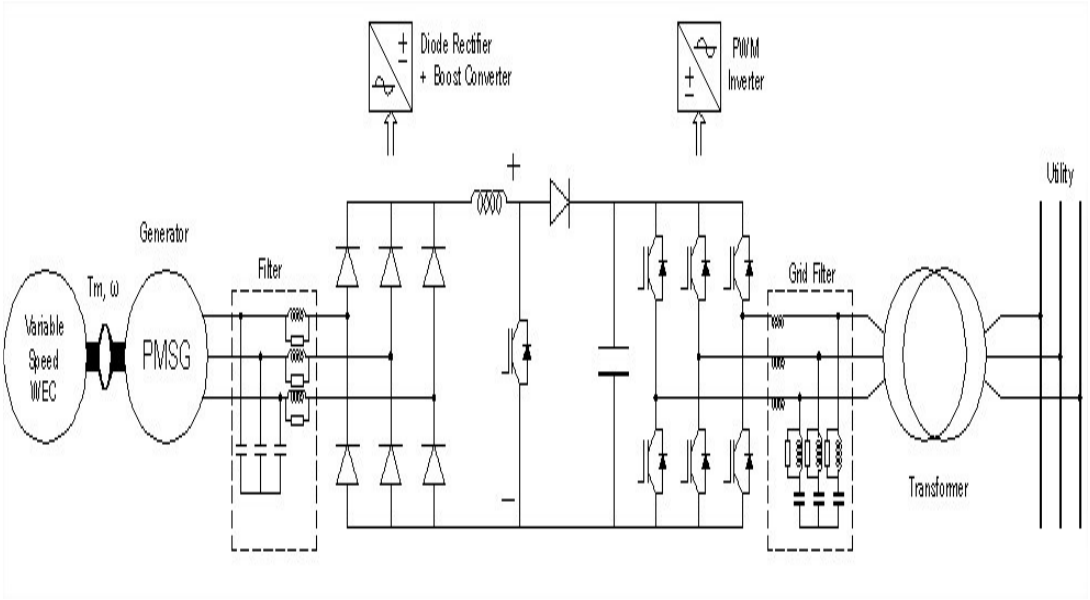

Figure Error! No text of specified style in document..**21 Variable speed generating system with boost converter**

The PWM rectifier of the back to back converter can be replaced by the uncontrolled rectifier and boost converter to achieve the same level of control as shown in figure 3.3 (Martha et al. 2007, Tarek et al. 2010 , Feng et al. 2008).

System description

Wave energy technology is still in R&D stage, struggling to go through to a commercial implementation. Wind energy technology has matured to a level where the turbine designs, electrical system configurations are converging to a small number of options. Generators, power electronic technology for grid interface options and control of generators in variable speed wind energy systems connected to the grid have been widely discussed. Several issues related to power quality are being investigated for wind energy system (Gabriele et al. 2007, Monica Chinchilla et al. 2006, Bhim Singh et al. 2008). The focus of wave energy developers so far has been basically on the sea performance, developing WEC which can withstand severe conditions and on the primary power take off mechanisms rather than electrical power take off. Among the various wave energy converters, converters based on OWC have

reached the pre-commercial stage. Therefore it is necessary to examine the different elements of the electrical system in detail with an objective of system optimization as well as the overall system control.

It is has been shown in wind and wave power conversion that variable speed turbines can capture energy 5% greater than the fixed speed technology and that the active and reactive power generated can easily be controlled. Variable speed operation is possible if the electrical grid frequency and the rotor frequency are decoupled. Hence the power electronic technology plays an important role in integration of the renewable sources into the electrical grid. To maximize power take off efficiency for a wide range variable speed operation the indirect connection using bi-directional power converter can be employed. The system uses full scale power electronics for converting the variable speed variable frequency power generated by the WEC to a constant voltage constant frequency power supplied to the grid. The generating system can make use of a PMSG. The full scale back to back voltage source converter by which the generator is connected to power grid allows the full controllability of the system. Due to the intensified grid codes full scale converter might be favored in future in spite of the additional cost incurred. The converter allows the variable speed operation and thereby the speed can be varied over a relatively wide range depending upon the input conditions where the turbine can extract maximum power at different input conditions. LCL filter is used between the inverter and the grid in order to achieve low levels of harmonic distortion (Erika Twinning et al. 2003, Milan Prodanovic et al. 2003).

Although the topology causes extra losses in the power conversion system this design allows the WEC to operate in a variable speed mode allowing more energy of the wave to be captured. The generator is decoupled from the grid by a voltage sourced dc link. Therefore this power electronic interface provides excellent controllable characteristics for the WECS. The power converter to the grid enables the fast control of active and reactive power. This will have a significant impact on the grid integration system and reduces the harmonic currents in order to keep the harmonic voltage within the acceptable limits and meet the grid code.

Taking into account all the above aspects wave energy harnessing system shown in figure 3.4 is considered for study. Here a variable speed Wells turbine driven PMSG

is connected to the grid through a LCL filter by means of fully controlled frequency converter which consist of a Pulse Width Modulated (PWM) rectifier, an intermediate dc circuit and a PWM inverter.

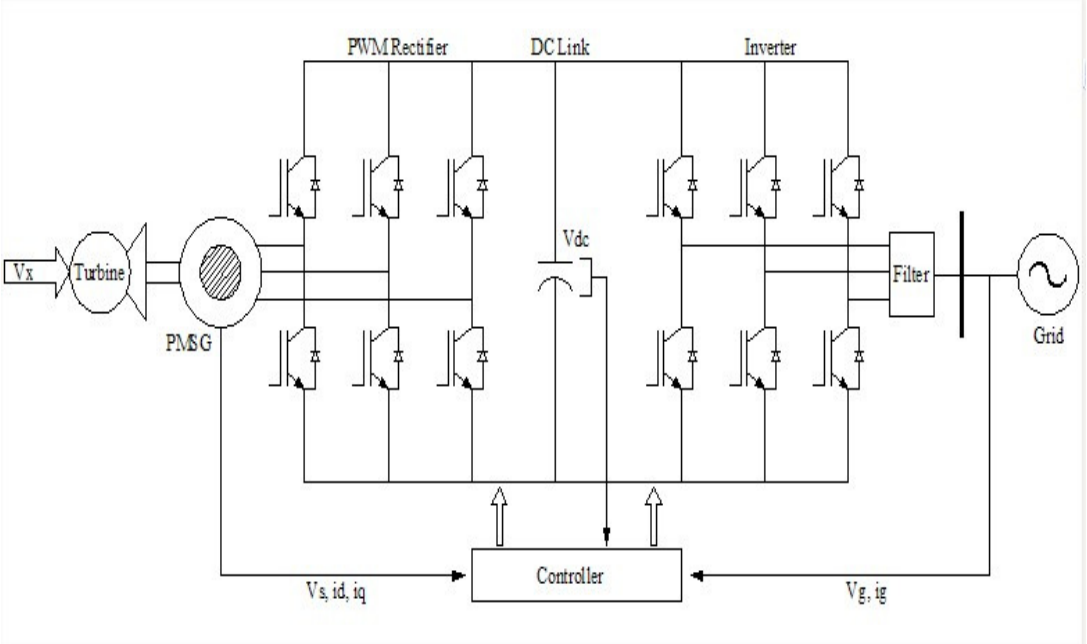

Figure Error! No text of specified style in document.**.22 Basic system of study**

Modeling of PMSG

Introduction

Permanent magnet electric machine is a synchronous machine which is magnetized from permanent magnets placed on the rotor instead of using a dc excitation circuit. With magnets on the rotor, electrical losses of the machine are reduced and the absence of field losses improves the thermal characteristics of the permanent magnet machines. The absence of mechanical components such as slip rings and brushes make the machine lighter resulting in higher power to weight ratio, which means higher efficiency and reliability. Permanent magnet machines have already become an attractive solution for wind turbine applications. The major disadvantages of permanent magnet machines are high cost of permanent magnet material, difficulties

to handle in manufacture, demagnetization of permanent magnets at high temperatures. These machines are classified into two group namely permanent magnet DC (PMDC) machines and permanent magnet AC (PMAC) machines. The PMDC machines are similar to dc commutator machines; the only difference is that the field winding is replaced by the permanent magnets. In case of PMAC the field is generated by permanent magnets located on the rotor and the brushes and the commutator does not exist. For this reason this machine is simple to use instead of PMDC. PMAC machines can be further classified depending on the type of back electromotive force into trapezoidal and sinusoidal machines. The trapezoidal machines, also called as brushless dc motors induce trapezoidal back emf voltage waveform in each stator phase winding during rotation while the sinusoidal PMAC machines, called synchronous machines require sinusoidal current excitation of the stator. Depending upon the rotor configuration PM synchronous machine (PMSM) can be classified in to surface mounted magnet type (SPMSM) and interior magnet type (IPMSM). In case of surface mounted magnet type the magnets are mounted on the surface of the rotor. The magnets can be regarded as air because the permeability of magnets is close to unity and the saliency is not present as a consequence of the same width of the magnets. From this the inductances expressed in the quadrature coordinates are equal ($L_d = L_q$). In case of interior magnet type the magnets are placed inside the rotor. In this configuration of the machine saliency appears and the air gap of d axis is increased compared to with q axis resulting that q axis inductance has a different value than d axis inductance. In case of SPMSM the design is easy due to the absence of saliency and hence becomes an attractive solution for wind or wave turbine application (Krishnan 2007).

Modeling of the generator

The generator can be electrically represented by the one phase equivalent circuit as shown in Figure 3.5 and the corresponding phasor diagram is shown in Figure 3.6. If a surface mounted PMSG (SPMSG) is used the magnetic flux distribution in the rotor is approximately sinusoidal. With this assumption the flux can be entirely described by a

vector and thus electromotive force E induced in the stator by the permanent magnet flux ψ_{pm} can be expressed as given in equation 3.1.

$$E = j\omega_r \psi_{pm} = j2\pi f \psi_{pm} \quad \text{(Error! No text of specified style in document.23)}$$

Internal voltage E depends on the actual rotor speed of the generator. Under load the stator current I_s and the stator reactance X_s also cause a magnetic field which is superposed to the field of the rotor. The voltage drop over the machines reactance X_s provokes a phase delay (load angle δ) between the internal voltage E and the stator voltage V_s which are equal only for no load. PMSG are normally not equipped with a damper winding. In the case when PMSG is connected to a frequency converter which provides a variable stator frequency according to the actual rotor speed, no relative movement between the stator and rotor field exists which could induce a voltage in the damper winding. Hence in case of transients, damper windings cannot contribute to damping. PMSG connected to a frequency converter is therefore a system without inherent damping. Thus no transient and subtransient reactances as known for wound rotor synchronous generator can be defined for the PMSG.

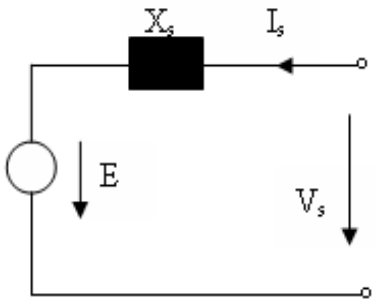

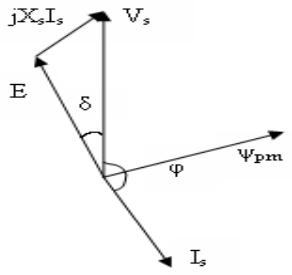

Figure Error! No text of specified style in document.**23 Equivalent circuit of PMSG**

Figure Error! No text of specified style in document.**24 Phasor diagram of PMSG**

In order to model the PMSG it is necessary to develop the mathematical model of the machine that is derived from the space vector form of the stator voltage equation as in 3.2.

$$V^{s}_{abc} = R_s I^{s}_{abc} + \frac{d}{dt}\lambda^{s}_{abc}$$ (Error! No text of specified style in document..**24**)

where R_s is the stator winding resistance per phase, I^s_{abc} is the stator current, V^s_{abc} is the stator voltage and λ^s_{abc} is the flux linkage. It is desirable to transform from abc to synchronous dq reference frame to have a simpler model (Krishnan 2007).

The two axes Permanent Magnet Synchronous Machine stator winding can be considered to have equal turns per phase. The rotor flux can be assumed to be concentrated along d axis while there is no flux along the q axis. Rotor flux is assumed to be constant at a given operating point. If the effect of variations of rotor temperature on the magnet flux is neglected, the rotor voltage equations are not necessary as in the induction machine, since there is no external source connected to the rotor. Rotor frame of reference is chosen because the position of rotor magnets determines the instantaneous induced voltage and subsequently the stator currents and the torque of the machine. In the rotor reference frame equivalent q and d axes of the stator winding are transformed into reference frames that are revolving at rotor speed.

Rotor magnet axis is the d axis and stator d and q axis windings have fixed phase relationship with the rotor magnet axis. The stator flux linkage equations are given by equations 3.3-3.4 (Krishnan 2007).

$$V^{r}_{qs} = R_q i^{r}_{qs} + P\lambda^{r}_{qs} + \omega_r \lambda^{r}_{ds}$$ (Error! No text of specified style in document..**25**)

$$V^{r}_{ds} = R_d i^{r}_{ds} + P\lambda^{r}_{ds} - \omega_r \lambda^{r}_{qs}$$ (Error! No text of specified style in document..**26**)

R_d and R_q are the direct and quadrature axis winding resistances.

The q and d axis stator flux linkages in rotor reference frame are given by the equations 3.5-3.6.

$$\lambda^{r}_{qs} = L_S i^{r}_{qs} + L_m i^{r}_{qr}$$ (Error! No text of specified style in document..**27**)

$$\lambda^{r}_{ds} = L_S i^{r}_{ds} + L_m i^{r}_{dr}$$ (Error! No text of specified style in document..**28**)

Self inductances of the stator q and d axes windings are equal to L_s only when the rotor magnets have an arc of electrical 180^0. When the stator winding d axis is in alignment with rotor magnet axis, the reluctance of the path is highest. The magnet reluctance is almost same as the air gap reluctance and hence its inductance is the lowest at this time. The inductance is referred to as the direct axis inductance L_d. At this time q axis winding faces the inter polar path in the rotor, where the flux path encounters no magnet but only the air gaps and iron in the rotor resulting in lower reluctance and higher inductance. The inductance of q axis winding is L_q at this time. In order to compute stator flux linkages in q and d axis the current in the rotor and stator are required. The permanent magnet excitation can be modeled as a constant current source i_{fr} . Since the rotor flux is along the d axis, d axis rotor current is i_{fr} and q axis rotor current is zero. Then the flux linkages can be written as shown in equations 3.7-3.8.

$$\lambda_{qs}^{r} = L_q i_{qs}^{r} \quad \text{(Error! No text of specified style in document..29)}$$

$$\lambda_{ds}^{r} = L_d i_{ds}^{r} + L_m i_{fr} \quad \text{(Error! No text of specified style in document..30)}$$

L_m is the mutual inductance between stator windings and rotor magnets. Substitution of equation 3.7 and 3.8 in the equation 3.3 and 3.4 gives stator voltage equations in terms of the direct and quadrature axis inductances as in equation 3.9.

$$\begin{bmatrix} V_{qs}^{r} \\ V_{ds}^{r} \end{bmatrix} = \begin{bmatrix} R_q + L_q P & \omega_r L_d \\ -\omega_r L_q & R_d + L_d P \end{bmatrix} \begin{bmatrix} i_{qs}^{r} \\ i_{ds}^{r} \end{bmatrix} + \begin{bmatrix} \omega_r L_m i_{fr} \\ 0 \end{bmatrix}$$

(Error! No text of specified style in document..31)

The torque equation of PMSG can be derived from the power balance equation. The power flowing into the machine can be expressed in dq reference frame as shown in equation 3.10.

$$P_{in} = \frac{3}{2}\left(v_{ds}^{r} i_{ds}^{r} + v_{qs}^{r} i_{qs}^{r}\right) \quad \text{(Error! No text of specified style in document..32)}$$

Substituting stator voltage equations in dq reference frame into equation 3.10 and separating the power quantities gives the power equation in the form as given in equation 3.11.

$$P_{in} = \frac{3}{2}\left(R_S {i_{ds}^r}^2 \right) + \frac{3}{2}\left(\frac{d}{dt} L_d \frac{\left({i_{ds}^r}^2 \right)}{2} + \frac{d}{dt} L_q \frac{\left({i_{qs}^r}^2 \right)}{2} \right) + \frac{3}{2}\left(\omega_r \lambda_{ds}^r i_{qs}^r - \omega_r \lambda_{qs}^r i_{ds}^r \right)$$

(Error! No text of specified style in document..**33**)

The first term represents the power loss in the conductors, the second term indicates the time rate of change for stored energy in the magnetic fields and the third term express the energy conversion from electrical to mechanical energy. The third term represents the electromagnetic torque because the power output from the motor shaft must be equal to the electromechanical power P_e as indicated in equation 3.12.

$$P_e = \omega_m T_e = \frac{3}{2}\left[\omega_r \lambda_{ds}^r i_{qs}^r - \omega_r \lambda_{qs}^r i_{ds}^r \right]$$

(Error! No text of specified style in document..**34**)

The relation between the electrical velocity ω_r and mechanical angular velocity ω_m of the machine depends on the number of pole pairs as shown in equation 3.13.

$$\omega_r = \frac{p}{2} \omega_m$$

(Error! No text of specified style in document..**35**)

The electromagnet torque is therefore given by the equation 3.14.

$$T_e = \frac{3}{2}\frac{P}{2}\left(\lambda_{ds}^r i_{qs}^r - \lambda_{qs}^r i_{ds}^r \right)$$

(Error! No text of specified style in document..**36**)

Substituting the flux linkages in terms of inductances and currents from 3.7 and 3.8 in the torque equation 3.14 gives the electromagnet torque in terms of the direct and quadrature axis inductances as shown in the equation 3.15.

$$T_e = \frac{3}{2}\frac{p}{2}\left\{ \lambda_{af} i_{qs}^r + \left(L_d - L_q \right) i_{qs}^r i_{ds}^r \right\}$$

(Error! No text of specified style in document..**37**)

λ_{af} is the rotor flux linkages that link the stator given by equation 3.16.

$$\lambda_{af} = L_m i_{fr}$$

(Error! No text of specified style in document..**38**)

In the expression for torque it can be observed that there are two terms. The first term represents the synchronous torque and is produced by the flux of the permanent magnets and the second term represents the reluctance torque which is the torque produced due to the difference in the inductances in dq reference frame. In case of surface mounted permanent magnet machines the inductances in dq reference frame are equal resulting in a simpler expression for the electromagnetic torque without the reluctance torque. With the assumption expressed above equation 3.15 has the following form

$$T_e = \frac{3}{2}\frac{P}{2}\left\{\lambda_{af}\, i_{qs}^{r}\right\} \quad \text{(Error! No text of specified style in document..39)}$$

Active and reactive powers of the permanent magnet generator are

$$P_s = \frac{3}{2}\left(V_{ds}^{r}\, i_{ds}^{r} + V_{qs}^{r}\, i_{qs}^{r}\right)$$

$$Q_s = \frac{3}{2}\left(V_{qs}^{r}\, i_{ds}^{r} + V_{ds}^{r}\, i_{qs}^{r}\right) \quad \text{(Error! No text of specified style in document..40)}$$

Electromechanical dynamic equation is given by

$$T_t = J\frac{d\omega_m}{dt} + B\omega_m + T_e \quad \text{(Error! No text of specified style in document..41)}$$

T_t is the torque of the turbine, T_e is the electromagnetic torque of the PMSG, J is the moment of inertia of the system, B is the friction coefficient, ω_m is the mechanical angular velocity of the machine. The modeling of PMSG has been implemented in MATLAB using the equations 3.9-3.19. The input to the PMSG is the mechanical speed developed by the Wells turbine and its outputs are the three phase voltage and the electromagnetic torque (Krishnan 2007).

Modeling of converters

The PWM rectifier and the inverter modeling is implemented using switching function concept (Byoung et al. 2001). Switching function concept is a powerful tool in understanding and optimizing the performance of static power converters. Using this concept power converter circuits can be modeled according to their function

rather than circuit topologies. As this method is not based on the state equation the tedious task of obtaining the state equations is avoided. Also with this, model convergence problem is avoided and simulation run time can be reduced. Design parameters such as the voltage, current ratings of the power switches and load currents can easily be calculated.

Functional models for the rectifier and the inverter are done based on transfer function theory. According to the transfer function theory for the PWM voltage source inverter input current I_v and the output line to line voltages (V_{ab},V_{bc},V_{ca}) are dependent variables and input dc voltage V_{dc} and load currents (I_a,I_b,I_c) are independent variables. Relationship between input and output can be expressed as in equations 3.20 and 3.21.

$$[V_{ab}, V_{bc}, V_{ca}] = (TF) V_{dc} \quad \text{(Error! No text of specified style in document..42)}$$

$$I_{in} = (TF)[I_a, I_b, I_c]^T \quad \text{(Error! No text of specified style in document..43)}$$

TF is the transfer function of the voltage source inverter and V_{dc} is the dc input voltage to the inverter. TF consist of several switching functions defined by the control strategy used. Sinusoidal pulse width modulation (SPWM) technique is used for both the rectifier and inverter circuits. For SPWM, two switching functions are used, one for the generation of line to line voltage and the other for the generation of currents within the inverter circuit. The overall model for the inverter consist of sinusoidal pulse width modulating signal generation block, switching function generation block, inverter block, load current generating block, pure switch and diode current generating block.

Sinusoidal pulse width modulating signal generation block compares the carrier signal V_{tri} with three control signals V_{cont_a} , V_{cont_b} , V_{cont_c} as shown in figure 3.7. Two sets of switching function signals SF1 and SF2 as shown in the figures 3.8-3.9 for each of the three phases are generated in the switching function block.

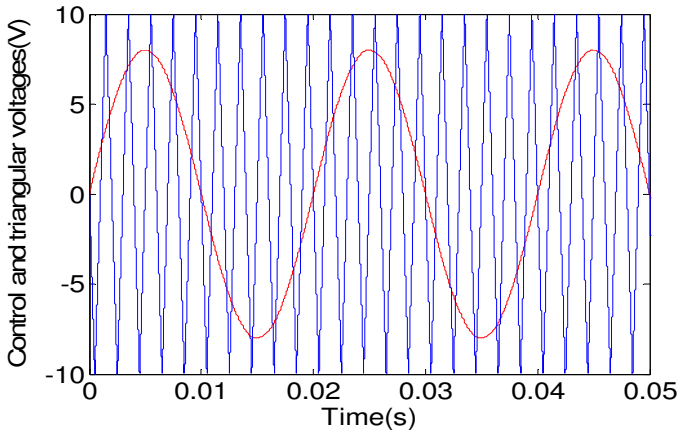

Figure Error! No text of specified style in document.**.25 Comparison of V_{tri} with control signal V_{cont_a}**

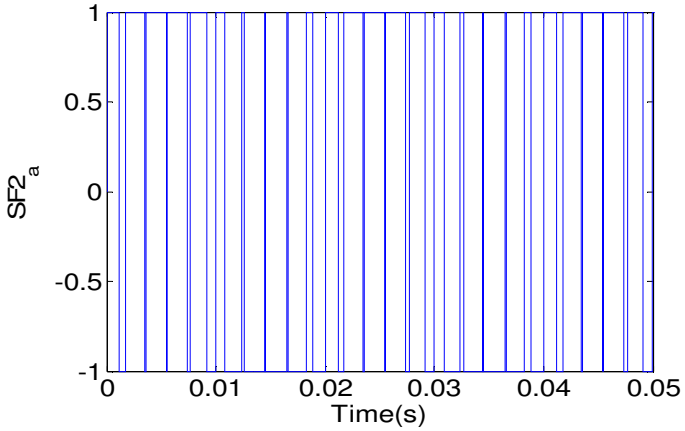

Figure Error! No text of specified style in document.**.26 Control signal SF2 for phase a**

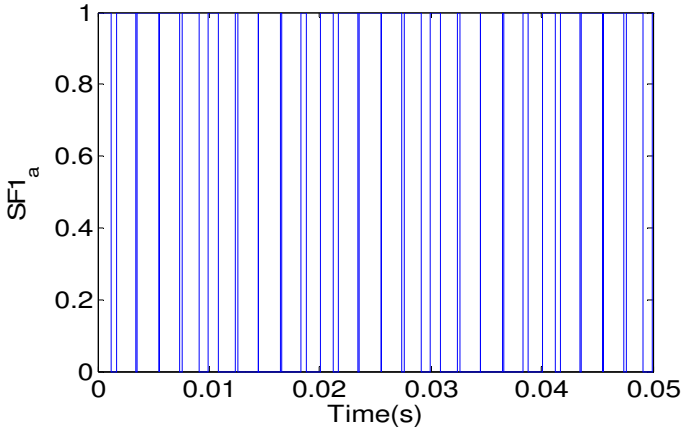

Figure Error! No text of specified style in document.**.27 Control signal SF1 for phase a**

Using the switching function signal SF_1 the inverter line and phase voltages are obtained using the equations 3.22- 3.24 in the inverter block.

$$\begin{bmatrix} V_{ao} \\ V_{bo} \\ V_{co} \end{bmatrix} = \frac{Vdc}{2} * \begin{bmatrix} SF_{1\_a} \\ SF_{1\_b} \\ SF_{1\_c} \end{bmatrix}$$

(Error! No text of specified style in document..**44)**

Inverter line to line voltages are derived using V_{ao}, V_{bo} and V_{co}. Inverter phase voltages V_{an},V_{bn} and V_{cn} are obtained as in equations 3.23.

$$\begin{aligned} V_{an} &= V_{ao} - V_{no} \\ V_{bn} &= V_{bo} - V_{no} \\ V_{cn} &= V_{co} - V_{no} \end{aligned}$$

(Error! No text of specified style in document..**45)**

$$V_{no} = \frac{1}{3}\left(V_{ao} + V_{bo} + V_{co}\right)$$

(Error! No text of specified style in document..**46)**

Using the phase voltages load currents for the three phases namely I_a, I_b and Ic are derived in the load current block. Switch currents I_{s1}, I_{s3} and I_{s5} for the upper leg devices and input current of the inverter are calculated using the corresponding load currents and the switching function SF_{2_abc} in the pure switch and diode current block according to the equations 3.25 - 3.26.

$$\begin{bmatrix} I_{s1} \\ I_{s2} \\ I_{s3} \end{bmatrix} = \begin{bmatrix} I_a & 0 & 0 \\ 0 & I_b & 0 \\ 0 & 0 & I_c \end{bmatrix} \begin{bmatrix} SF_{2\_a} \\ SF_{2\_b} \\ SF_{2\_c} \end{bmatrix}$$

(Error! No text of specified style in document..**47)**

From the switch currents inverter input current is derived as in equation 3.26.

$$Iv = I_{s1} + I_{s2} + I_{s3}$$

(Error! No text of specified style in document..**48)**

Similar concept is used to model the three phase PWM rectifier.

Modeling of dc link

In the system under study, power electronic interface between the generator and the grid consists of two controlled voltage source converters (VSC) and a capacitor as

shown in figure 3.10. One of the VSC is connected to the stator of PMSG named generator side converter, which converts ac power to dc power and stores it in the capacitor. The other VSC named the grid side converter being connected to the grid using PWM technique outputs power and voltage with a constant magnitude and frequency to the power grid. The capacitance called dc link capacitance between the two converters absorbs the instantaneous active power difference between the two converters. Modeling of the dc link capacitor is done based on the following equations.

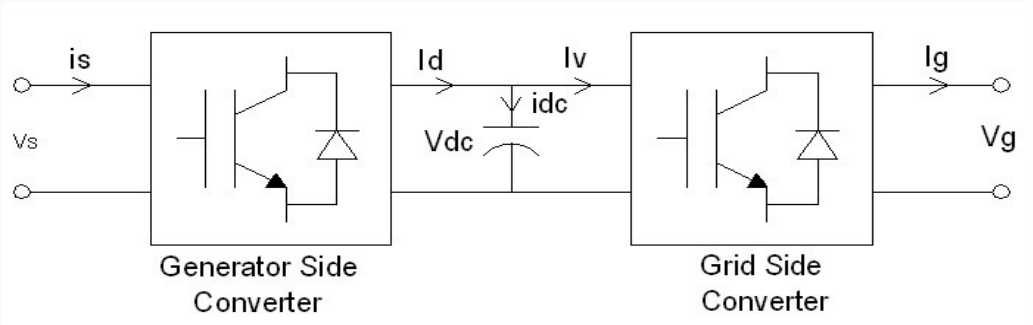

Figure Error! No text of specified style in document.**.28 DC link**

The dynamic equation for dc link is given by the equation 3.27.

$$\frac{dv_{dc}}{dt} = \frac{1}{C_k}(i_v - i_d) \quad \text{(Error! No text of specified style in document.}\mathbf{.49)}$$

I_d is the current flowing out of the generator side converter given by equation 3.28 and I_v is the current flowing into the grid side converter given by equation 3.29.

$$I_d = \frac{1}{V_{dc}}\left(v_{ds} i_{ds} + v_{qs} i_{qs} - P_{rlosss}\right) \quad \text{(Error! No text of specified style in document.}\mathbf{.50)}$$

$$I_v = \frac{1}{V_{dc}}\left(v_{dg} i_{dg} + v_{qg} i_{qg} - P_{dloss}\right) \quad \text{(Error! No text of specified style in document.}\mathbf{.51)}$$

v_{dg}, v_{ds} are the direct axis voltage components of grid voltage and the stator voltage and v_{qg}, v_{qs} are the quadrature axis voltage components of grid voltage and the stator voltage. i_{ds}, i_{dg} are direct axis components of grid and the stator current and i_{qg}, i_{qs} are

the quadrature axis components of grid and the stator current. By substituting equation 3.27 and 3.28 in 3.26 the dynamic equation of the dc link voltage could be defined as shown in equation 3.30.

$$\frac{dV_{dc}}{dt} = \frac{1}{C_k V_{dc}} \left[\left(v_{qg} i_{qg} + v_{dg} i_{dg} \right) + \left(v_{qs} i_{qs} + v_{ds} i_{ds} \right) - \left(P_{rloss} + P_{dloss} \right) \right] \quad \text{(Error! No text of specified style in document..52)}$$

P_{rloss} and P_{dloss} are the converter losses.

Results and discussion

The WECS model developed is validated by applying different inputs like constant axial velocity, varying axial velocity and the actual wave pattern. Figure 3.11 shows the torque, speed, three phase AC voltage generated by PMSG, dc link voltage and the output voltage of the inverter when the input to the Wells turbine namely the axial velocity is set at a constant value. Figure 3.12 shows the change in the torque, speed, voltage generated and the stator current of the generator when the input to the Wells turbine namely the axial velocity is initially set at a constant value and then changed in steps. Figure 3.13 shows the torque (T_e), speed (ω_m), voltage generated by PMSG (V_s), dc link voltage (V_{dc}) and the output voltage of the inverter (V_{in}) when the input to the Wells turbine namely the axial velocity is set at a constant value and then decreased in steps.

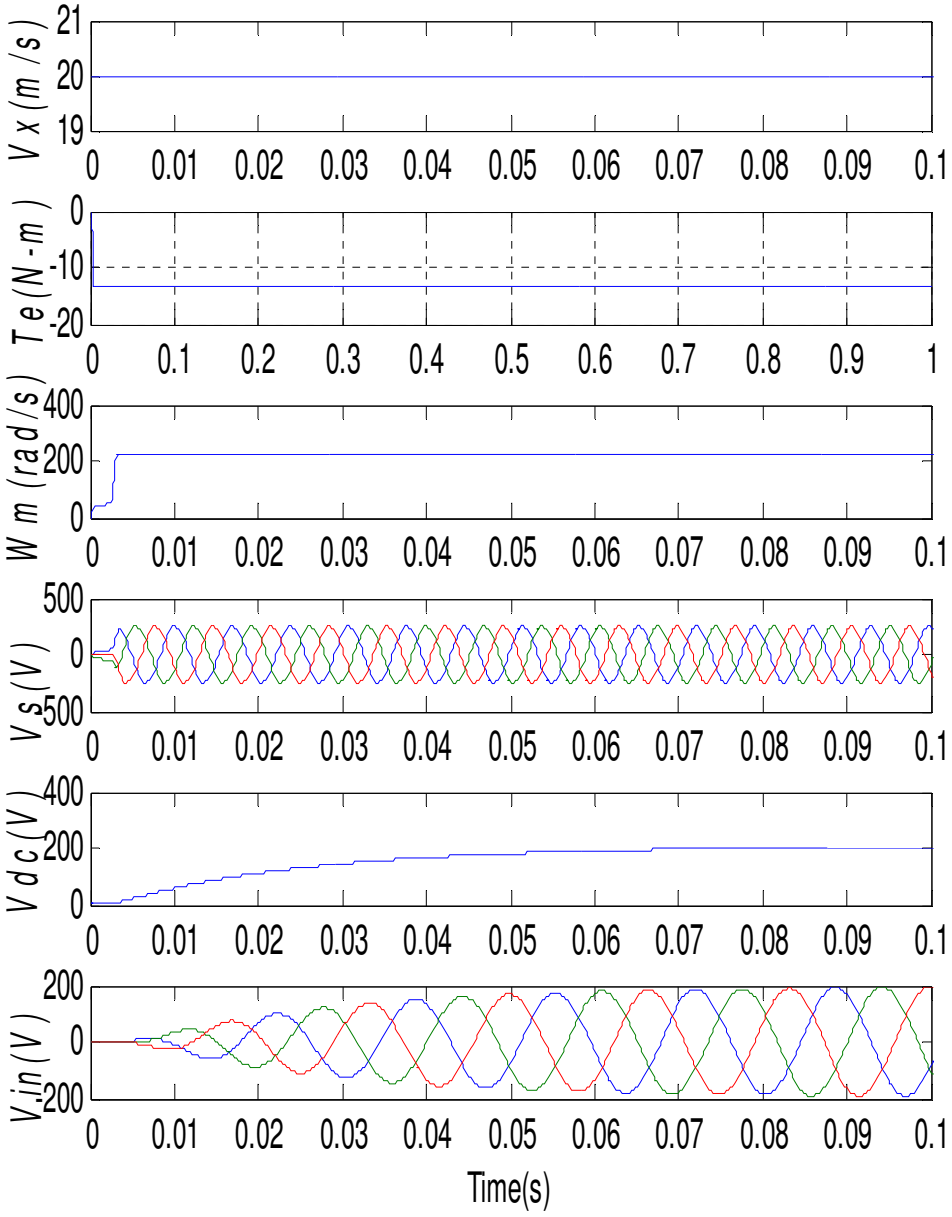

Figure Error! No text of specified style in document..**29 Performance of WECS with constant axial velocity**

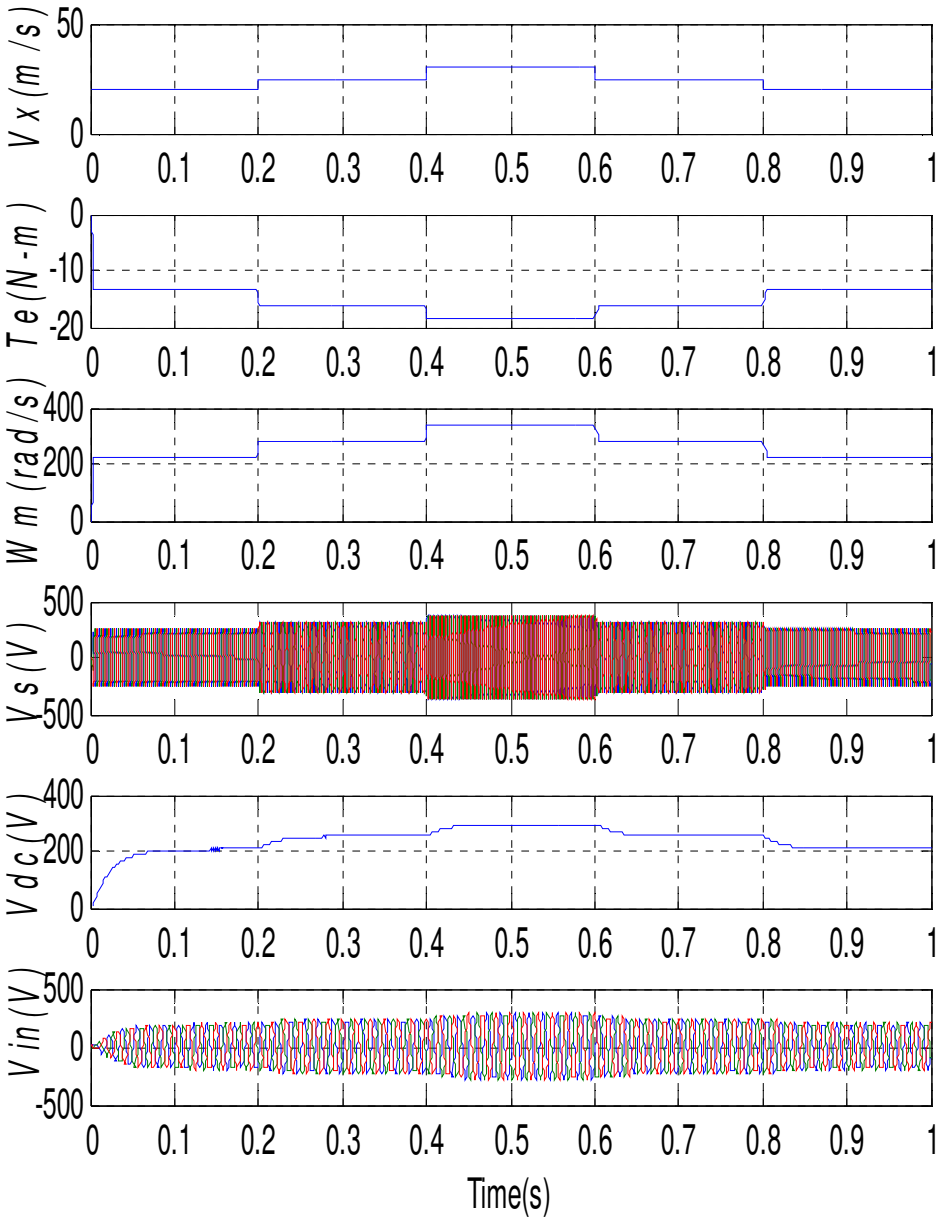

Figure Error! No text of specified style in document.**.30 Performance of the WECS with axial velocity is changed in steps**

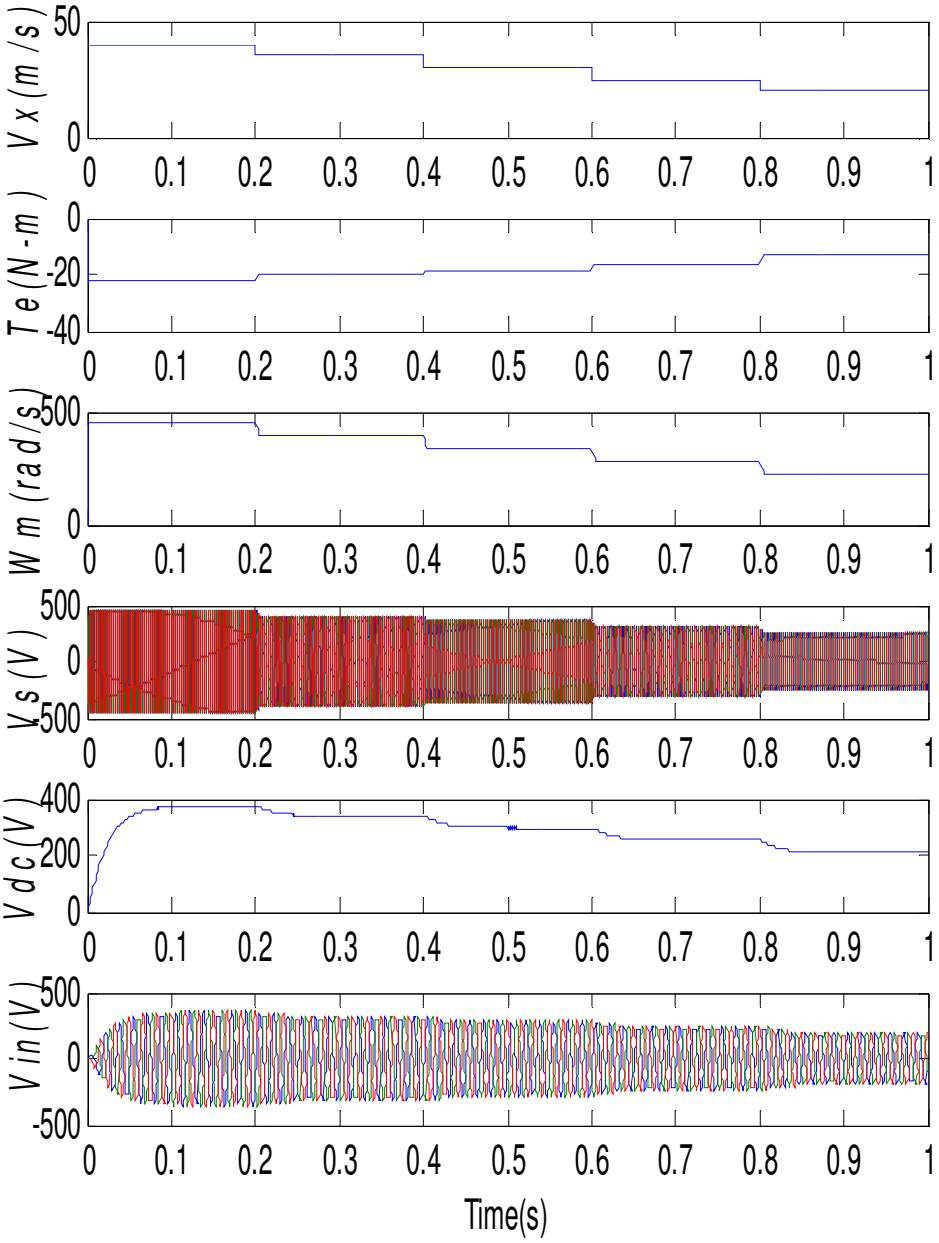

Figure Error! No text of specified style in document.**.31 Performance of the WECS with axial velocity is decreased in steps**

When OWC model is applied with a wave pattern for 500s which has a significant wave Height (H_s) of 1.55m and wave period of 18.57s, speed, power developed by the PMSG, torque developed by the PMSG, the three voltage generated by PMSG are as shown in figures 3.14 - 3.17. Figure 3.18 shows the part of the three phase voltage generated by PMSG and figure 3.19 shows the rms value of the generated voltage.

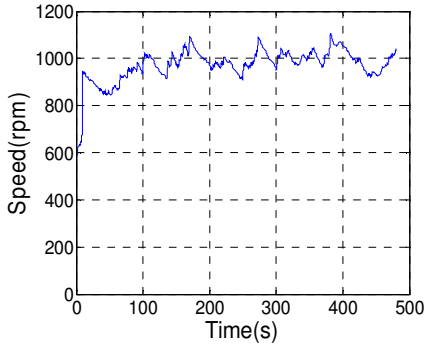

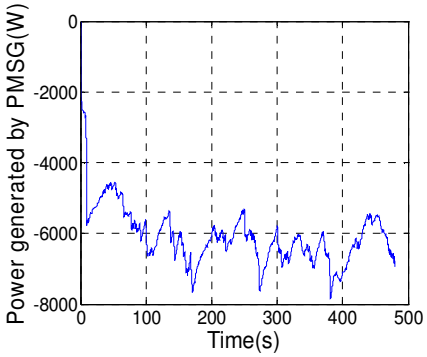

Figure Error! No text of specified style in document.**..32 Turbine Speed**

Figure Error! No text of specified style in document.**..33 Power developed by PMSG**

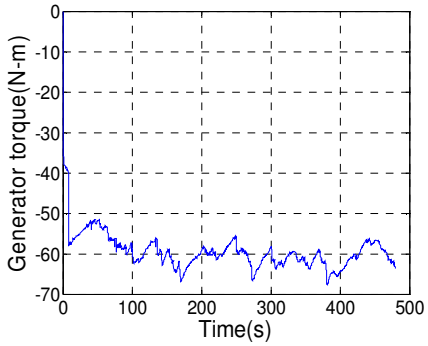

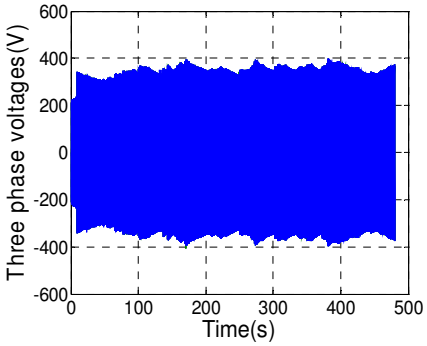

Figure Error! No text of specified style in document.**..34 Torque developed by PMSG**

Figure Error! No text of specified style in document.**..35 Voltage generated by PMSG**

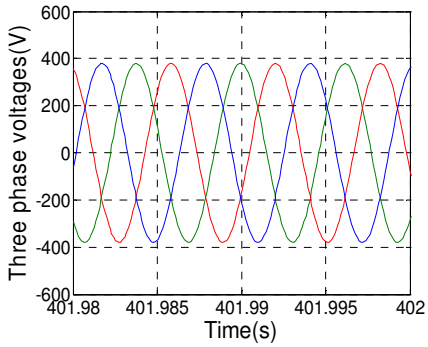

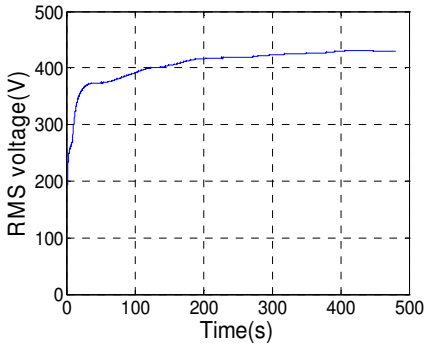

Figure Error! No text of specified style in document.**..36 AC voltage generated**

Figure Error! No text of specified style in document.**..37 RMS voltage generated**

Results demonstrate the randomness in the various quantities like speed, torque and powers developed of the turbine and the generators when the axial velocity input to the turbine is varying randomly. Modeling and design of controllers for grid connected WECS is presented in the next chapter.

CHAPTER 4
MODELING AND DESIGN OF CONTROLLERS FOR A GRID CONNECTED WECS

INTRODUCTION

Power possessed by a wave which has a length of 1m along the wave front with a height H & period T is given by $P = \rho_w g^2 H^2 T (1/32\pi)$ W/m where, ρ_w is mass density of water, g is the acceleration due to gravity. In nature waves are far from ideal and are irregular. With wave height and period both varying over a wide range, the power available for extraction from the waves varies from instant to instant. Deriving a constant average electrical power out of this for exporting to grid in case of grid connected operation and supplying an isolated load in case of standalone operation are both challenging jobs. Fluctuations in the power fed to the grid are not desirable and therefore characteristics and control of generator needs to be studied intensively to improve the performance and efficiency of such power plants if they are to become economically feasible. Control of fluctuations in an OWC wave energy device is more difficult in view of pulsating nature of input power unlike in wind energy schemes where air velocity is practically steady with superimposed ripple. In OWC based wave energy device, in addition to statistical variation of air speed due to statistical variations of wave, there is cyclical variation of air velocity due to bidirectional nature of air flow. Therefore, axial velocity of air swings from zero to a maximum value and back to zero in a period of typically 4 - 5s in a periodically repeated manner. The extent of variation in speed of Wells turbine due to cyclical input power depends on turbine output, rotational inertia of the system, torque speed characteristics of generator, wherein the turbine output itself is a function of speed. Of these, only generator characteristics can be modified during operation. The generator performance should be controlled so as to improve overall efficiency and to reduce power fluctuation or ripple to an acceptable value.

In wind power conversion system several issues concerned to the power control, power quality are investigated and solved. These solutions can be applied to wave energy systems, but need further research in order to extract electrical energy from the sea waves in a commercially and technologically acceptable manner. Several issues are to be considered and solved such as control applied to the generator, the power conditioning system for the increased production and reduced voltage harmonics. In addition, power fluctuations introduced should comply with new grid codes for renewable energy sources. Control of variable speed wind energy conversion system has been widely discussed in the bibliography. Several control schemes suitable for grid connected voltage source inverters and for isolated power systems for wind power conversion system are proposed (Juan Mauel et al.2006, Monica Chinchilla et al. 2006).

This chapter deals with the design of controllers for the generator side converter and the grid side converters for a grid connected wave energy conversion system. Since the output power of the wave energy converter fluctuates, the frequency and the magnitude of the ac voltage generated vary. Full scale back to back converters are employed to interface the energy conversion system to the grid. The back to back converters consist of two controlled voltage source converters (VSC) and a capacitor. One of the VSC named generator side converter, is connected to the stator of PMSG. This converts ac power to dc power and stores it in the capacitor. The other VSC called the grid side converter is connected to the grid. This outputs power and voltage with a constant magnitude and frequency to the power grid using PWM technique. The capacitance called dc link capacitance between the two converters absorbs the instantaneous active power difference between the two converters. The power converter control is achieved in two stages namely with a controller for the generator side converter and a controller for the grid side converter. Since the ac system of the generator and the grid are decoupled by the dc link they can operate at different ac frequencies. Hence independent direct and quadrature axis reference frames for the control of generator side and the grid side converters can be used. Control of the system is realized by coordinated control of generator side converter and the grid side converter (Fotios et al. 2006, Feng et al. 2008).

Generator side converter control

Generator side converter consists of active elements such as IGBTs. This provides best utilization and control of the PMSG. Several control strategies have been discussed in the literature namely maximum torque control, unity power factor control and constant stator voltage control (Fotios et al. 2006, Feng et al. 2008).

In the maximum torque control strategy d axis current is kept zero while the current vector is aligned with the q axis in order to maintain the torque angle equal to 90°. If stator current is controlled to have q component only the generator provides maximum possible torque. With this strategy reactive power demand of the generator is not zero which increases the converter rating. In unity power factor control strategy d axis current component of the stator is used to compensate the reactive power demand of the generator. The main advantage of this control strategy is that the generator operates at unity power factor which minimizes the converter rating. However there is risk of over voltages due to over speeds since the stator voltage is not directly controlled and stator voltage varies depending upon the speed. The risk of over voltage at over speeds can be avoided with constant stator voltage control.

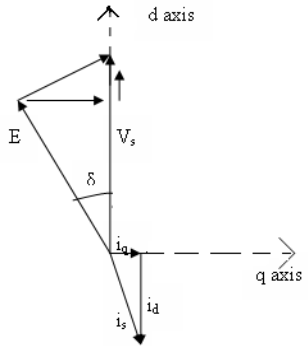

Figure Error! No text of specified style in document.**..38 Phasor diagram for constant stator voltage control**

In this control strategy, stator voltage is controlled instead of reactive power, thereby limiting stator voltage to the rated value. Control is done in stator voltage oriented reference frame where d axis is aligned to the stator voltage vector. The phasor diagram of this control strategy is shown in the figure 4.1. The Active power

depends on direct axis stator current and the reactive power depends on the quadrature axis stator current. Active and reactive powers are given by equation 4.1.

$$P_s = \frac{3}{2} V_{ds}^{s} i_{ds}^{s}$$

$$Q_s = -\frac{3}{2} V_{qs}^{s} i_{qs}^{s}$$

(Error! No text of specified style in document..**53**)

where V_{ds} and V_{qs} are the direct and quadrature axis components of stator voltages and i_{ds} and i_{qs} are the direct and quadrature axis currents of the stator current. Direct axis stator current component i_{ds} is determined by active power production of generator and quadrature axis stator current component i_{qs} can be used to control stator voltage to its rated value. With this control both generator and converter always operate at rated values for which they are designed. But the converter rating increases with the reactive power demand of the generator. As constant stator voltage control is assessed to be most beneficial, this control strategy is implemented in the simulation model. So as to ensure that the active power generated is fed to the grid via the dc link, dc link voltage must be kept constant. Assuming a loss less converter active power of the generator and dc link power can be equated as in the equation 4.2

$$P_s = P_{dc} = V_{dc} I_d = \frac{3}{2} v_{ds} i_{ds}$$

(Error! No text of specified style in document..**54**)

where V_{dc} is the dc link voltage and I_d is the output current of the generator side converter. Above expression indicates that dc link voltage as well as active power can be controlled using i_{ds}. Stator voltage control is achieved by controlling the current i_{qs}. Block diagram of the control scheme is shown in figure 4.2. V_{ac} is the measured stator voltage and i_{qs} and i_{ds} are quadrature and direct axis stator currents derived from the measured three phase stator currents.

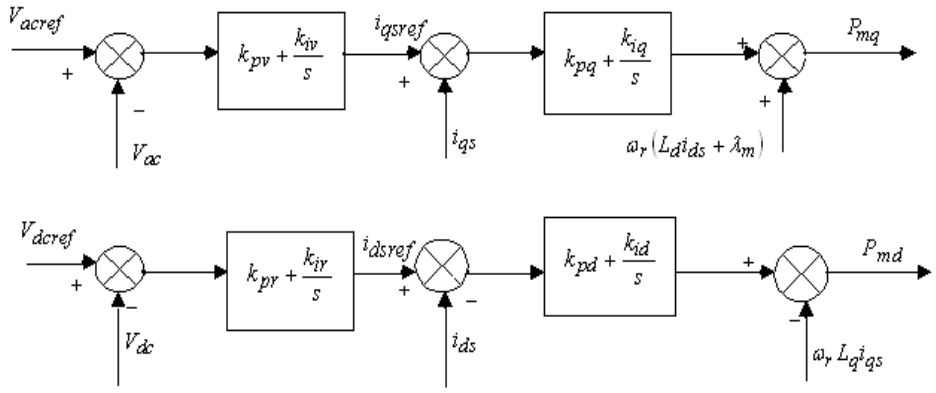

Figure Error! No text of specified style in document..**39 Block diagram of the control scheme for generator side converter.**

Control scheme has fast responding inner current loop controlling d axis and q axis stator currents and outer slower loop for controlling dc link voltage and stator voltage. Based on the stator voltage error, q axis reference current i_{qref} is determined through a PI controller as in equation 4.3, where

$$i_{qref} = k_{pv} e_v + k_{iv} \int e_v dt \quad \text{(Error! No text of specified style in document..55)}$$

k_{pv} and k_{iv} are proportional and integral gains of the PI controller, and e_v is the error between reference stator voltage and measured stator voltage. Similarly d axis current reference i_{dref} is determined through a PI controller based on the dc link voltage error as given in equation 4.4, where

$$i_{dref} = k_{pr} e_r + k_{ir} \int e_r dt \quad \text{(Error! No text of specified style in document..56)}$$

k_{pr} and k_{ir} are proportional and integral gains of the PI controller and e_r is the error between reference dc link voltage and measured dc link voltage.

Based on the current errors d and q axis reference voltages P_{md} and P_{mq} are determined by a PI controller. Decoupling terms for d and q axis obtained from stator voltage equations are used as shown in equations 4.5 and 4.6 in order to have simple and independent control of direct and quadrature axis currents.

$$P_{md} = k_{pd} e_d + k_{id} \int e_d dt - \omega_r L_q i_{qs} dt$$ (Error! No text of specified style in document..**57)**

$$P_{mq} = k_{pq} e_q + k_{iq} \int e_q dt - \omega_r (L_d i_{ds} + \lambda_m)$$ (Error! No text of specified style in document..**58)**

k_{pd}, k_{pq} are the proportional gains of the PI controllers and k_{id}, k_{iq} are the integral gains. e_d is the d axis current error and e_q is the q axis current error. Decoupling terms for d axis namely $(- \omega_r L_q i_{qs})$ and q axis $\omega_r(L_d i_{ds} + \lambda_m)$ are used. Control signals P_{md} and P_{mq} are then transformed into a, b, c components and given to PWM converter to generate pulses for the machine side converter.

Design structure of q axis current controller is shown in figure 4.3. The controller block is chosen to be PI controller as it offers zero error in steady state. Transfer function of a PI controller is the ratio between the output signal and the error signal as shown in equation 4.7, where

$$G_c(s) = k_{pq} + \frac{k_{iq}}{s} = k_{pq} \frac{1 + T_{iq} s}{T_{iq}}$$ (Error! No text of specified style in document..**59)**

k_{pq} represent the proportional gain, k_{ii} is the integrator gain and T_{ii} is called the integrator time and represents the ratio between k_{pq} and k_{ii}.

Transfer function of inverter modeled as a gain with a time lag is given by equation 4.8.

$$G_i(s) == \frac{K_i}{1 + sT_i}$$ (Error! No text of specified style in document..**60)**

Plant transfer function is determined from the dq voltage equations considering current as input and voltage as output as given by equation 4.9, where

$$G(s) = \frac{i_{qs}(s)}{V_{qs}(s)} = \frac{K}{1 + sT_q}$$ (Error! No text of specified style in document..**61)**

T_q is the time constant of the machine and K is the inverse of stator resistance.

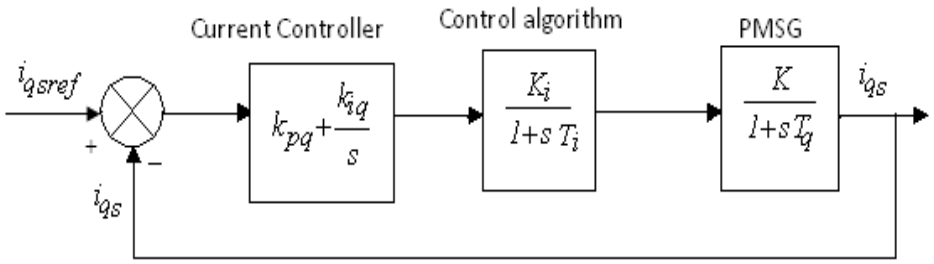

Figure Error! No text of specified style in document.**.40 Structure of q axis current controller**

The open loop transfer function of the current controller is

$$G_{OL}(s)=k_{pq}\frac{1+T_{iq}s}{T_{iq}s}\quad\frac{K_i}{T_is+1}\quad\frac{K}{1+sT_q}$$

(Error! No text of specified style in document.**.62)**

The slowest pole is one of the PMSG transfer function and is meant to cancel the zero of the controller making the system more stable. This implies

$$T_{iq}=T_q$$

(Error! No text of specified style in document.**.63)**

With this assumption open loop transfer function simplifies to

$$G_{OL}(s)=k_{pq}\frac{K}{T_{iq}s}\quad\frac{K_i}{T_is+1}$$

(Error! No text of specified style in document.**.64)**

The value of k_{pq} is determined by comparison of the open loop transfer function with second order system with a damping factor of 0.707.

Closed loop transfer function is given by equation 4.13.

$$G_{CL}(s)=\frac{G_{OL}(s)}{1+G_{OL}(s)}$$

(Error! No text of specified style in document.**.65)**

Grid side converter control

The main objective of the control scheme is to modulate the inverter to regulate the magnitude and phase angle of the grid supply current so that the real and the reactive power entering the network can be controlled. The criteria for judging the performance of the control schemes for the grid side converter are, their steady state

and dynamic response characteristics, harmonic distortion of the output currents and the quality of power injected to the grid. Both switching frequency effects and the preexisting grid voltage distortion can contribute to poor power quality. Although current and voltage control schemes are possible, current control principle is used for its excellent dynamic characteristics.

The use of LCL filter between the inverter and the grid enhances the performance of the inverter but increases the complexity of the control scheme. LCL filter is a low pass filter, having improved harmonic performance at low switching frequency, which is a significant advantage at high power applications. However, the systems incorporating LCL filters are sensitive to grid voltage harmonics due to resonance. In the present research work the scheme used for regulating the grid current makes use of a synchronous frame PI controller. The reference grid currents in direct and quadrature axis are generated in a reference current calculating block, and synchronized to the grid voltage, with active and reactive power references as inputs (Erika Twinning et al. 2003, Miloan Prodanovic et al. 2003 and Monica Chinchilla et al. 2006). Figure 4.4 shows the three phase voltage source inverter system connected to the grid through LCL filter.

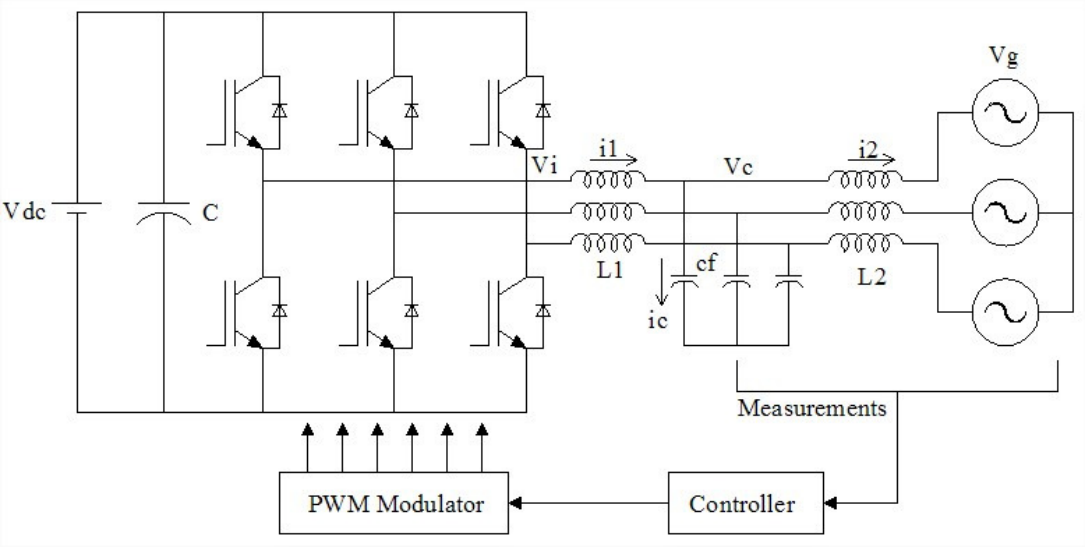

Figure Error! No text of specified style in document..**41 Three phase VSI connected to the grid through LCL filter.**

The voltage source inverter can be considered to be driven from a constant dc bus and connected to the grid through LCL filter. DC link voltage is maintained constant within reasonably good margin using the generator side converter. For the VSI system shown in figure 4.4 the relationship between the inverter output voltage V_i and the voltage at the filter capacitor terminal V_c can be expressed as in equation 4.14.

$$\begin{bmatrix} v_{ia} \\ v_{ib} \\ v_{ic} \end{bmatrix} = \begin{bmatrix} R_{1a} + L_{1a}p & 0 & 0 \\ 0 & R_{1b} + L_{1b}p & 0 \\ 0 & 0 & R_{1c} + L_{1c}p \end{bmatrix} \begin{bmatrix} i_{1a} \\ i_{1b} \\ i_{1c} \end{bmatrix} + \begin{bmatrix} v_{ca} \\ v_{cb} \\ v_{cc} \end{bmatrix} \quad \text{(Error! No}$$

text of specified style in document..**66)**

Relationship between i_1 the current through L_1, i_c the current through C_f, i_g the current through L_2 are given by equation 4.15.

$$\begin{aligned} i_{1a} - i_{ga} &= i_{ca} \\ i_{1b} - i_{gb} &= i_{cb} \\ i_{1c} - i_{gc} &= i_{cc} \end{aligned} \quad \text{(Error! No text of specified}$$

style in document..**67)**

i_{ca}, i_{cb} and i_{cc} are the currents through similar capacitors of a, b and c phases respectively. Voltages at the capacitor terminals for the three phases are given by equation 4.16.

$$\begin{aligned} v_{ca} &= \frac{1}{c_f}\int i_{ca}\,dt \\ v_{cb} &= \frac{1}{c_f}\int i_{cb}\,dt \\ v_{cc} &= \frac{1}{c_f}\int i_{cc}\,dt \end{aligned} \quad \text{(Error! No text of}$$

specified style in document..**68)**

The relationship between the grid voltage V_g and voltage at the filter capacitor terminal V_c can be expressed as in equation 4.17.

$$\begin{bmatrix} v_{ca} \\ v_{cb} \\ v_{cc} \end{bmatrix} = \begin{bmatrix} R_{2a} + L_{2a}p & 0 & 0 \\ 0 & R_{2b} + L_{2b}p & 0 \\ 0 & 0 & R_{2c} + L_{2c}p \end{bmatrix} \begin{bmatrix} i_{ga} \\ i_{gb} \\ i_{gc} \end{bmatrix} + \begin{bmatrix} v_{ga} \\ v_{gb} \\ v_{gc} \end{bmatrix}$$ (Error! No text

of specified style in document..**69)**

LCL filter and the grid are modeled based on the equations 4.14 - 4.17. Figure 4.5 represents the single phase equivalent representation of the inverter system with controller, filter and the grid connection where i_g* is the reference grid current signal, V_i is the voltage at the output terminals of the inverter, V_c is the voltage at the filter capacitor terminal, i_1 is the current through filter inductor L_1, i_c is the current through the filter capacitor, i_g is the grid current flowing through the filter inductor L_2 and V_g is the grid voltage.

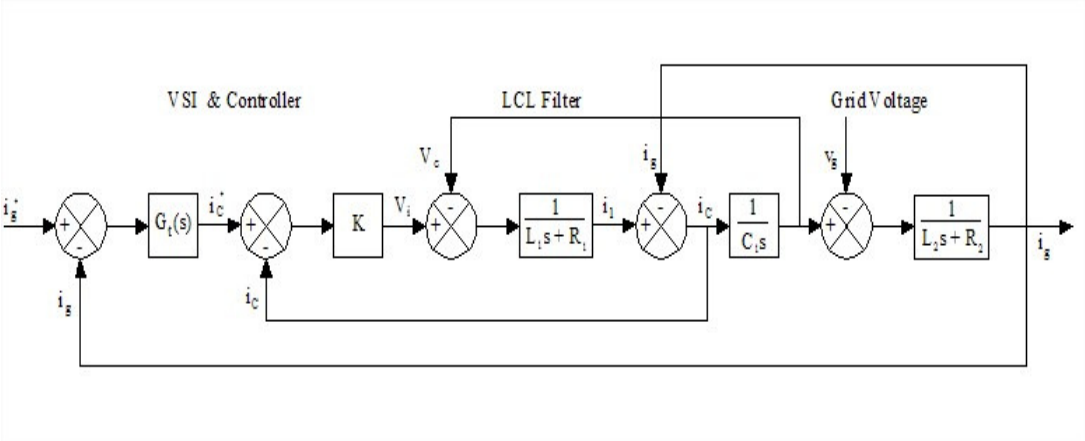

Figure Error! No text of specified style in document..**42 Single phase equivalent representation of the inverter system**

The measured three phase ac currents are transformed into dc components in a synchronously rotating frame with the intention that, the steady state error that is normally associated with the application of PI control to ac quantities can be eliminated. Also this has the advantage of controlling the real and reactive power independently. The reference grid currents in the direct and quadrature axis are obtained from the active and reactive power reference set points. The generation of

reference currents needs to be synchronized to the grid voltage. The active and reactive power reference in terms of direct and quadrature axis currents is given by equations 4.18 - 4.19.

$$P_{ref} = \frac{3}{2}\left(v_{dg}\ i_{dgref} + v_{qg}\ i_{qgref}\right)$$

(Error! No text of specified style in document..**70**)

$$Q_{ref} = \frac{3}{2}\left(v_{qg}\ i_{dgref} - v_{dg}\ i_{qgref}\right)$$

(Error! No text of specified style in document..**71**)

The direct and quadrature axis reference currents can be derived from equation 4.18 and 4.19 as given by equation 4.20 and 4.21.

$$i_{gdref} = \frac{2}{3}\frac{(P_{ref}V_{dg} + Q_{ref}V_{qg})}{({V_{dg}}^2 + {V_{qg}}^2)}$$

(Error! No text of specified style in document..**72**)

$$i_{gqref} = \frac{2}{3}\frac{(P_{ref}V_{qg} - Q_{ref}V_{dg})}{({V_{dg}}^2 + {V_{qg}}^2)}$$

(Error! No text of specified style in document..**73**)

V_{gd} and V_{gq} are the direct and quadrature axis components of the grid voltage and i_{gd} and i_{gq} are the direct and quadrature axis components of the grid current. These calculations are performed in reference current calculating block.

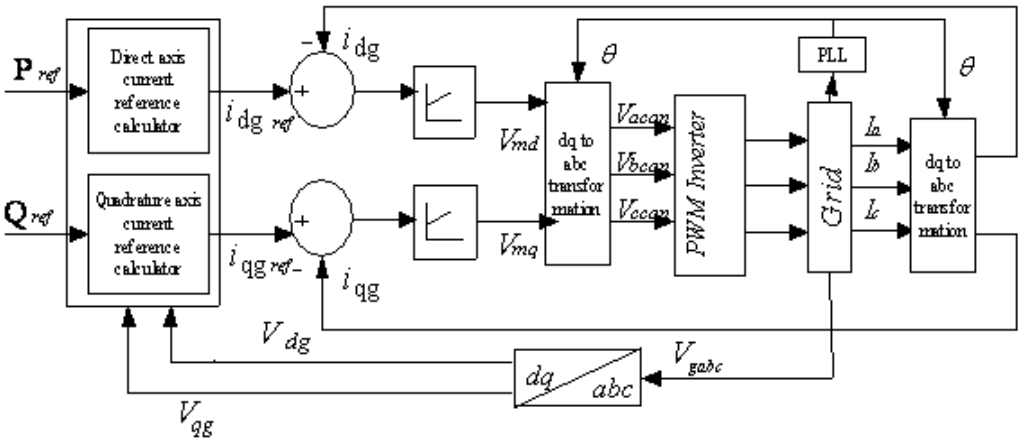

Figure Error! No text of specified style in document.**.43 Block diagram of the control strategy for grid side converter.**

Figure 4.6 shows the control strategy used for the generation of reference currents and PI control scheme for the control of active and reactive power flow into the grid. The controller is equipped with current controllers. Active power control is possible through the d axis component of grid current and the reactive power control through the q axis component of grid current. The d and q axis reference currents are calculated as per the equations 4.20 and 4.21 respectively in the calculating blocks. The three phase grid currents i_a, i_b and i_c are sensed and transformed to dq0 reference frame, rotating at electrical frequency of grid voltage. Synchronization of the reference frame to the grid voltage is achieved by PLL method. The control voltages for the three phases VSI are generated based on the errors in d axis and q axis currents through PI controllers. The PI controllers produce the control voltages for the inverter in d and q axis based on the equations 4.22.

$$V_{md} = K_{Ph} i_h + K_{ih} \int i_h dt$$

$$V_{mq} = K_{Pj} i_j + K_{ij} \int i_j dt \qquad \text{(Error! No text of specified style in document.**.74**)}$$

i_h and i_j are the errors in d axis and q axis grid currents, K_{ph}, K_{pj} are the proportional and K_{ih}, K_{ij} are the integral gains of the PI controllers. The voltages V_{md}, V_{mq} are then transformed into a b c coordinates to get control voltages V_{acon}, V_{bcon} and V_{ccon} for the PWM inverter. Reference value for the active power can be obtained through a maximum power tracking characteristic, however the model developed has the option of setting it at any suitable value. Reference value for the reactive power in this model is obtained through a voltage controller which will enable the unity power factor operation or can be set at any desired value.

Evaluation of controller performance under dynamic conditions

In order to evaluate the performance of the control scheme the model is examined under various operating conditions. Conditions include steady state, dynamic and transient state such as changes in input power, changes in the active and reactive power references, grid voltage disturbances and grid faults. In each case the grid

current distortion is evaluated and system performance is analyzed. DC link voltage is maintained constant at 800 V, minimum value of dc reference voltage is determined by the inverter output voltage as in equation 4.23.

$$V_{dcref} = 2\sqrt{2/3}V_{iline} \quad \text{(Error! No text of specified style in document..75)}$$

V_{iline} is the line to line voltage at the inverter output. The inverter is connected to a 440 V LV grid through a LCL filters; hence the output of the inverter is taken10% more than the grid voltage for the calculation of the reference for the dc link voltage.

Table 4.1 presents some of the cases considered to evaluate the performance of the controller for changes in the input power without any grid disturbance and fixed power references.

Table 4.1 Cases considered for evaluating the performance of controller for changes in the input

Case no	Action	Reason for considering the case
Case1	Axial velocity input to the turbine is held constant. Active and reactive power references are also held constant.	To assess the steady state response under steady input condition.
Case2	Axial velocity input to the turbine is changed in steps. Active and reactive power references are held constant.	To assess the dynamic response of the system for step change in the input condition.
Case3	Axial velocity input to the turbine is varying. Axial velocity of air swinging from zero to a maximum value and back to zero in a period of typically 4 -5 sec in a periodically repeated manner as a typical sinusoidal wave. Active and reactive power references are held constant with no grid disturbance.	To study the response under varying input condition.
Case 4	Actual wave pattern is applied as input to the model. Active and reactive power references are held constant, with no grid disturbance.	To study the response under real input condition.

Case1: To assess the steady state response under steady input condition, axial velocity input to the turbine is held constant. Active and reactive power references are also held constant with no grid disturbances. Figures 4.7 and 4.8 illustrate the response of the active and reactive powers following closely the respective references values. Response of the active and reactive powers is quite fast, response time is less than 1s. Figures 4.9 and 4.10 display the responses of the d axis and q axis components of the grid current respectively.

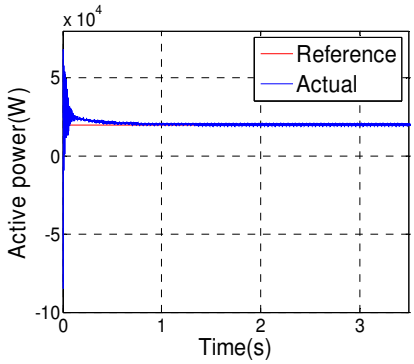

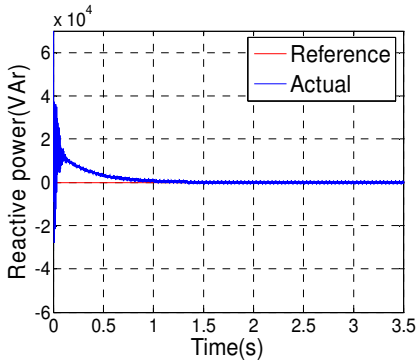

Figure Error! No text of specified style in document.**.44** **Active power response**

Figure Error! No text of specified style in document.**.45** **Reactive power response.**

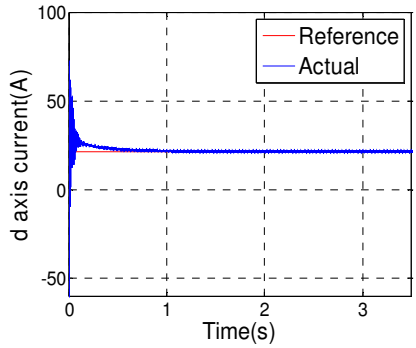

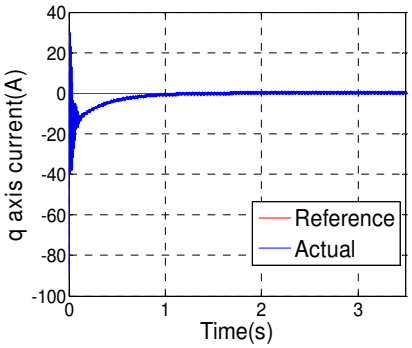

Figure Error! No text of specified style in document.**.46** **d- axis current response**

Figure Error! No text of specified style in document.**.47** **q- axis current response**

Figure 4.11 shows the response of the dc link voltage which is maintained constant at 800 V, ripple in the dc link voltage is about 1.25%, with a rise time of 0.021s. Figure 4.12 shows the grid current for one of the three phases. Figure 4.13 shows the grid

current and the grid voltage for one of the three phases with grid current scale multiplied by a factor of 20 for clarity. Figure 4.14 shows the THD of the grid current which is 2.55 % which implies high quality of current.

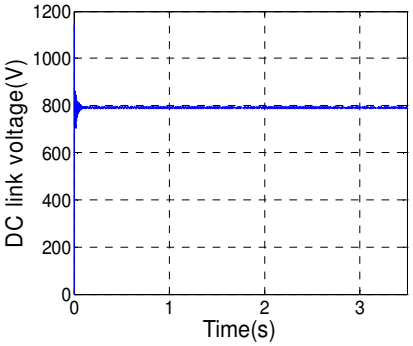

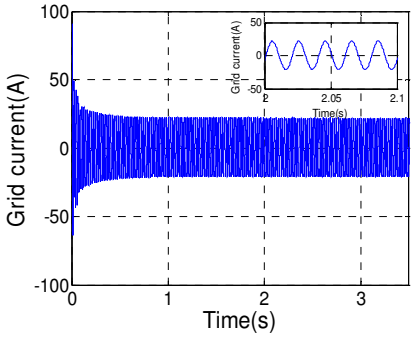

Figure Error! No text of specified style in document..**48** **DC link voltage response**

Figure Error! No text of specified style in document..**49** **Grid current response.**

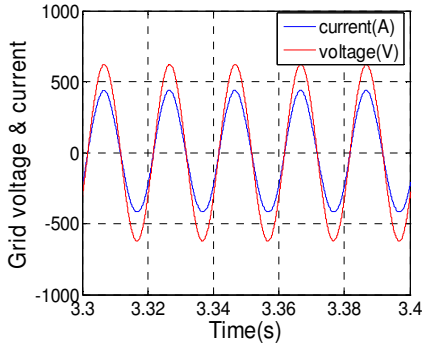

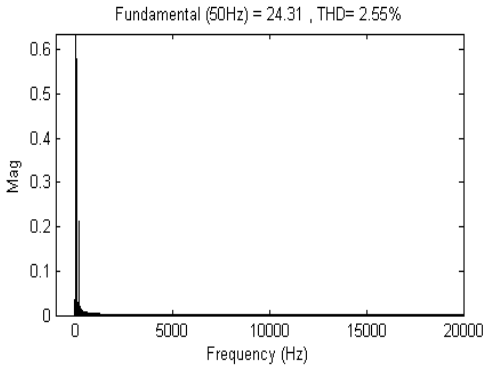

Figure Error! No text of specified style in document..**50** **Grid current and voltage response.**

Figure Error! No text of specified style in document..**51** **THD of the grid current**

Case 2: To assess the dynamic response of the system for step change in the input power, axial velocity input to the turbine is changed in steps with active and reactive power references held constant. Axial velocity is varied in steps as shown in figure 4.15. Figure 4.16 is the power generated for the input shown in figure 4.15. Reference for active power is set at 20 kW and the reference for the reactive power is set at zero. Figures 4.17 and 4.18 illustrate the response of the active and reactive powers following closely the respective references values which implies that average power

control has been achieved. Figure 4.19 shows the response of the dc link voltage which is maintained constant at 800 V, the ripple voltage decreases with lower value of axial velocity. Figure 4.20 shows the THD of grid current.

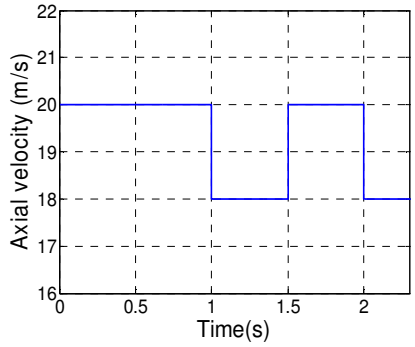

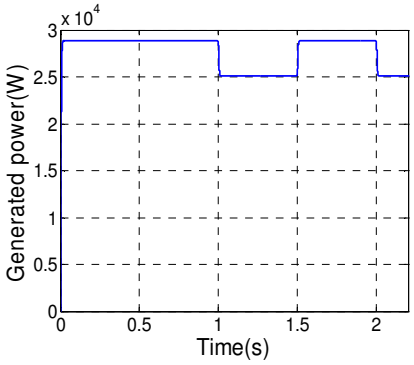

Figure Error! No text of specified style in document..**52** **Axial velocity**

Figure Error! No text of specified style in document..**53** **Power generated**

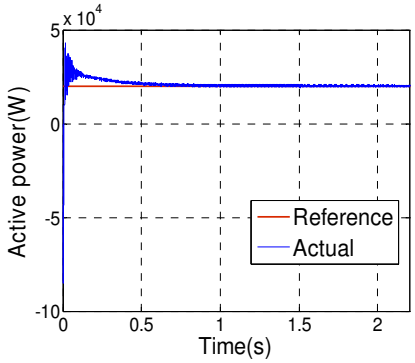

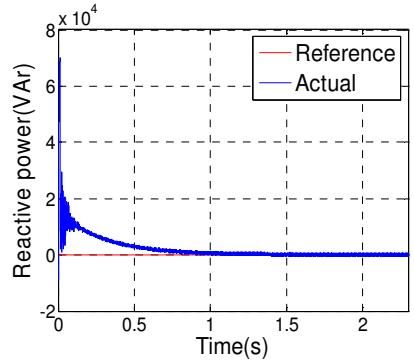

Figure Error! No text of specified style in document..**54** **Active power response**

Figure Error! No text of specified style in document..**55** **Reactive power response**

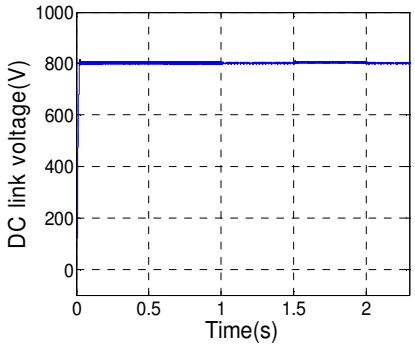

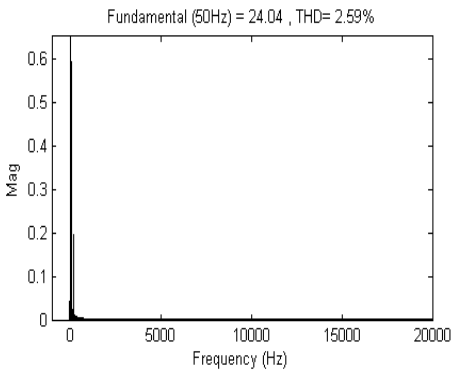

Figure Error! No text of specified style in document..**56** **DC link voltage response**

Figure Error! No text of specified style in document..**57** **THD of grid current**

It is seen from the results that the turbine power and generated power response is in accordance with the change in the axial velocity. Active and reactive powers follow the respective references; response time is less than 1s. THD of grid current and ripple in the dc link voltage are low as the previous case.

Case 3: In case of WECS in addition to statistical variation of air speed due to statistical variations of wave there is cyclical variation of air velocity due to bidirectional nature of air flow. Hence axial velocity of air swings from zero to a maximum value and back to zero in a period of typically 4 -5s in a periodically repeated manner. To study the response under varying input condition, model is applied with varying axial velocity as shown in figure 4.21. Active and reactive power references are held constant with no grid disturbance.

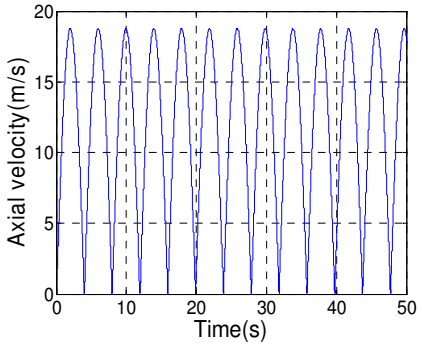

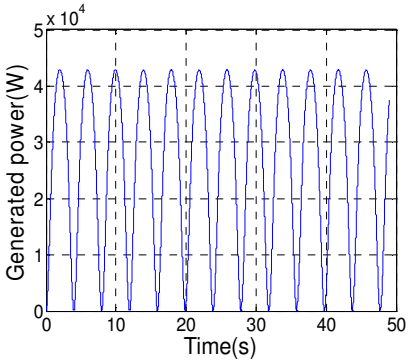

Figure Error! No text of specified style in document..**58** **Axial velocity**

Figure Error! No text of specified style in document..**59** **Power generated by PMSG**

Power generated by the permanent magnet synchronous generator for varying input conditions is shown in figure 4.22 which indicates that the power generated follows the axial velocity variations. DC link voltage response is shown in figure 4.23. Ripple of dc link voltage increases to about 4.5% with a response time of 20s. Although the power generated by the generator varies in accordance with variations in the axial velocity, the controller maintains the power fed to the grid at the reference value as shown in figures 4.24 and 4.25, response time of the active power increases to 5s and that of the reactive power to 7s, with initial spikes, but exhibits stable and fast

response. The grid current of one phase for the above condition is shown in figure 4.26. THD of the current is within the standards about 3.5%.

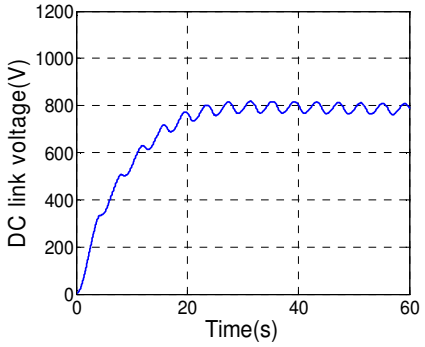

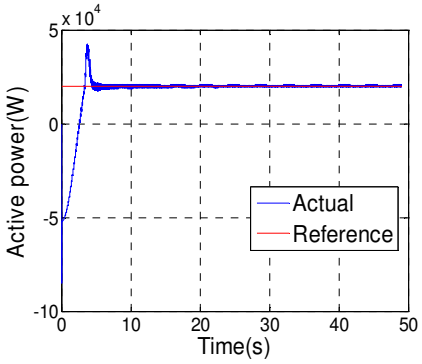

Figure Error! No text of specified style in document.**.60** **Response of dc link voltage**

Figure Error! No text of specified style in document.**.61** **Response of active power**

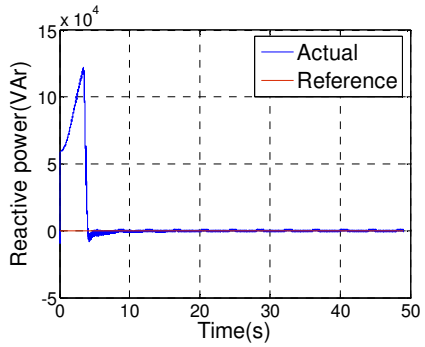

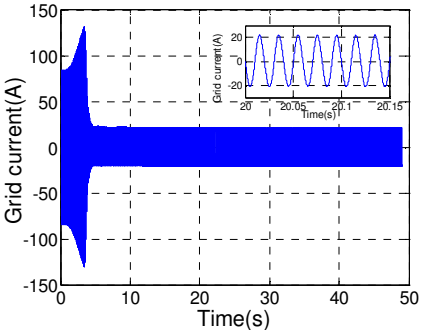

Figure Error! No text of specified style in document.**.62** **Response of reactive power**

Figure Error! No text of specified style in document.**.63** **Response of the grid current**

Case 4: To study the response under real input condition, actual wave pattern is applied as input to the OWC turbine model. Active and reactive power references are held constant, with no grid disturbance. Input to the turbine namely axial velocity is obtained from the OWC model. The OWC model is applied with the actual wave pattern as shown in figure 4.27. This pattern has a significant wave height of 1.005m and period of 16.733s. The variation of axial velocity from the OWC model is as shown in figure 4.28. Reference for active power is set at 20 kW and the reference for the reactive power is set at zero. Response of the active and reactive powers is shown in figure 4.29 which is stable without much disturbance and the response time is low. DC link voltage response is shown in figure 4.30. Ripple of dc link voltage is

increased further to 20% compared to case when the input wave pattern considered is sinusoidal as in case 3. Grid current harmonics increase to 4.3%. This is reflected in the power responses.

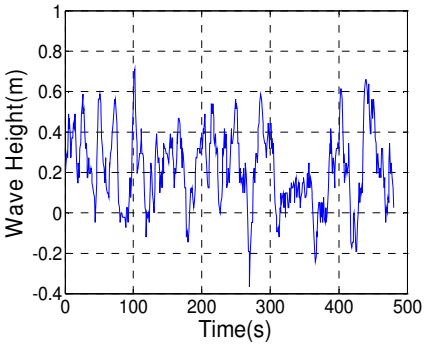

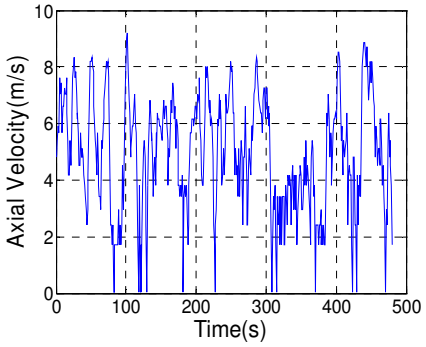

Figure Error! No text of specified style in document.**.64 Wave pattern**

Figure Error! No text of specified style in document.**.65 Axial velocity**

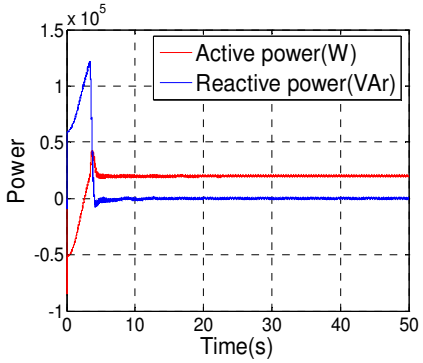

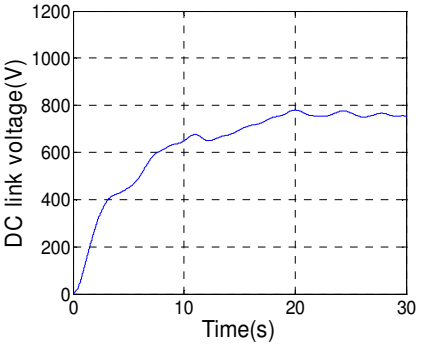

Figure Error! No text of specified style in document.**.66 Power response**

Figure Error! No text of specified style in document.**.67 DC link voltage response**

To study the dynamic response of the controller for changes in the power reference values, when the input to the turbine is held constant and with no grid disturbance, active power and reactive power references is changed in steps. Table 4.2 presents some of the cases considered to evaluate the performance of the controller for step changes in the power references.

Table 4.2 Cases considered for evaluating the performance of the controller for changes in the power references

Case no	Action	Reason for considering the case
Case 5	Axial velocity input to the turbine is held constant. With no grid disturbance, active power reference is changed in steps and the reactive power reference held constant.	To study the response of the controller for changes in the reference value for given constant input to the turbine.
Case 6	Axial velocity input to the turbine is held constant. With no grid disturbance, active power reference is held constant and the reactive power reference changed in steps.	To study the response of the controller for changes in the reference value for given constant input to the turbine.

Case 5: Input to the Wells turbine namely axial velocity is held constant. No grid disturbance is applied. Reference for active power is varied in steps and the reference for the reactive power is set at zero. Reference for the active power is set at 10 kW from zero to 1.5s, 20kW from 1.5 to 2.5s, 10 kW from 2.5 to 3.5s and 20Kw from 3.5s onwards. Figures 4.31 and 4.32 illustrate the instantaneous response of the active and reactive powers following closely the respective references values.

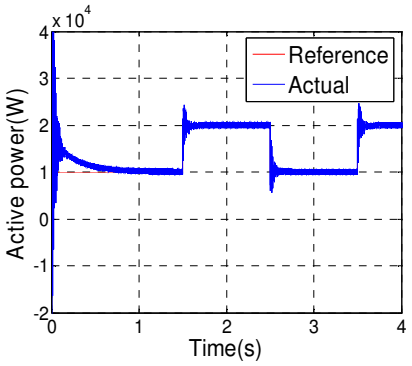

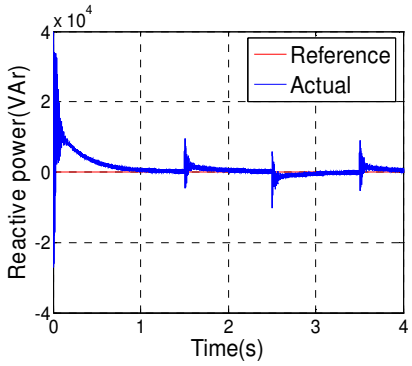

Figure Error! No text of specified style in document..**68** **Active power response**

FigureError! No text of specified style in document..**69** **Reactive power response**

Figures 4.33 and 4.34 show the response of the corresponding d axis and q axis components of the grid current. Figure 4.35 shows the response of the dc link voltage which is maintained constant at 800 V, ripple is quite low, rise time is 1s. Figure 4.36 shows the three phase grid current. The power control results have shown stable and

fast response of both active and reactive power demands. The power control transient response time is of the order of 0.1s. Calculated THD values show high quality grid current with THD of 2.1%.

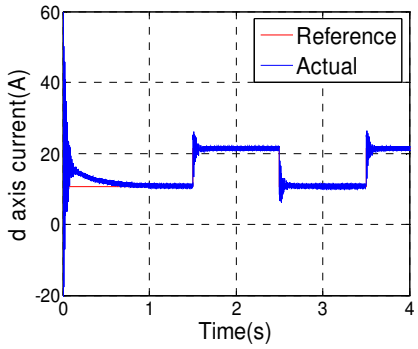

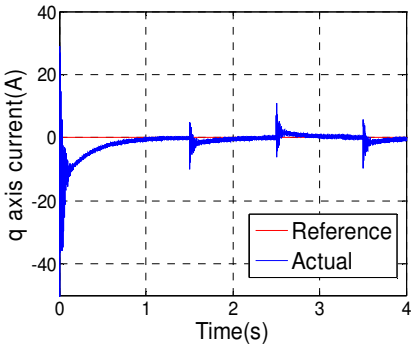

Figure Error! No text of specified style in document.**.70** **d axis current response**

Figure Error! No text of specified style in document.**.71** **q axis current response**

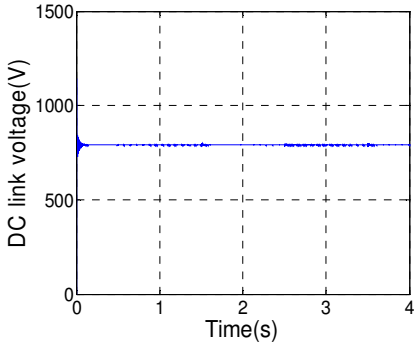

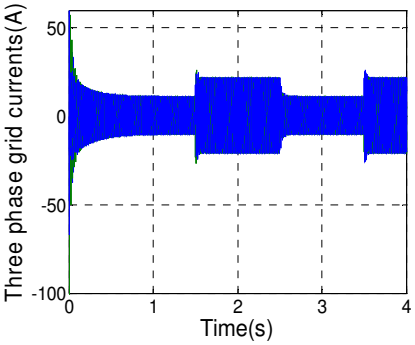

Figure Error! No text of specified style in document.**.72** **DC link voltage response**

Figure Error! No text of specified style in document.**.73** **Grid current response**

Case 6: The input to the turbine is maintained fixed and active power reference is set at 20 kW. The reference for reactive power is set initially at 0kVAr and changed to 10 kVAr lagging at 1s once the steady state is reached. Figure 4.37 illustrates the response of the reactive power following closely the respective reference value with dynamic response time of about 0.1s. The corresponding grid current and grid voltage is shown in figure 4.38 where the current scale is multiplied by a factor of 20 for the sake of clarity.

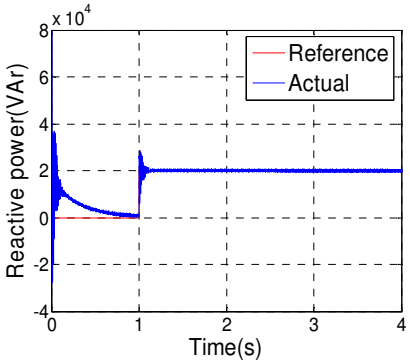

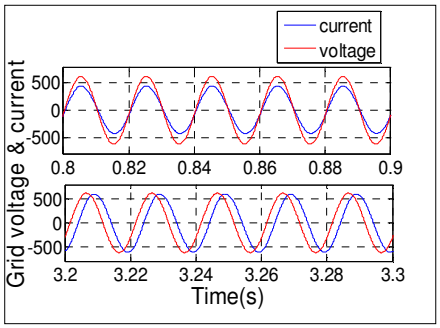

Figure Error! No text of specified style in document.**.74** **Reactive power response**

Figure Error! No text of specified style in document.**.75** **Grid voltage and current**

From the results presented it is found that the controller responds quickly for changes in the power reference values and delivers high quality current to the grid.

To assess the transient response of the controller under steady input condition, with active and reactive power references held constant, different grid faults and grid voltage and frequency disturbances are simulated. Table 4.3 presents some of the cases considered to evaluate the controller performance for grid disturbances and grid faults.

Table 4.3 Cases considered for evaluating the performance of the controller for grid disturbances

Case no	Action	Reason for considering the case
Case7	Axial velocity input to the turbine is held constant. Active and reactive power references are also held constant, single line to ground fault of the grid is imposed.	To study the response of the controller for disturbances in the grid voltage for given constant input to the turbine.
Case8	Axial velocity input to the turbine is held constant. Active and reactive power references are also held constant. Grid voltage sag 20% is imposed.	To study the response of the controller for disturbances in the grid voltage for given constant input to the turbine.
Case9	Axial velocity input to the turbine is held constant. Active and reactive power references are also held constant. Grid voltage frequency change of 4% is imposed, magnitude being constant.	To study the response of the controller for disturbances in the grid frequency for given constant input to the turbine.

Case 7: To analyze the response of the controller for single line to ground fault at the grid axial velocity input to the turbine is held constant, active and reactive power references are also held constant and single line to ground fault of the grid is simulated. Single line to ground fault is imposed at time 1.5s and the fault is cleared at

time 2 seconds. Figure 4.39 shows the response of the dc link voltage for a single line to ground fault, the link voltage oscillates during the fault by about 32%. Figures 4.40 and 4.41 illustrate the response of the active and reactive powers following closely the respective references values once the fault is cleared. During the fault, distortion in the grid current is high and these distortions are reflected in the active and reactive power responses. Figure 4.42 shows the response of the three phase grid current. Figure 4.43 shows the grid current of the faulted phase along with the voltage just before the fault and during the fault with current scale multiplied by a factor of 20 for clarity. Figure 4.44 shows the distorted three phase grid current during single line to ground fault.

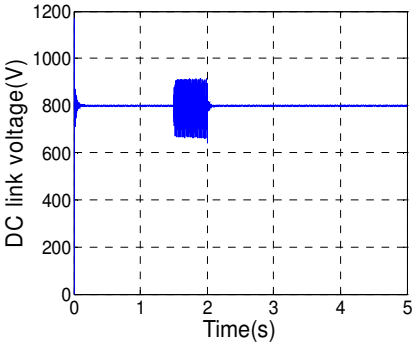

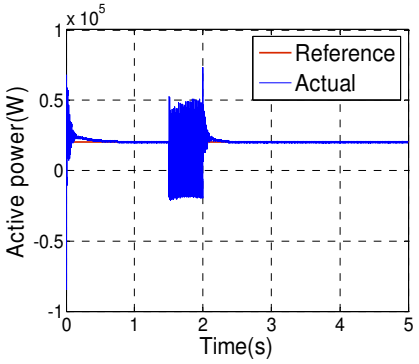

Figure Error! No text of specified style in document.**..76 Response of the dc link voltage**

Figure Error! No text of specified style in document.**..77 Active power response**

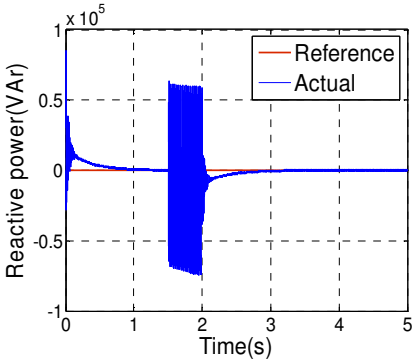

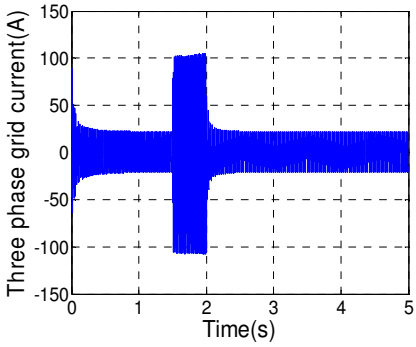

Figure Error! No text of specified style in document.**..78 Response of the reactive power**

Figure Error! No text of specified style in document.**..79 Grid current response**

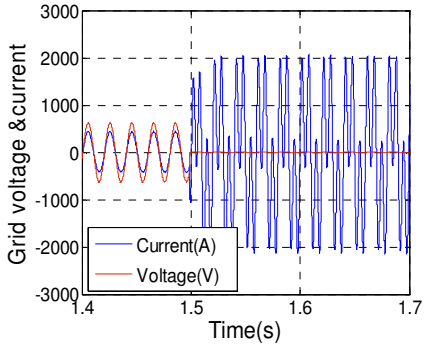

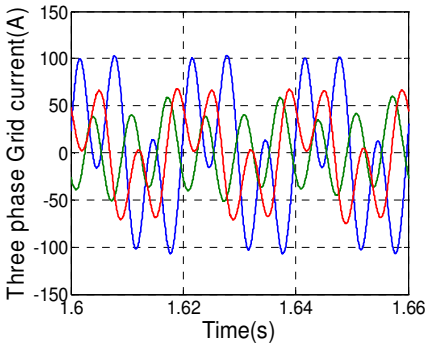

Figure Error! No text of specified style in document.**.80** **Grid current and voltage**

Figure Error! No text of specified style in document.**.81** **Distorted grid current**

From the results it is found that the grid current distortion increases during fault. Dc link voltage distortion increases by 32% during the fault, however response of the controller is fast and stable with active and reactive powers following the reference within 1 seconds of the fault being cleared.

Case 8: To study the response of the controller for disturbances in the grid voltage both symmetrical and unsymmetrical grid voltage sag of 20% is considered. Input to the Wells turbine namely axial velocity is held constant. Reference for active power is set at 20 kW and the reference for the reactive power is set at zero. Symmetrical voltage sag of 20% is imposed at time 2.2s and is cleared at time 3.2s. Figures 4.45 and 4.46 illustrate the response of the active and reactive powers following closely the respective reference values, which indicates that the studied system can stably be operated under grid voltage disturbance of 20%. Figure 4.47 shows the response of the dc link voltage for the above condition. Figure 4.48 shows the response of the three phase grid current. THD of the grid current with 20% symmetrical voltage sag is found 4.85% initially when the sag is applied and reduces to 2.10% within 0.6s. This is due to increase in all the harmonic components with significant increase in the third harmonic component from 0.03% to 2.16%. Figure 4.49 indicates that THD of grid current is 2.10%.

Grid current distortion increases when the grid voltage contains harmonics. This is shown figure 4.50 in where the grid voltage contains 5% third harmonic component.

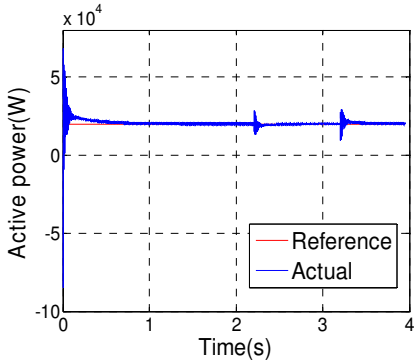

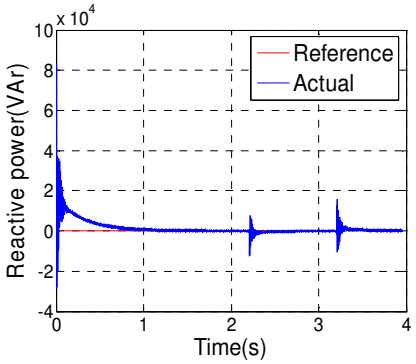

Figure Error! No text of specified style in document..**82** **Active power response**

Figure Error! No text of specified style in document..**83** **Reactive power response**

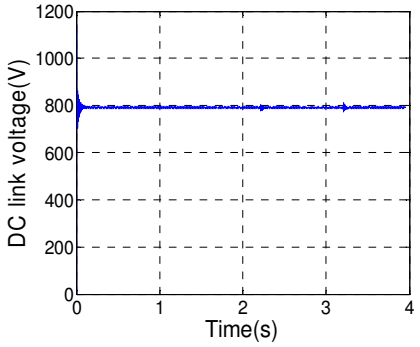

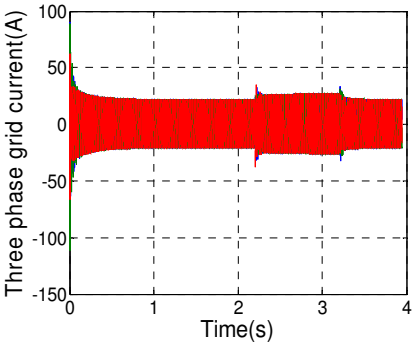

Figure Error! No text of specified style in document..**84** **Response of the dc link voltage**

Figure Error! No text of specified style in document..**85** **Grid current response**

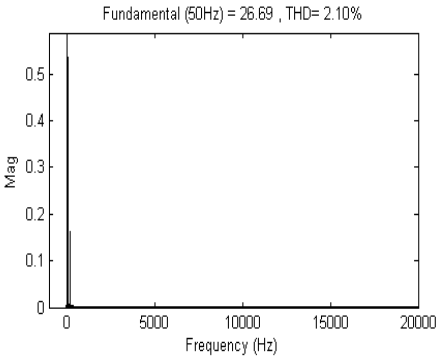

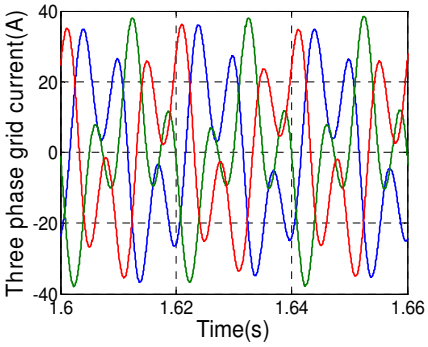

Figure Error! No text of specified style in document..**86** **THD of grid current**

Figure Error! No text of specified style in document..**87** **Distorted grid current**

From the results presented it is found that the THD of the grid current with symmetrical and unsymmetrical voltage sag is found to be within 5%. In both cases power response is quick and stable.

Case 9: To study the response of the controller for disturbances in the grid frequency grid voltage frequency change of 4% is imposed with constant magnitude. Input to turbine namely axial velocity is held constant. Reference for active power is set at 20 kW and the reference for the reactive power is set at zero. A dip in the frequency by 4% is imposed at time 2.2s and is cleared at time 3.2s. Figures 4.51 and 4.52 illustrate the response of the active and reactive powers following closely the respective references values once the frequency disturbance is cleared. Figure 4.53 shows the response of the dc link voltage for the above condition. Figure 4.54 shows the response of the three phase grid current. THD of the grid current rises to 15.25% at the instant of the disturbance, but reduces to 2.73% as shown in figure 4.55 within 0.5s.

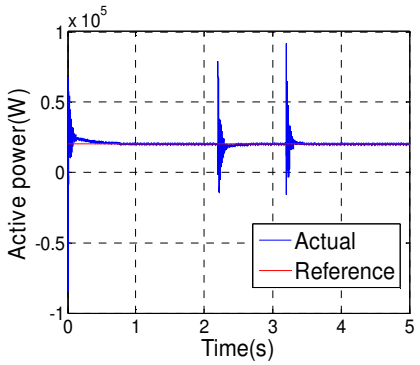

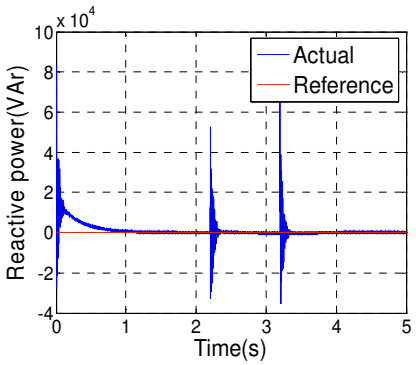

Figure Error! No text of specified style in document.**.88** **Response of the active power**

Figure Error! No text of specified style in document.**.89** **Reactive power response**

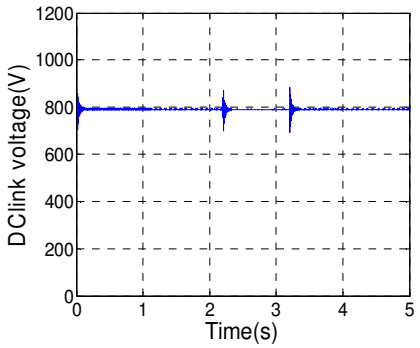

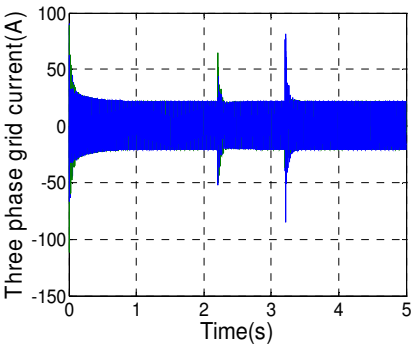

Figure Error! No text of specified style in document.**.90** **DC link voltage response**

Figure Error! No text of specified style in document.**.91** **Grid current response**

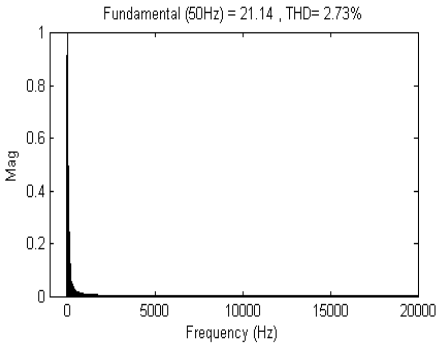

Figure Error! No text of specified style in document.**.92** **THD of grid current**

DC link voltage oscillates by about 25% at the instant of frequency change by 4%, oscillations damps out in 0.2s. This is also reflected in the active and reactive power responses and grid current response. From the results it can be concluded that the controller is able to bring the system to the normal condition for changes in the frequency within a short time of 0.2s which indicates that the studied system can stably be operated under grid voltage frequency disturbance without much effect on the power response characteristics and the power quality.

Results and discussion

From the results under different operating conditions it is observed that the control scheme provides a good response in terms of power quality and power control. Under unsymmetrical unbalance of the grid voltage and under fault conditions the distortion in the grid current increases significantly. However power control results indicate stable characteristics, capable of bringing back the system to the normal quickly once the fault is cleared and a fast response. Hence it can be concluded that studied model with the proposed controller provides overall average power control under steady state and transient conditions. Next chapter deals with the development of wave turbine emulator in the laboratory and studies on the PMSG coupled to the emulator developed.

CHAPTER 5
DEVELOPMENT OF WAVE TURBINE EMULATOR

INTRODUCTION

Wave Turbine Emulator (WTE) is an important equipment for developing the WECS. The Emulator reflects the actual behavior of the wave turbine without reliance on natural wave resources and actual wave turbine. It offers a controllable test environment that allows the evaluation and improvement of control schemes for electric generators which is hard to achieve with an actual wave turbine. The WTE can accurately reproduce the characteristics of real wave turbine. The Emulator can be used for research applications to drive an electrical generator in a similar way as a practical wave turbine. General structure of a WTE consists of a personal computer (PC) where the characteristics of the turbine are implemented, dc or ac drive to

emulate the turbine rotor, feedback mechanism from the drive and power electronic equipment to control the drive. The feedback signal is generally acquired by the PC through an A/D converter and the signal for driving the power electronic device comes from the PC through a D/A converter. This chapter presents the development of WTE.

Review of turbine emulators

Emulator is fundamentally a demonstration of a practical turbine in the laboratory environment. A number of wind turbine Emulators have been presented in the literature. Emulator can be used for development and research applications to drive electric generators by reproducing the torque or speed developed by the real turbine for different input conditions. It allows the testing without construction of costly turbine and help in determining the strength and weakness of energy conversion scheme and the related control technologies. Emulator can be used to drive different kinds of electric generators like Induction generator, DFIG and the PMSG and their performance can be evaluated easily (Bunlung et al. 2007, Hossein et al. 2004). Emulator should basically mimic the actual turbine characteristics showing the same mechanical behavior of the actual turbine rotor along with generator it is driving under dynamic conditions. There have been studies on wind turbine emulators based on dc motor, induction motor, permanent magnet synchronous motor (PMSM) and permanent magnet dc motor.

Wind turbine emulator based on a DSP system and a separately excited dc motor that can be used in research activities of wind turbine control in a controllable experimental platform without reliance on natural wind resources and actual wind turbines is proposed by several authors in the literature (Arifujjaman et al. 2006, Arifujjaman et al. 2008, Mohammad et al. 2008, Battaiotto et al. 1996, Luiz et al. 2005, Wozniak et al. 1991). A laboratory set up to be used as wind turbine emulator consisting of a real time control program and a commercial dc drive is presented by (Chinchilla et al. 2004). Modeling and design for a wind turbine generation control system using doubly fed induction machine and DSP based experimental setup is proposed by (Rebelo et al. 2004). However there have been no reports of development of wave turbine emulators. A solid state wave energy emulator for two rectifier

topologies have been proposed for extracting power from direct drive wave energy converters by Nei and others (Nei Z et al. 2008).

Realization of wave turbine emulator

A Wave turbine Emulator (WTE) developed in the present work is a configuration that simulates the practical behavior of the wave turbine in laboratory environment. The actual system to be emulated consists of OWC with Wells turbine is as shown in the figure 5.1. In order to develop WTE, model of the system is first implemented in MATLAB and its characteristics are studied. Input to the model is the actual wave pattern, which is the variation of wave height with time and its outputs are the turbine torque and the speed. The model is applied with several wave patterns of different wave height and period. From the speed characteristics it is observed that the maximum speed is in the range 800 to 1200 rpm for wave patterns with significant wave height in the range 0.8 to 2.5 m and period in the range 10-30 seconds.

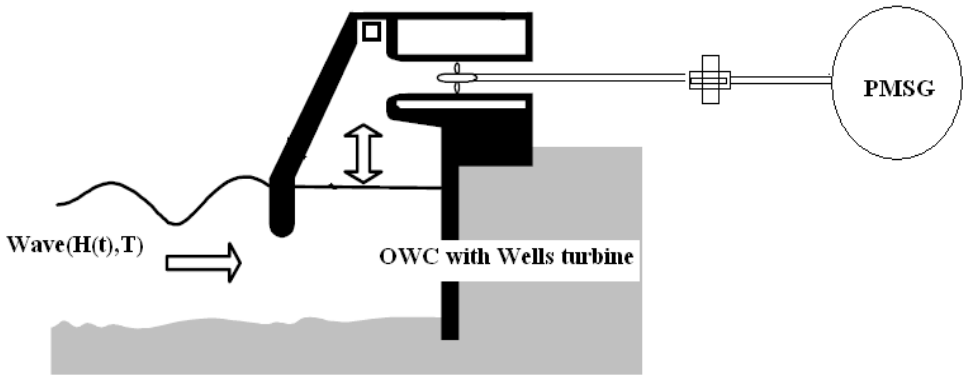

Figure Error! No text of specified style in document.**.93** **System to be emulated**

Acceleration during start up is as high as 3500 rpm/s and rise time is of the order of 1 to 2 s. Maximum acceleration and deceleration at steady state is 110rpm/s and 25rpm/s. For a particular wave pattern for 500s shown in figure 5.2 corresponding to group of wave data 4, with significant wave height 1.0050 m and period of 16.7333s the variation of speed from the model is shown below in figure 5.3.

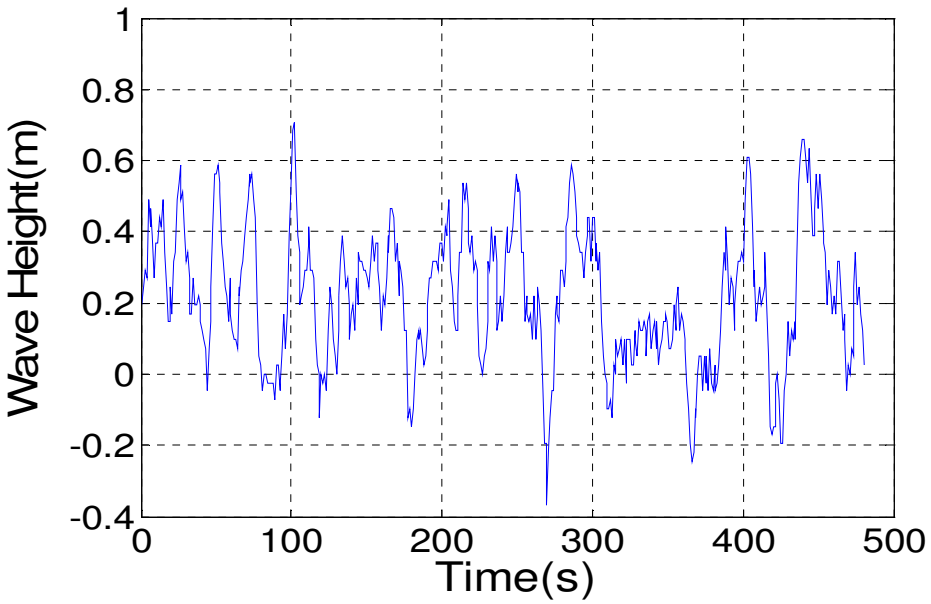

Figure Error! No text of specified style in document.**.94** **Wave pattern**

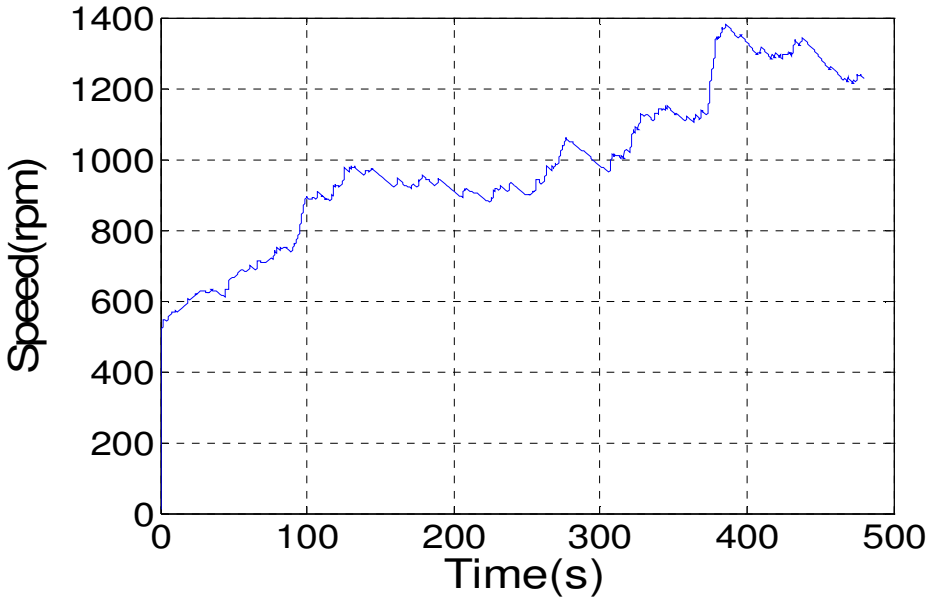

Figure Error! No text of specified style in document.**.95** **Turbine speed**

The emulator developed should be able to track the speed characteristics. In general speed to be traced is not a fixed reference value but varies in accordance with the variation of the wave pattern and therefore the control strategy needed is different

from the common control of regulating speed in closed loop, rather a velocity controller is required.

In order to realize the wave turbine rotor different types of machines can be used. Both induction machines and dc motors have been used to develop wind turbine emulators. However PMSM would be ideal in terms of power quality, inertia, impulse torque and speed response. PMSM have an impulse torque two orders of magnitude larger than that of a dc servomotor and have greater power density than dc machines and induction machines. Therefore for the emulator developed, a PMSM is used to reproduce the dynamics of the speed of the turbine.

General form of the emulator consists of a PMSM with VSC controller as a drive. Control commands to VSC controller is supplied through serial communication port of PC and control inputs are fed through analog output card functioning as daughter board in PCI slot of PC. These control inputs are obtained from the model of the system to be emulated and the characteristics of the wave turbine simulated.

The speed control of PMSM is to be performed equivalent to that of the dc motor by a decoupling control, which is also known as field oriented control or vector control. The purpose of speed controller is to take a signal representing the demanded speed, and to drive the motor at that speed. The design of speed controller is essential in emulating desired transient and steady state characteristics of turbine under consideration. The speed controller calculates the difference between the reference speed and the actual speed producing an error, which is fed to the PI controller. This generates the torque command which is processed either in the constant torque controller or in the flux weakening controller depending on the mode of operation. For operation up to rated speed, the controller will operate in constant torque region and for the speeds above rated speed the controller will operate in flux-weakening region. The outputs of these controllers are stator current command and torque angle command. These, together with electrical rotor position provide phase current commands. These commands along with current feedback control are used in realizing PWM current control scheme of VSC. PMSM position and speed are to be sensed through an encoder and the required signals from the voltage and current sensors are to be processed using A/D board. The connection of computer and controller hardware can be established using RS232 serial interface.

Selection of drive system

To achieve the above job the Rexroth IndraDrive with drive controller CHS 0.1.1C and Rexroth Indradyn synchronous motor can be used (Rexroth IndraDrive C drive controllers manual). IndraDrive firmware supports drive control both in open-loop and closed-loop operation. In the closed loop control, the drive controller has a cascade structure, i.e. the individual loops (position, velocity and torque or current) are connected into one another as shown in the figure 5.4. Depending on the operating mode there are different control loop structures with different points of input and paths of the command values. Based on the selection of active operating mode it is possible to close the torque control loop, the torque and velocity control loop or additionally the position control loop in the drive. The velocity and position control loops are closed by means of the encoder feedback. Motor control is achieved by field-oriented closed-loop current control. The velocity control mode is used as it is suitable for the above application. In the velocity control mode an external velocity command value can be preset via analog inputs or master communication interface.

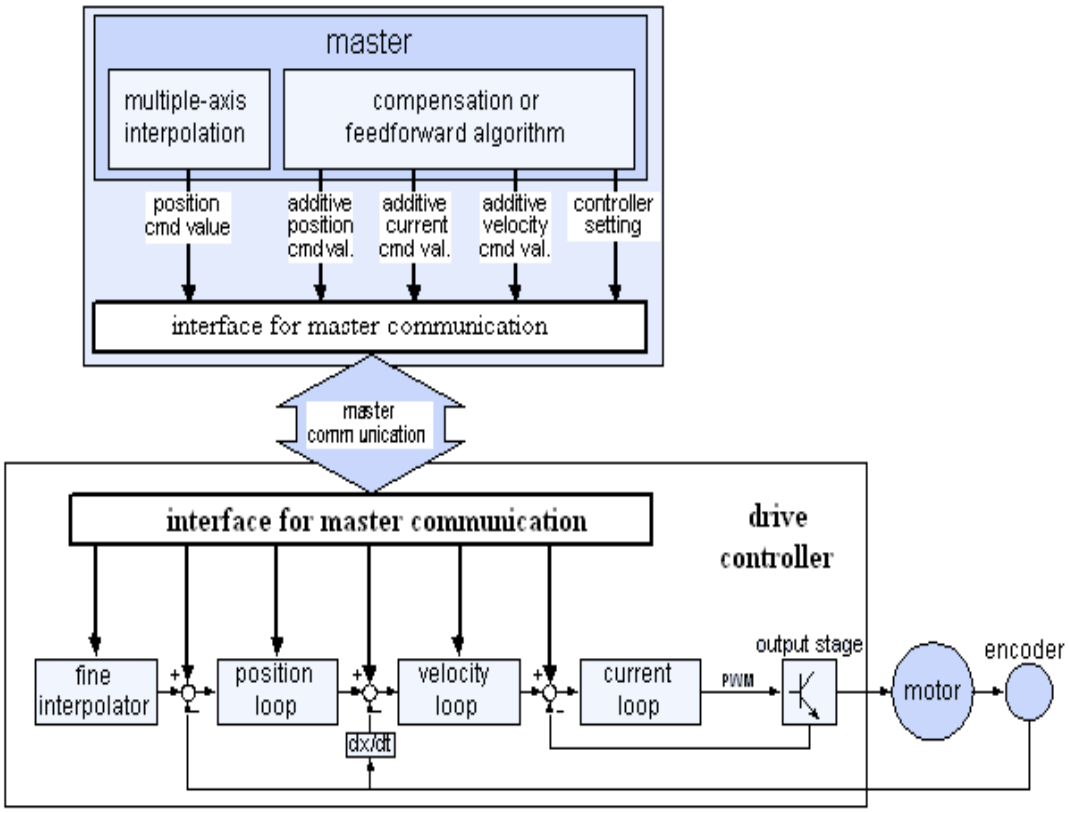

Figure Error! No text of specified style in document.**.96 Closed loop structure of the controller**

Velocity control is achieved through a digital PI loop with extensive filter measures and has the option of smoothing of velocity control loop difference through filter that can be parameterized. Velocity control loop monitoring is accessible to prevent the drive from running away. Velocity loop internally generates the torque/force command value to which additive torque/force command value can be added as an additive component. It also has the option of selecting predefined and internally stored velocity command value steps through digital inputs, window comparator for masking critical velocity ranges in the command value channel, ramp generator with separately adjustable two-stage acceleration and deceleration limits of the preset velocity command value. There is a feature to limit the acceleration and deceleration of the velocity command value in steps by means of two ramps whose parameter values can be entered by the user suitably. This allows parameterising of different

ramps for the acceleration and braking process. There is also a parameter called velocity command filter used to round acceleration jumps in the velocity command value characteristics in order to have a smooth initialization or deceleration of the drive in velocity control mode. The limited command value available at the output of command value processing can be adjusted, by means of linear fine interpolation, for further processing in the velocity loop. With field oriented closed-loop current control, the internal control task provides closed loop control of the motor current according to the principle of field orientation, i.e. separate closed-loop control of the torque-generating current and the flux-generating current. It also offers compensation for the cross coupling of the d and q axes to increase dynamics and voltage loop for operation in the field weakening range. The switching frequency of the output stage can be set in the range 4 to 16 kHz. The minimum possible controller cycle time of the velocity loop depends on the available control section and on switching frequency of the power output stage. Higher the switching frequency selected, shorter is the cycle time. Cycle time for velocity loop can be adjusted in the range 250- 125μs and for the current loop 62.5-125μs.

With such authoritative, adoptable controllers of the IndraDrive it is possible to control both synchronous motors and asynchronous motors. Further, the IndraDrive controllers can be adjusted to the motor to be controlled by providing or inputting the motor-specific data. In the case of Rexroth motors this can be done without any problem because the manufacturer provides a specific data set for adjusting each motor type. The data are documented by the manufacturer as parameter values, stored and made available in motor-specific parameters. With the firmware available for the controller, synchronous motors can be operated in the entire speed range, including field weakening. This includes base speed range for constant torque, field weakening range for constant power and field weakening range for power limit range. Indradyn motors are characterized by dynamics, compact construction, a high torque density and an extremely high degree of precision due to new optical encoder systems. Optical encoder has an accuracy of ± 80 angular seconds. The motor used has a speed range of 4500rpm, with rotor moment of inertia of 0.002910 kg m^2.

For synchronous motors, the field-oriented closed-loop current control of the controller has additional features of limitation of the I_q command value at the voltage

limit for protection against too little control margin, utilization of the reluctance effect to increase the available torque in the basic speed range and support of synchronous motors with reluctance torque, i.e. motors with significantly different inductances in the d and q axes. In view of all the above, Rexroth Indradyn three phase synchronous motor driven by Rexroth IndraDrive controller is used for the implementation of the turbine emulator. Further details of Rexroth IndraDrive controller and the Rexroth Indradyn motor is given in Appendix II.

Selection of data acquisition card

From the OWC-turbine model built in MATLAB, speed data has to be acquired. Keithley data acquisition card KPCI 3102 is used for this purpose as it is compatible with MATLAB data acquisition toolbox. MATLAB, toolboxes are comprehensive collections of MATLAB functions (M-files) that extend the MATLAB environment to solve particular classes of problems. The data acquisition toolbox is a collection of M-file functions and MEX-files, the dynamic link libraries (DLLs) built on MATLAB® environment. The toolbox provides with a framework for bringing live, measured data into MATLAB using PC-compatible, plug-in data acquisition hardware as shown in figure 5.5. Keithley adaptor is the critical interface that enables the data acquisition toolbox to communicate with DriverLINX device drivers for Keithley data acquisition boards. Data acquisition toolbox supports most Keithley data acquisition boards with 32-bit Driver LINX drivers. DriverLINX has to be properly loaded first in order to use the hardware. The Keithley KPCI-3102 data acquisition card is used in this work to send or receive data to or from the emulator hardware. KPCI-3102 is provided with external peripheral STA-300 screw terminal panel. On this panel three 8 bit digital output ports and 16 channel analog input ports are provided. The digital I/O port of KPCI-3102 has sampling rate of 3 mega samples per second; whereas the analog port has maximum sampling frequency of 225 kHz. Internal architecture of the Keithley data acquisition card is shown in figure 5.6 and additional details are included in Appendix III.

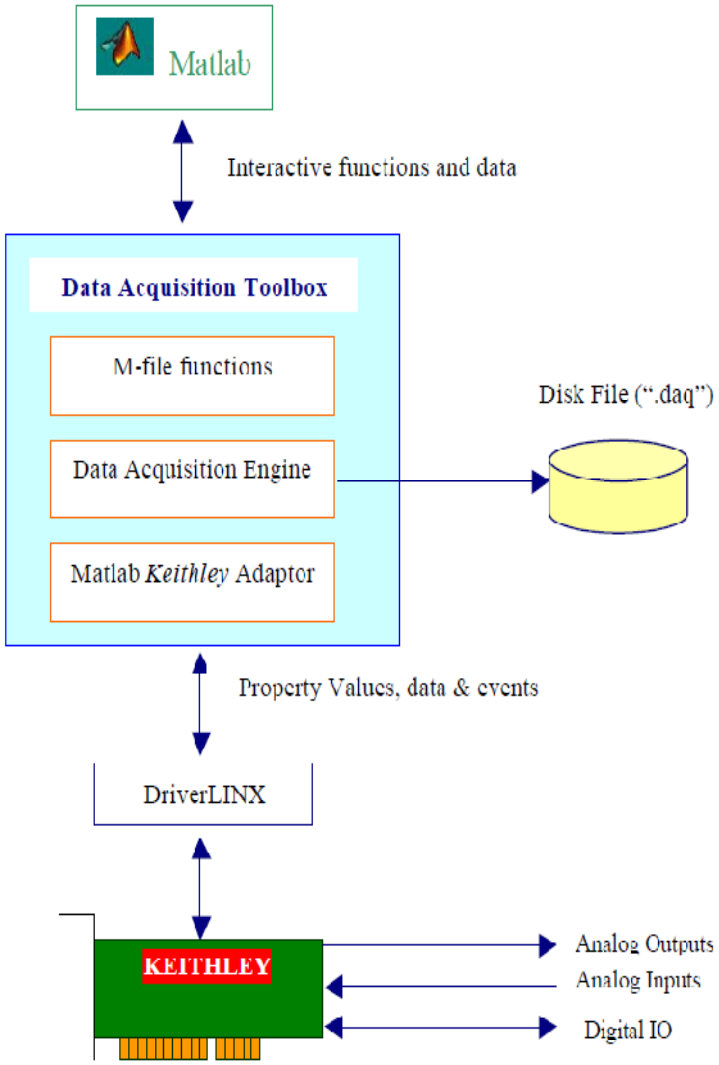

Figure Error! No text of specified style in document..**97 Using Matlab with Data Acquisition Toolbox & Keithley boards.**

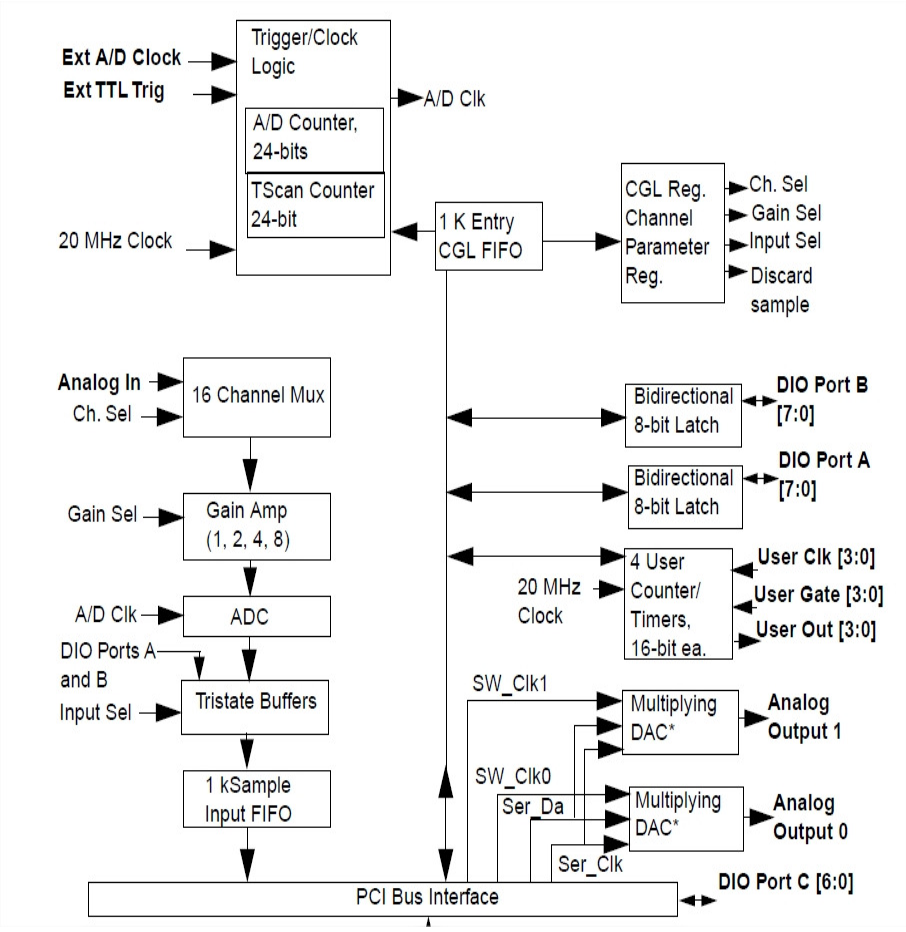

Figure Error! No text of specified style in document.**.98** **Architecture of data acquisition card**

Digital to analog converter

The digital signal from the digital I/O port of Keithley data acquisition card is converted into analog signal using DAC 813 digital to analog converter. The DAC 813 is a complete monolithic 12-bit digital to- analog converter with a flexible digital interface. It includes a precision +10V reference, interface control logic, double-buffered latch and a 12-bit D/A converter with voltage output operational amplifier. Fast current switches and laser-trimmed thin-film resistors provide a highly accurate, fast D/A converter. Figure 5.7 shows circuit diagram of DAC card. Further details of the DAC 813 IC and circuit design are included in the Appendix IV.

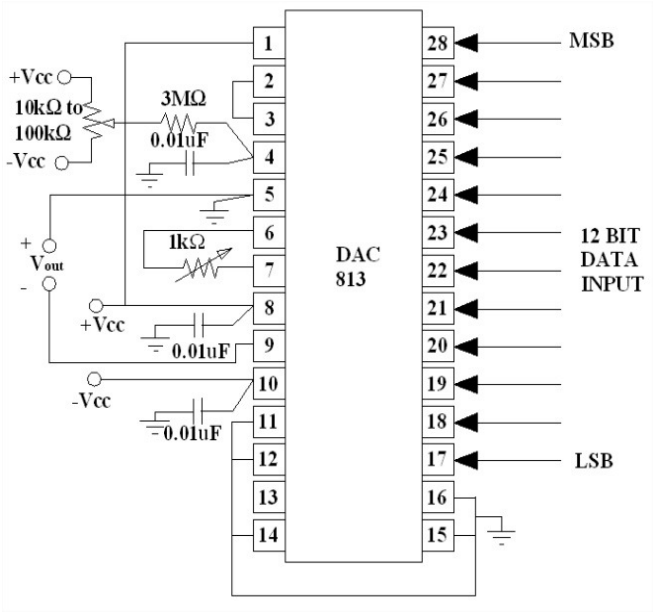

Figure Error! No text of specified style in document.**.99 DAC Circuit**

The block diagram of the developed wave turbine emulator is shown in figure 5.8.

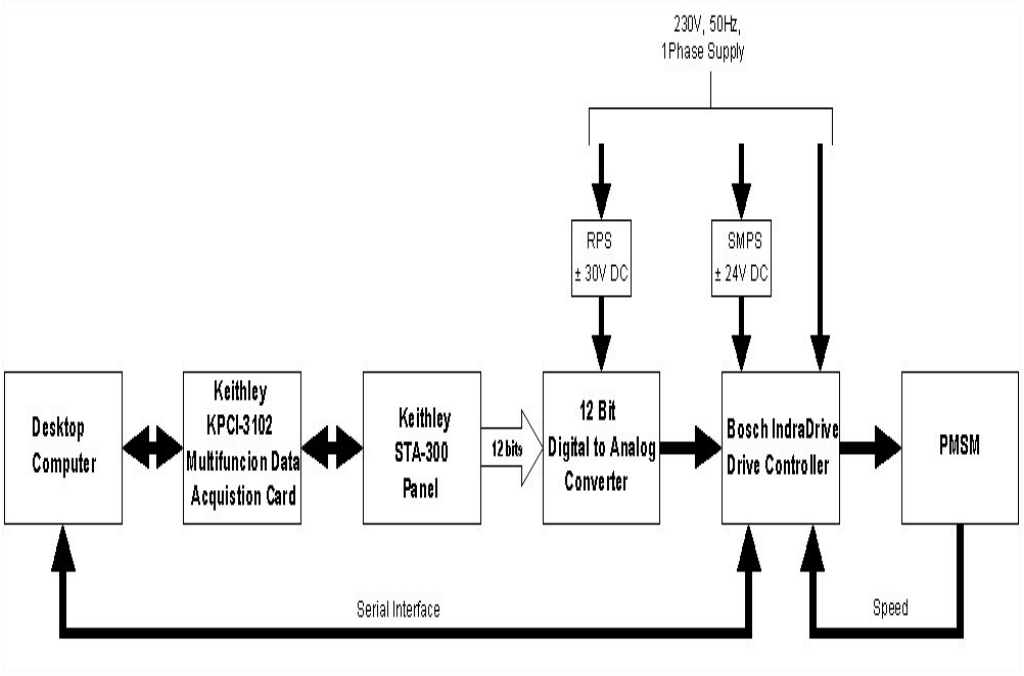

Figure Error! No text of specified style in document.**.100 Block Diagram of Wave Turbine Emulator.**

Laboratory implementation of wave turbine emulator:

The overall schematic of the wave turbine emulator showing both software and hardware component is shown in figure 5.9. Software part comprises of model of OWC, Wells Turbine model and PMSG model. Modeling of OWC and the Wells turbine are presented in chapter 2. Modeling of the PMSG is explained in detail in chapter 3. For the hardware implementation three phase PMSM driven by Rexroth IndraDrive Controller, is used along with data acquisition card and digital to analog converter.

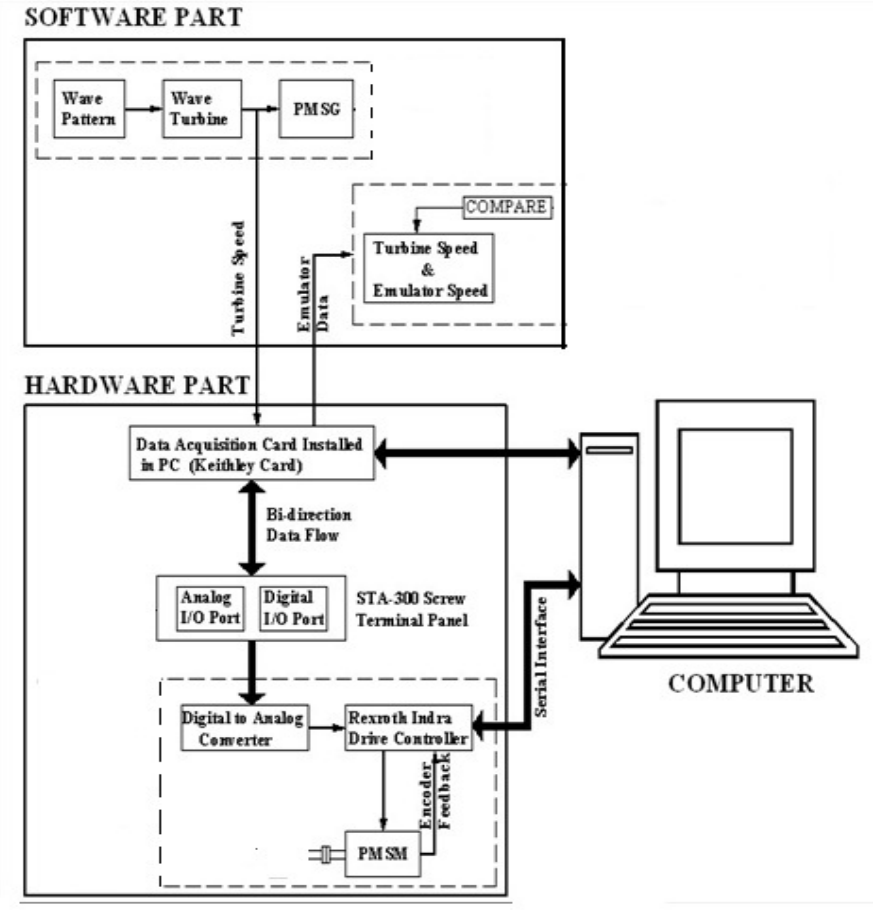

Figure Error! No text of specified style in document.**.101 Structure of Wave Turbine Emulator**

A Photograph of Wave Turbine Emulator implemented in the laboratory as shown in 5.10.

Figure Error! No text of specified style in document..**102 Laboratory setup of wave Turbine Emulator**

Waves are characterized based on spectral analysis to differentiate different wave pattern data and then to be able to explain the behavior of the emulator developed based on wave pattern. The Oscillating water column is modeled based on Energy balance concept. The measured data of wave height obtained from the Indian wave energy plant located at Vishinjam in Kerala coast is given as input to the OWC model. The output of OWC model is the axial velocity for a particular wave pattern which is given as input to the wave turbine model. The speed data from the turbine model is transferred to digital I/O port of data acquisition card which is used as an interface between Matlab and the controller. The data acquisition card is installed in PCI slot of the computer. The acquired data is given to STA-300 screw terminal panel which gives an 8-bit digital data. The digital and analog ports of the data acquisition card are first calibrated. The procedure of calibrating the data acquisition card is given in Appendix III. These digital and analog ports are then programmed through Matlab code to receive or send the data. The digital data is then converted to analog voltage signal using 12 bit DAC Circuit. This analog voltage signal ranging 0-10V is given as

input to the control section of the controller which drives the 3-phase PMSM. Since the maximum input voltage to the analog channel is limited to 10V, scaling factor is used with the aid of Indraworks engineering software.

From the laboratory setup of wave turbine emulator speed data is extracted by means of optical encoder. The speed data is then transferred to the PC through RS232 cable and then compared with the speed of the turbine from the WEC model. Comparison is done for the different types of wave patterns to assess the behavior of the wave turbine emulator. The Speed of synchronous motor is controlled in the same manner as the turbine model for different wave pattern inputs and hence the whole assembly will replicate the speed characteristics of the actual wave turbine.

Response of the emulator developed

The response of the Emulator is tested for different cases of wave pattern in comparison with the model are presented in the figures 5.11-5.13 and the statistics are given in the table 5.1.

Case 1: Input to the WEC model is the wave pattern corresponding to the group of wave data 1 which has significant wave height of 1.9189m, time period 36.48s and wave power of 316.8kW. Figure 5.11 shows speed response of wave turbine emulator and the model.

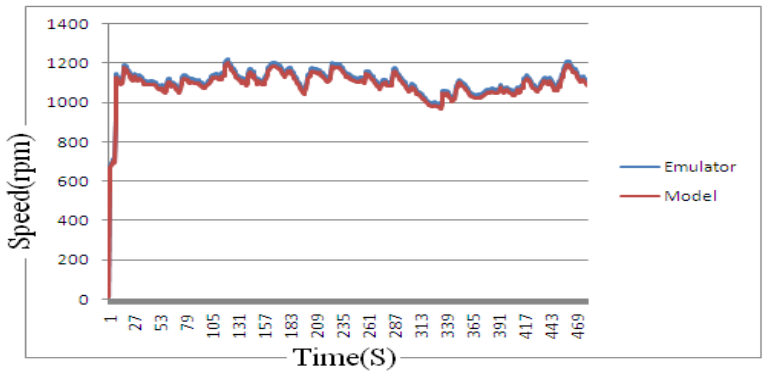

Figure Error! No text of specified style in document.**.103 Comparison of the Speed for wave data 1**

Case 2: Input to the WEC model is the wave pattern corresponding to the group of wave data 2 which has significant height of 1.9562 m, significant time period 19.025 s

and wave power of 212.9 kW. Figure 5.12 shows speed response of wave turbine emulator and WEC system model.

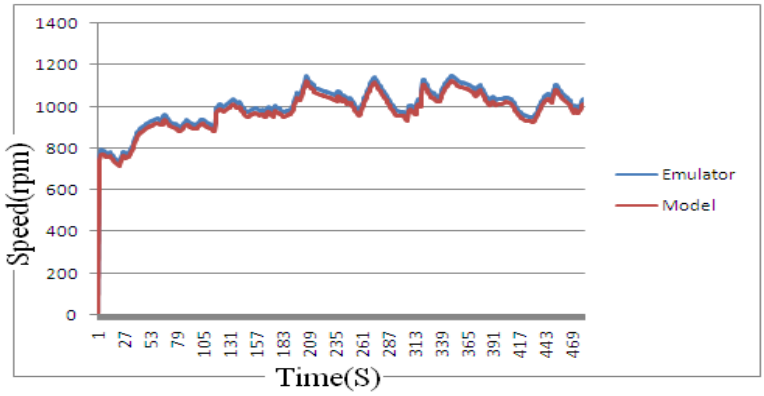

Figure Error! No text of specified style in document.**.104 Comparison of the Speed for wave data 2**

Case 3: Input to the WEC model is the wave data pattern corresponding to the group of wave data 5 which has significant height of 1.552 m, period of 18.887s and wave power of 143.2 kW. Figure 5.13 shows speed response of wave turbine emulator and the WEC system model.

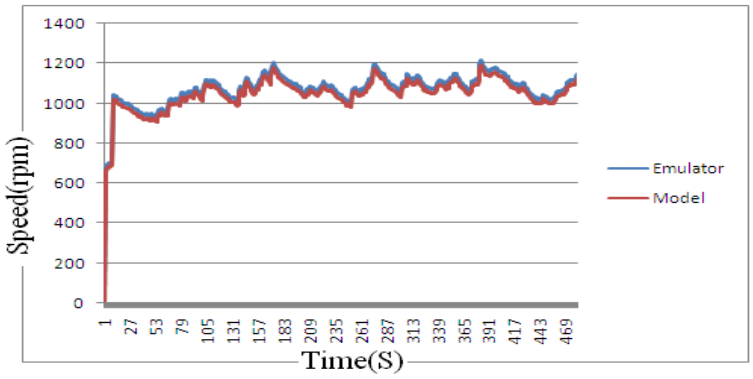

Figure Error! No text of specified style in document.**.105 Comparison of the Speed for wave data 5**

Results presented above for different wave patterns as input indicate that the speed dynamics of the WEC system model is exactly followed by wave turbine emulator implemented in laboratory. It is found that the error in the average speed is within

2%. Errors in the maximum, minimum and the standard deviation are also within the tolerable limits as given in table 5.1.

Table 5.1 Comparison of the speeds of the model and emulator

Wave Data	Average speed(rpm)			Maximum speed(rpm)			Minimum speed(rpm)			Standard deviation		
	Model	Emula--tor	% Error	Model	Emula-tor	% Error	Model	Emula-tor	% Error	Model	Emula-tor	% Error
Wave data 1	1079	1099	-1.86	1200	1222	-1.83	967	985	-1.86	7.11	7.28	-2.4
Wave data 2	1076	1096	-1.87	1192	1214	-1.81	983	1001	-1.83	66	68	-2.7
Wave data 3	988	987	0	1336	1341	-0.37	856	875	-2.22	166	158	4.8
Wave data 4	970	988	-1.87	1132	1153	-1.85	862	879	-1.97	18	19	-3.1
Wave data 5	954	972	-1.85	1124	1145	-1.86	882	898	-0.67	85	86	-1.7

Dynamics of the PMSG coupled to the emulator

A three phase PMSG of same rating as that of the PMSM is coupled to the emulator built which will generate three phase ac voltage. The frequency and the amplitude of the voltage generated by the variable speed PMSG changes according to the variations in the speed with which it is driven. This voltage is rectified using three phase uncontrolled bridge rectifier. The diode 1N5408 is used for this purpose with the following specifications namely Maximum peak reverse voltage: 1000 V, Maximum RMS voltage: 700 V, Maximum dc blocking voltage: 1000 V, Maximum average rectified current: 3 A. Open circuit voltage of the rectifier is sensed using Hall effect voltage sensor card. Circuit diagram of Hall Effect voltage sensor card, details of circuit design and specifications are included in Appendix V. The magnitude of dc voltage is sensed by Hall Effect voltage sensor card and this data taken back to Matlab through analog port of Keithley data acquisition card for analysis and comparison. Flow of sensor data and control signals between the functional units of wave turbine emulator is as shown in the figure 5.14 below.

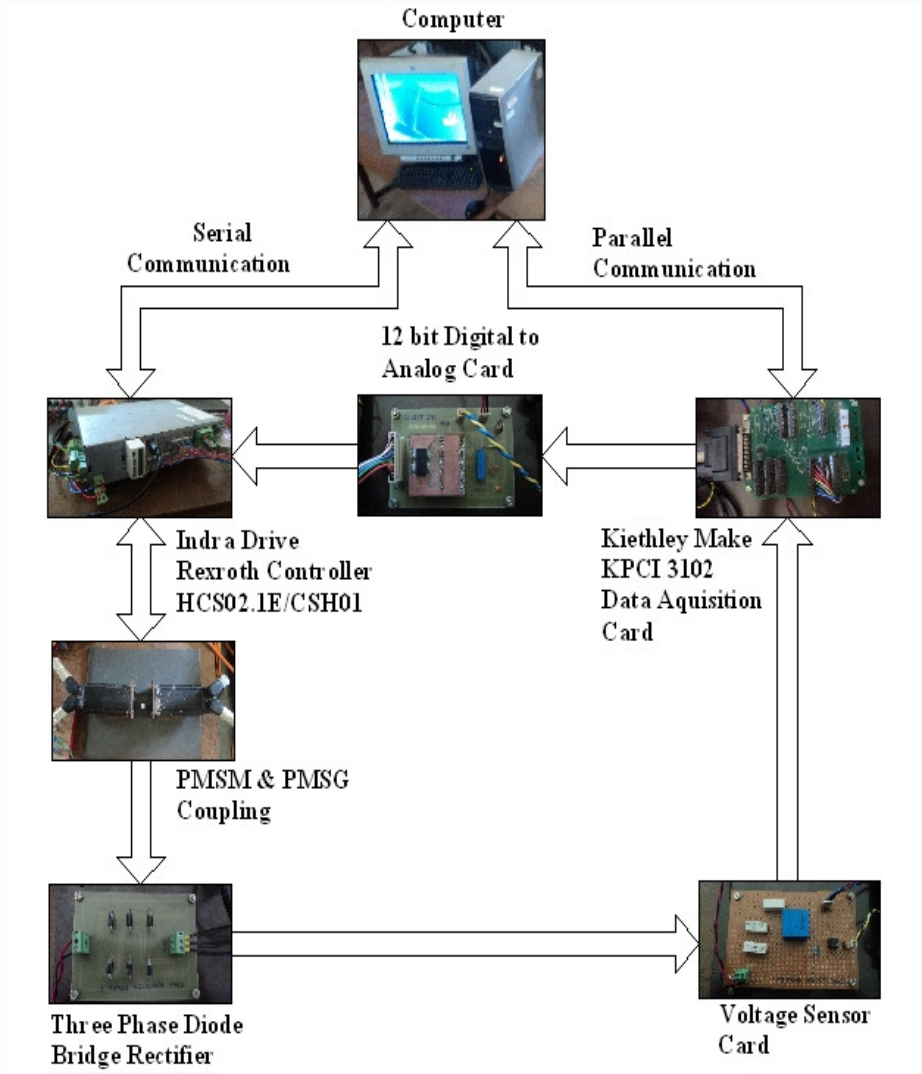

Figure Error! No text of specified style in document.**.106 Flow of sensor data and control signals**

Response of the dc voltage

From the laboratory setup of wave turbine emulator, dc voltage magnitude data from the uncontrolled rectifier circuit is sensed. This dc voltage is compared with the dc voltage at the output of the model. The dc voltage magnitude measured using the sensor card is scaled down to 200:1 ratio before it is transferred to the analog port of the data acquisition card. This is because the data acquisition card has voltage band

limit on its I/O ports. Comparison is done for the different type of wave pattern to assess the behavior of the PMSG coupled to the PMSM which is acting like the wave turbine emulator. Figures 5.15 and 5.16 show the dc voltages of the model and that obtained from the hardware setup for wave patterns corresponding to the group of wave data 1 and wave data 2. It is found that the error in the average dc voltage is within 5%. Errors in the maximum, minimum and he ripple are also within the tolerable limits as given in table 5.2.

Table 5.2 Comparison of dc voltage from the model and hardware set up.

Wave Data	Average dc voltage(V)			Maximum dc voltage(V)			Minimum dc voltage(V)			% Voltage ripple		
	Model	Emula -tor	% Error	Model	Emula -tor	% Error	Model	Emula -tor	% Error	Model	Emula -tor	% Error
Wave data 1	601	582	3.1	659	615	6.6	457	419	8.3	30.6	31.8	-3.1
Wave data 2	580	568	2.03	676	665	1.6	521	493	5.3	22.9	25.8	-6.2
wave data 3	568	555	-2.28	696	680	2.3	480	460	4.1	32.5	31	4.6
Wave data 4	518	510	1.37	753	735	2.3	423	412	2.6	43.8	43.4	-0.2
Wave data 5	515	506	-1.68	639	615	3.8	450	445	1.1	29.5	27.6	6.5

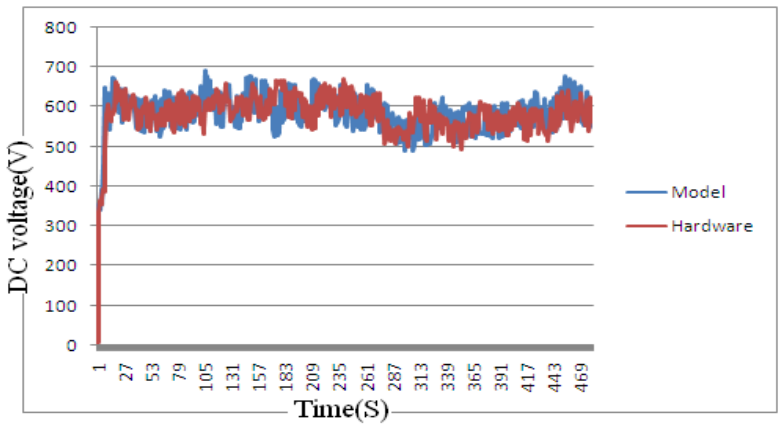

Figure Error! No text of specified style in document.**..107 Comparison of dc voltage for wave data 1**

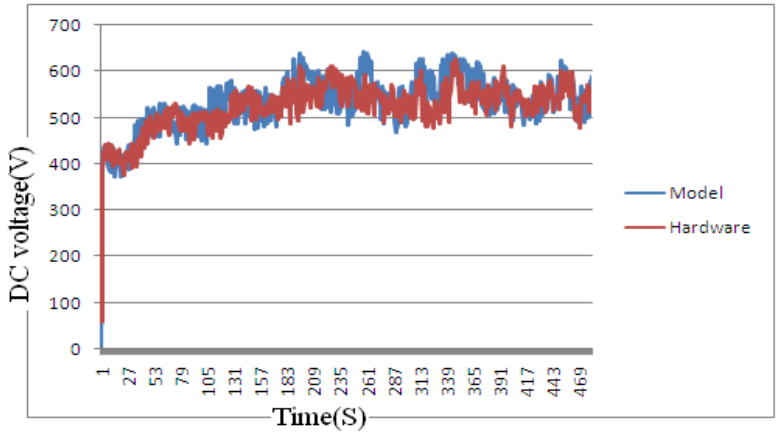

Figure Error! No text of specified style in document.**.108 Comparison of dc voltage for wave data 2.**

Results and discussion

From the speed response of the emulator presented above for different wave patterns as input show that the speed dynamics of the wave turbine emulator developed is similar to the speed dynamics of the WEC system model. So it can be concluded that the wave turbine emulator has been successfully implemented in laboratory.

From the response of dc voltage it can be concluded that the dc voltage dynamics obtained in WEC system model is followed by the dynamics of dc voltage measured using the sensor card at the output of the rectifier. Next chapter highlights the significant and striking conclusions drawn from the results presented in the above chapters 2 to 5. It also indicates the scope of future work that can be carried out based on the work executed in this thesis.

CHAPTER 6
CONCLUSIONS

The key points made in this thesis are summarized in chronological order and a general discussion of the results with reference to grid connected wave energy harnessing system and the development of a wave turbine emulator is presented. This is followed by the major contributions of the thesis and scope for future work.

In Chapter 1 general aspects to be taken into consideration in harnessing wave energy are discussed. Concept, history and classification of various types of WEC were introduced. Fundamentals of capturing wave energy and general aspects regarding the utilization of wave energy are discussed. Basic elements of WEC are introduced. The classification of WEC based on the positioning of the converter is presented. The technical challenges a wave energy converter has to tackle are discussed and a brief review of technological developments in wave energy conversion systems is presented. Furthermore, the gist of the work and contents of different chapters that follow are summarized.

In chapter 2, for the given wave pattern wave characterization is done based on the spectral analysis in order to distinguish different wave patterns. A model for OWC was proposed based on the energy balance theory. OWC model integrated with turbine model is applied with on site measured data of the wave pattern and the accuracy of the model is tested. The wave pattern data is obtained from the prototype of OWC based Indian wave energy plant installed at south western coast of India near Trivendrum in Kerala state. The model computes the differential pressure within the oscillating column, the axial velocity of air at the orifice and the gross torque. This in turn is used to calculate the pneumatic power and turbine power. These results are compared with the onsite measured values of the power. It is seen that the values obtained from the model are matching with the onsite measured values. From the results obtained from OWC model it can be concluded that the absolute axial velocity

of air in the OWC varies in accordance with the variations in the wave pattern input. These variations are reflected in the speed, torque and the power generated.

Chapter 3 presents the modeling of following: a) Variable speed permanent magnet synchronous generator to simulate dynamic behavior, b) Voltage source inverter and the PWM rectifier using switching function concept, c) Dynamic behavior of dc link, filter and ac grid. Performances of the generator under following conditions are analyzed: i) Constant axial velocity, ii) Varying axial velocity, iii) Real wave pattern input to the OWC model. Results demonstrate the randomness in the various quantities like speed of the turbine, torque and power developed at the turbine shaft when the axial velocity input to the turbine fluctuates randomly. This in turn influences the output of the generator. Hence the uncertainty in the wave power due to arbitrariness in the waves and the difficulties in developing an efficient wave harnessing system are illustrated.

Design of controllers for the generator side converter and the grid side converters for a grid connected wave energy conversion system are explained in Chapter 4. Implementation of constant stator voltage control scheme for the generator side converter, for maintaining the dc link voltage constant is presented. This chapter also presents the design of controller for the grid side converter with an objective of regulating the magnitude and phase angle of the grid supply current, so that the real and the reactive power entering the network can be controlled.

The overall scheme is evaluated under steady state, dynamic and transient operating conditions. From the results presented, it is observed that the control scheme provides a good response in terms of power quality and power control. It is also noted that the distortion in the grid current increases significantly under following conditions: unbalance in the grid voltage and electrical fault. However, the performance of power control unit indicates its stable behavior and fast response. This makes the system stable and brings back system quickly to the normal condition, once the disturbance is cleared. Hence with this it is shown that the proposed controller provides overall average power control under steady state, dynamic and transient conditions.

Chapter 5 explains the development of wave turbine emulator and its performance when it is coupled with PMSG. The emulator developed consists of a three phase PMSM with VSC controller as a drive. Control commands to VSC controller is supplied through serial communication port of PC and control inputs are fed through analog output card functioning as daughter board in PCI slot of PC. These control inputs are obtained from the model and the characteristics of the wave turbine simulated using MATLAB®. The speed control of PMSM is performed equivalent to that of the dc motor by a decoupling control, which is also known as field oriented control or vector control. PMSM position and speed are sensed through an encoder. To realize the emulator Rexroth IndraDrive controller with Rexroth Indradyn motor is used

In order to assess the performance of this laboratory setup of wave turbine emulator, its speed data is recorded over all ranges of control. This speed data of the PMSM is compared with the speed of the turbine obtained from the WEC software model. Comparative study is carried out for different types of wave pattern to appraise the behavior of the proposed wave turbine emulator. Results presented show that the speed dynamics of the WEC system model is exactly followed by wave turbine emulator implemented. Errors in the average speed, maximum and minimum speeds and standard deviation indicate that the emulator speed characteristics are matching with the characteristics of the model. Thus, the turbine speed characteristics are successfully reproduced by means of PMSM in the laboratory.

As a next phase of work a three phase PMSG is coupled to the emulator. AC voltage generated by PMSG is rectified using three phase uncontrolled bridge rectifier. Results presented show that the dc voltage dynamics obtained in WEC system model agree with the dynamics of dc voltage measured using the Hall effect voltage sensor card at the output of the three phase uncontrolled rectifier.

In brief the research work presented in this thesis is an effort to recognize the potential issues associated with harnessing wave energy using OWC principle. The following points highlight the major contributions of the thesis.

- Development of OWC model based on energy balance concept.

- Development of dynamic model for the representation of a variable speed Wells turbine driven PMSG connected to the grid by means of back to back converters.
- Implementation of control schemes for regulating the dc link voltage for varying input conditions and for regulating the grid current entering the distribution network and hence the power flow into the grid.
- Studies on the response of the controller under steady state at balanced grid voltage with constant input power, dynamic conditions like step variation in input power and step changes in the power references and transients such as balanced /unbalanced voltage disturbances, frequency changes and different grid fault conditions.
- Development of prototype of turbine emulator in the laboratory using a three phase PMSM.
- Study on behavior of the three phase PMSG coupled to the emulator developed.

Scope for future work

The laboratory set up implemented consists of wave turbine emulator coupled to PMSG and three phase uncontrolled rectifier converting ac voltage generated into dc voltage. Further, a boost converter can be implemented and controlled for stable dc voltage and the performance of the WECS can be analyzed for dc load. A three phase inverter can as well be realized to convert the dc voltage into a constant ac voltage and the behavior of the WECS for ac load can be analyzed. The present work carried out can be used as a platform for further research works involved in wave energy harvesting systems.

APPENDIX I

The parameters used in the model of the wave turbine and PMSG

A. Turbine parameters

Number of blades (n)	8
Blade chord length (l)	0.38 m
Blade height (b)	0.4 m
Cross section area of orifice (A_2)	2.0106 m^2
Mean Radius (r)	0.8 m
Moment of Inertia (J)	12.75 kgm^2
Gear Ratio (g_r)	1

B. PMSG Parameters

Stator resistance (Rs)	0.6 ohm
d-axis inductance (Ld)	0.0014 H
q-axis inductance (Lq)	0.0028 H
Rated power	20 kW
No of pole pairs (p)	8
Permanent magnet flux linkage (Ke)	0.52 Wb

APPENDIX II

Basic Components of Rexroth IndraDrive system

Rexroth IndraDrive controller is a controller designed by Bosch Group for controlling the three-phase synchronous motor using the Indraworks engineering software. Basic components of IndraDrive system is shown in figure A.1. The drive controller consists of two essential parts namely power Section and control Section.

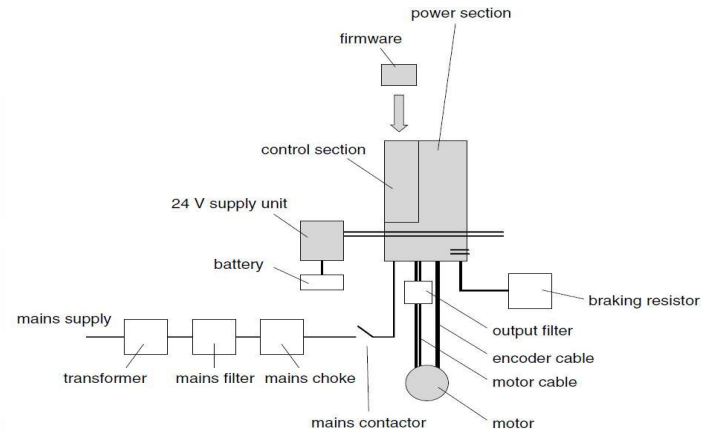

Figure A. 1 Basic components of IndraDrive system.

Power Section

The Power Section of the IndraDrive controller requires a 24V dc supply and has an option to work with 1-phase or 3-phase supply. Figure A.2 shows block diagram representation of power section unit, where L1, L2, L3 are the three phase input from the supply and A1, A2, A3 are the three phase voltage applied to the PMSM. The Basic components of power section are shown in figure A.3.

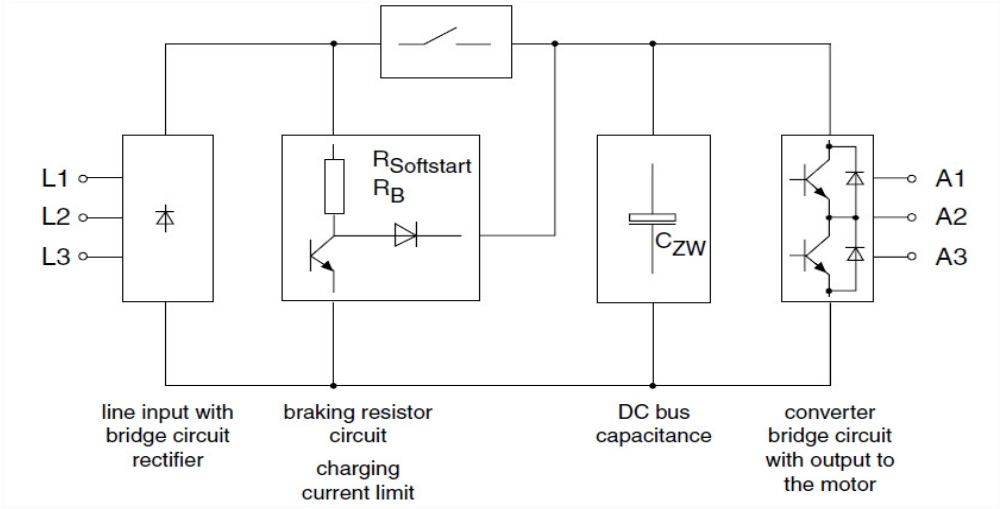

Figure A. 2 Block diagram of power section

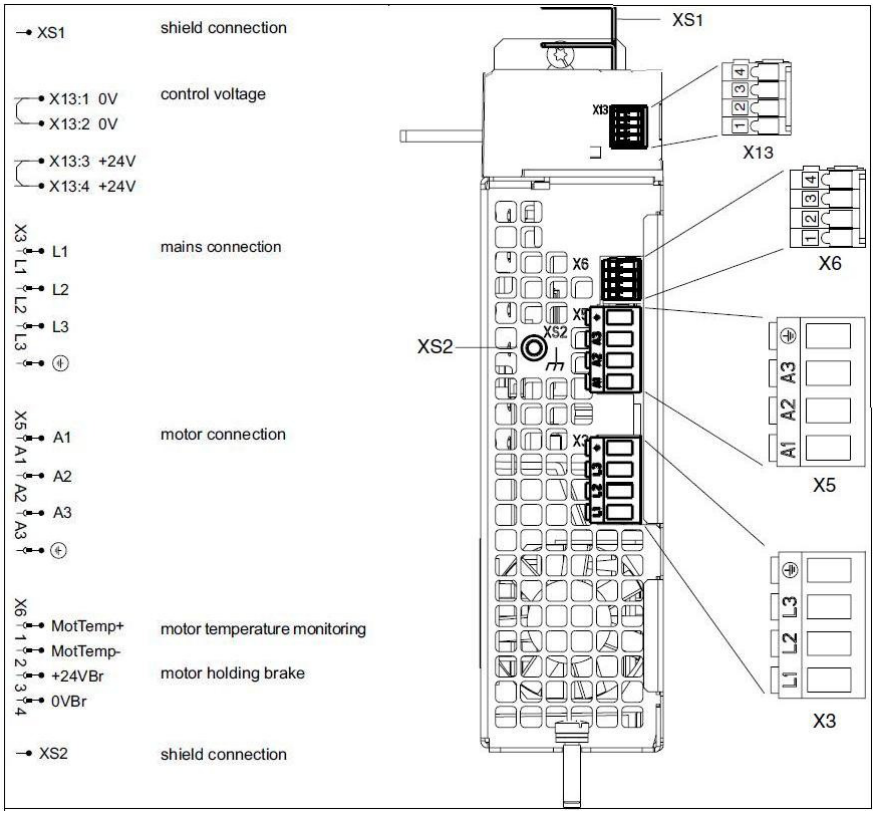

Figure A. 3 Basic components of power section.

First 24V dc voltage is supplied to the X13 pin “bb” is displayed on display panel of drive. Then single phase or three phase power supply is given to the Mains

connection(X3) which shows “Ab” on display panel indicating that drive is ready to Operate. Supply to 3-phase synchronous motor is taken from X5 of the power section of IndraDrive controller. X6 is for monitoring the temperature of the motor. For both X5 and X6 connections are done through a single cable from controller to motor.

Control Section

The control section is a separate section which is inserted into the power section. The interfaces provided on the drive and its function is shown in table A.1 and the layout of control section is shown in figure A.4. The details of each component are explained in the subsequent sections.

Table A. 1 Control section interface and Function

Interface	**Function**
X2	Serial Interface
X7	Multi Media card
X31/X32	Digital & Analog Input/Outputs
X*(X15)	Master Communication
H1	Interface for Control Panel (Display)
X4	Encoder
X8	Analog E/A Module
X10	Digital E/A Module
X41	Without Safety Technology

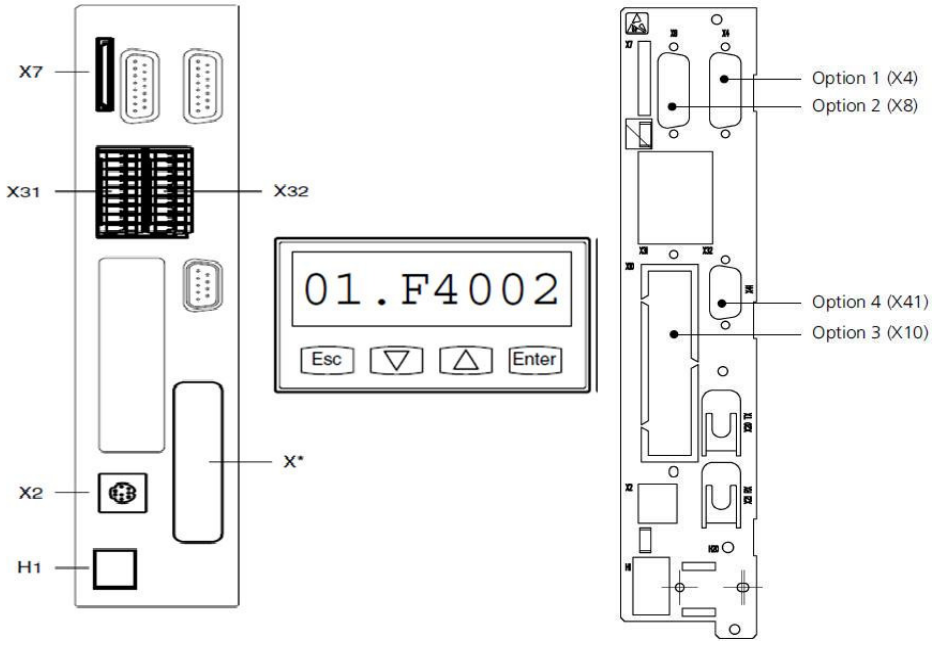

Figure A. 4 Basic components of control section.

X2, Serial Interface (RS 232)

The Serial interface (RS232) is required for programming, parameterization and diagnosis during commissioning and servicing. The interface permits:

- Maximum of one node.
- Transmission length of up to 15m.
- Baud rates of 9600/19200 baud.

X7, Multi Media card

X7 is for reading data (firmware, parameter, operating data) from respective storing data on a Multi Media Card (MMC).

X31/X32 Digital and Analog Input/Outputs

With 24V supplied to the X13 of power section the display on the panel will be “bb”. This closes the contact Bb1 and Bb2 of X31 as shown in figure A.5. Then “Ud” signal is checked & if it becomes high, 24V is applied at pin3 of X31 (P-0-4028 bit 15). Drive displays “AH”, holding torque will be available on the motor. By

applying 24V at pin4 of X31 (P-0-4028 bit 13) the brake gets released and the display on the panel is “AF”.

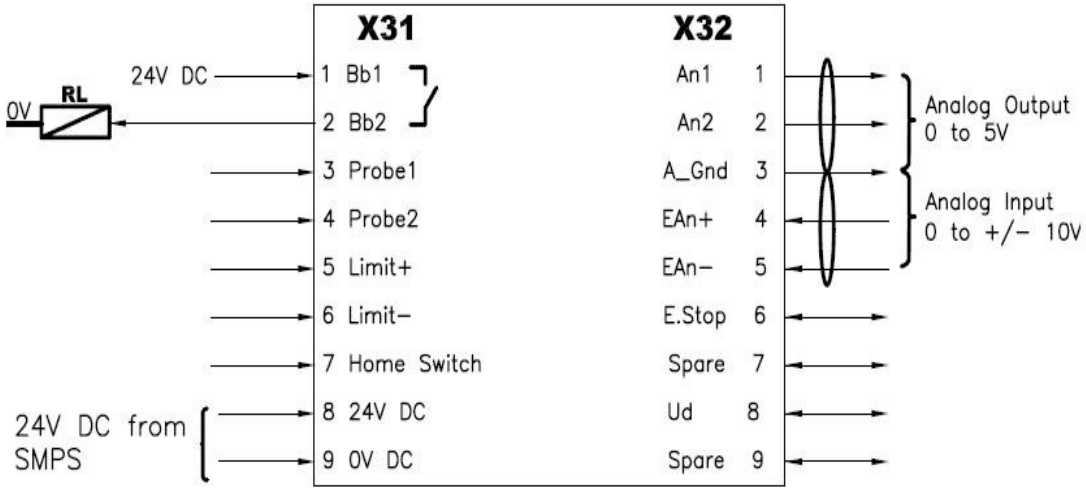

Figure A. 5 Pin configuration of Analog channel (X31/32).

X15, Master Communication

Figure A.6 gives the complete pin configuration of master Communication channel.

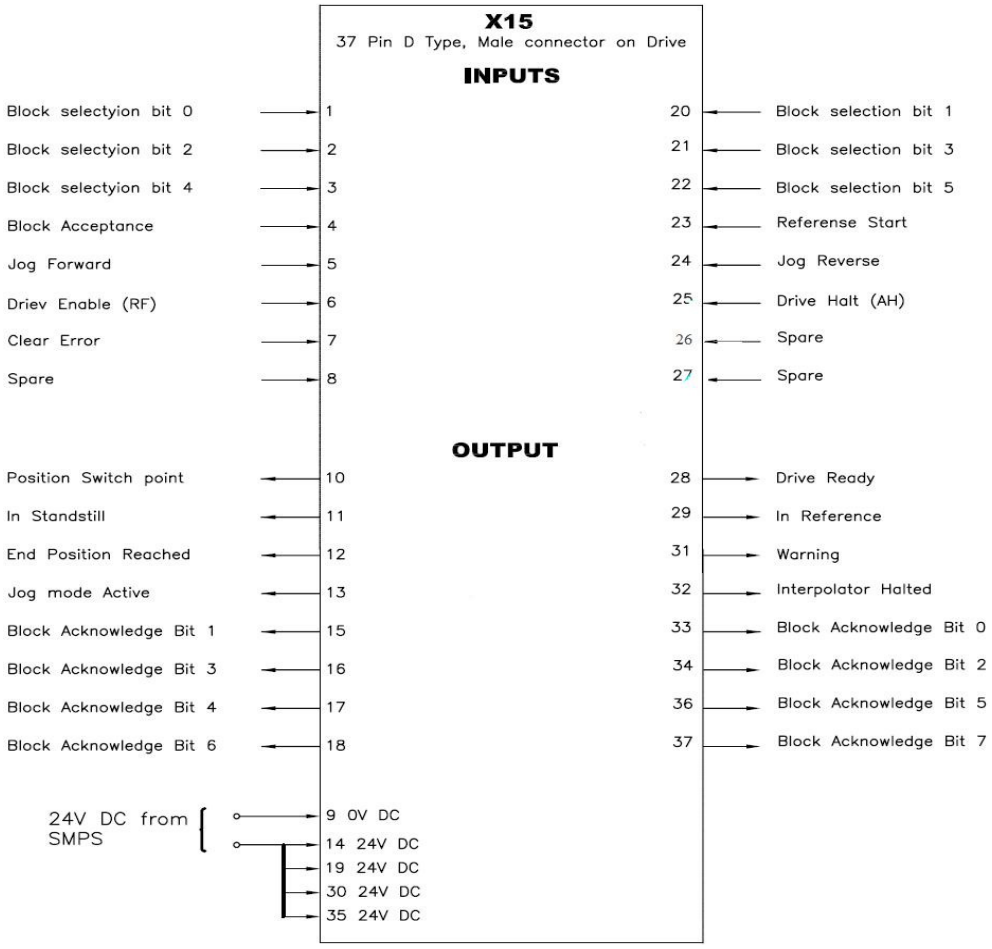

Figure A. 6 Pin configuration of Master Communication channel (X15).

X15 has 16 Digital input and 16 Digital output pins. The outputs are designed as groups. Each group is supplied with 24V. After getting Ab condition as explained in previous section 24V is applied at pin no. 6 of X15 (P-0-4028 bit 15). Then the Drive displays “AH” and holding torque will be available on the motor. By applying 24V at pin no 25 of X15 (P-0-4028 bit 13) the drive displays “AF”.

H1, Control Panel

The control panel is plugged into the H1 interface on the control section. Operating status, command and error diagnoses, and warnings for problems requiring attention are shown in the display. Using the four buttons on panel, the commissioning operator can opt to display further diagnoses on the drive controller and to activate simple commands.

Indra-Drive Start up Procedure

1. Encoder cable connection from the motor is connected correctly at X4 interface of the controller is ensured.
2. Power cable connections from AC mains to X3 of the power section and from X5 of the power section to the 3-phase synchronous motor are ensured.
3. 24V dc supply from Regulated power supply is applied to X13 connector of power section. X13/4: +24V X13/1: 0V
4. Drive internally checks for the required hardware connections, Feedback cable and temperature monitoring cable (X6).
5. If the display on the drive is "RL" for the first time, it means that the drive has detected a new motor. Now if the ESC button on the display module is operated, display on the drive will be "bb".
6. 3-phase power supply is switched on. Once 3 phase supply is available at X3 connector L1, L2, L3 terminals, drive displays "Ab"
7. Now "Ud" signal is checked at pin 8 of X31 & if it becomes high, 24V is applied at pin 3 of X31 (P-0-4028 bit 15).Drive displays "AH"
8. Holding torque will be available on the motor.
9. Brake gets released from motor by switching on 24 V to pin4 in X31 interface with parameter (P-0-4028 bit 13) high.
10. Now the drive & motor are ready to accept any analog signal input.

Indradyn 3-phase synchronous motor

The synchronous motor is driven as a wave turbine by using IndraDrive Controller. The motor has Encoder connector and power connector as shown in figure A.7. The power connector is provided to apply 3-phase power supply of 200-500V AC to the motor. The Encoder connector converts the speed of synchronous motor to voltage signals which is given as feedback to the X4 terminal of IndraDrive Controller. The synchronous motor has 6 pole pairs with holding torque of 23 Nm. The Input to the power connector is 3-phase 200V – 500V AC, 6A, 50-60Hz. The Drive is operated with both 1-phase and 3-phase supply. The supply to the motor is given by IndraDrive power section.

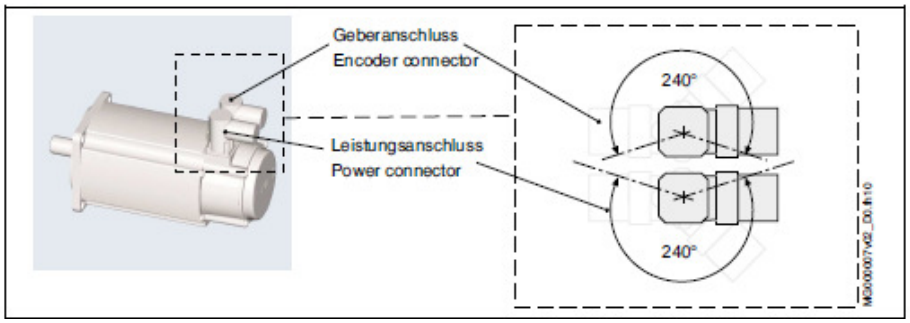

Figure A. 7 Indradyn 3-phase Synchronous motor

By using Indraworks engineering software the functionality of the Synchronous motor can be changed. The synchronous motor can be run in either velocity control mode or position control mode. Velocity control mode of operation is used in this work.

APPENDIX III

Installation and Calibration of KPCI-3102

The Keithley make KPCI -3102 data acquisition card is used as an interface between MATLAB and Rexroth IndraDrive controller. By using this data acquisition card the speed output of the wave turbine model is fed as input to the Rexroth IndraDrive controller.

Installation of KPCI-3102

The Keithley data acquisition card is installed in PCI slot of PC. The DriverLINX software is the driver support for Keithley data acquisition card. The Keithley data acquisition card is provided with STA-300 Screw terminal Panel. The CAB-305 cable is used to connect KPCI-3102 series board to STA-300 screw terminal panel. The STA-300 screw terminal panel consists of analog and digital I/O ports. Figure A.8 below shows connection between KPCI-3102 card and STA-300 screw terminal panel using CAB-305 communication cable.

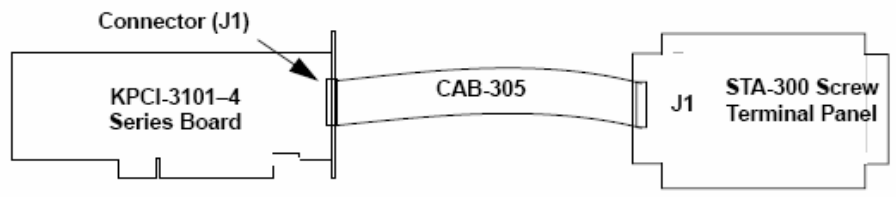

Figure A. 8 Connection between KPCI card and screw terminal panel

Figure A.9 shows the layout of STA-300 screw terminal panel. It has 16 analog Inputs (TB 1-16) and 2 analog output (TB 19-24) terminals provided with 8-bit digital Input/output terminals Port-A (TB 49-56) Port-B (TB 57-64) and Port-C (TB 65-71).

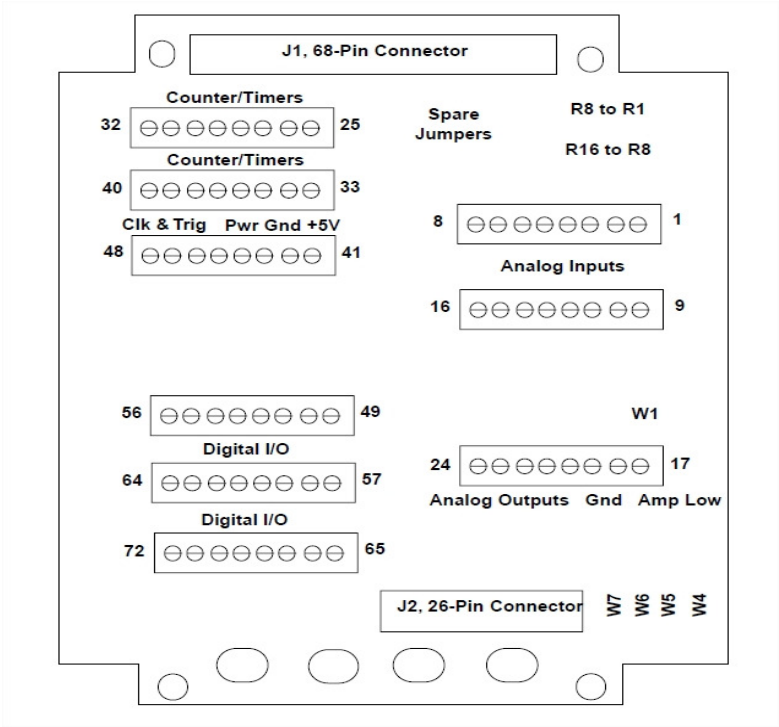

Figure A. 9 Layout diagram of STA-300 screw terminal panel

KCPI-3102 Calibration Utility

The DriverLINX KCPI-3100 calibration utility is an application that helps to calibrate data-acquisition boards in Keithley's KCPI-3100 Series. There is a gain adjustment potentiometer and an offset potentiometer. The calibration utility finds the best settings for the potentiometers by measuring a reference voltage with the board and automatically adjusting the settings. The series include models KCPI-3101, KCPI-3102, KCPI-3103, KCPI-3104, KCPI-3110 and KCPI-3116. To calibrate data acquisition board KCPI-3100 calibration utility is started from the Windows start menu under programs DriverLINX Test Panels. The calibration utility consists of three stages:

- Selection Device
- Calibration ADC
- Calibration DAC

First from the Device page device to be calibrated is selected. Then ADC and DAC systems are calibrated separately. Select Device page is used to select a KPCI-3102 series device to be calibrated and to display information about the selected device.

Selection of Device

Device page is used to select a KPCI-3102 series device to be calibrated and to display information about the selected device.

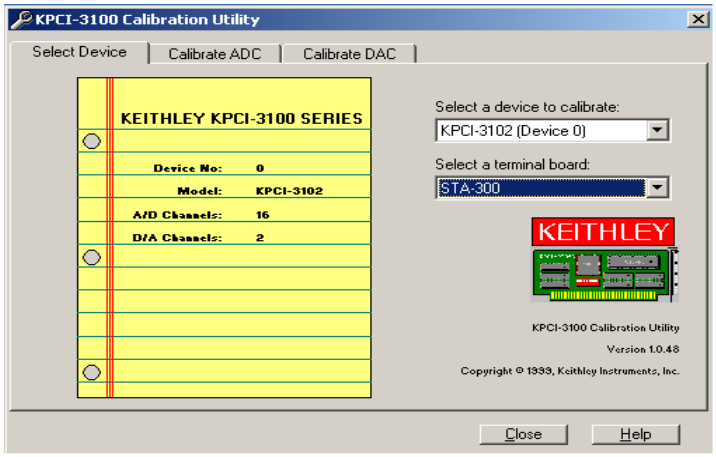

Figure A. 10 KPCI-3100 Calibration utility select device page

The Select Device Page as shown in figure A.10 contains a drop-down box labeled "Select a device to calibrate:" This box lists all of the devices in the systems that are loaded in the KPCI-3100 series. If no devices appear in the list, the device may be in use or may not be loaded. Status of the device is checked using the DriverLINX configuration panel. The Select Device page also displays the following information about the selected board:

- Device No—the board's DriverLINX Logical Device number
- Model—the board's model
- A/D Channels—the number of ADC channels the board supports
- D/A Channels—the number of DAC channels the board supports

Calibration of ADC

For analog inputs, the objective of calibration procedure is to zero the offsets and adjust the combined gain of the A/D converter and instrumentation amplifier. The

steps involved in setting offset and gain adjustments for the analog input and A/D Converter (ADC) circuits are given as follow:

1. In the KPCI-3101–4 series calibration utility dialog box, when A/D calibration tab is clicked, the A/D Calibration dialog box appears as shown in figure A.11.
2. To calibrate the analog inputs, on-screen instructions in the A/D Calibration dialog box are followed.
3. When finished with the analog input calibration, calibrate ADC page is used to determine new settings for selected ADC. The determined new settings are saved in the board.

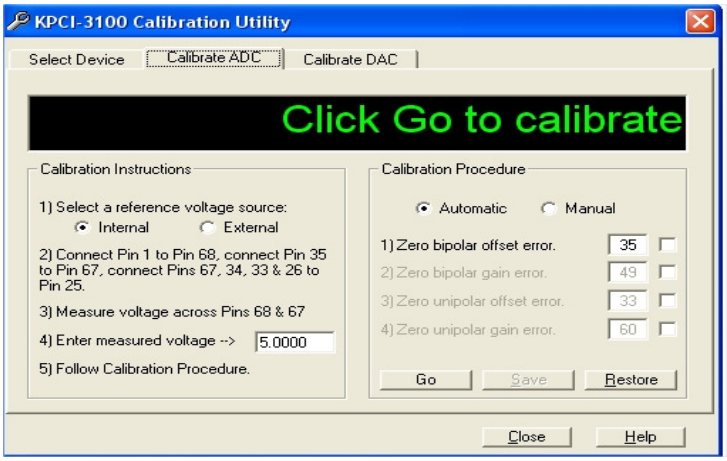

Figure A. 11 KPCI-3100 ADC calibration utility page

Calibration of DAC

For analog outputs, the objective of calibration is to independently zero the offset and adjust the gain for each of the digital-to-analog converters (DACs) on the KPCI-3102 series board. The KPCI-3101–4 Series boards each have two independent analog outputs, provided by two digital-to-analog converters (DACs or D/A converters). In this part of the procedure, offset and gain adjustments for the DACs are made.

1. In the KPCI-3101–4 Series calibration utility dialog box, when D/A Calibration tab is clicked, the D/A Calibration dialog box appears as shown in figure A.12.
2. To calibrate each DAC, on-screen instructions in the D/A Calibration dialog box are followed.

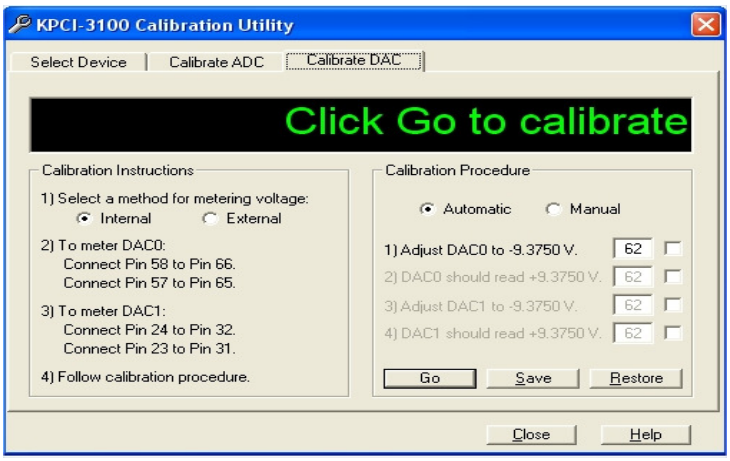

Figure A. 12 KPCI-3100 DAC calibration utility page

APPENDIX IV

Digital to analog converter

Features

- ±1/2LSB nonlinearity over temperature
- guaranteed monotonic over temperature
- low power: 270mw type
- digital interface double buffered: 12 and 8 + 4 bits
- specified at ±12v and ±15v power supplies
- reset function to bipolar zero
- 0.3" wide dip and so packages

Description

The DAC813 is a complete monolithic 12-bit digital to- analog converter with a flexible digital interface. It includes a precision +10V reference, interface control logic, double-buffered latch and a 12-bit D/A converter with voltage output operational amplifier. Fast current switches and laser-trimmed thin-film resistors provide a highly accurate, fast D/A converter. Digital interfacing is facilitated by a double buffered latch. The input latch consists of one 8-bit byte and one 4-bit nibble to allow interfacing to 8-bit (right justified format) or 16-bit data buses. Input gating logic is designed so that the last nibble or byte to be loaded can be loaded simultaneously with the transfer of data to the D/A latch saving computer instructions. A reset control allows the DAC813 D/A latch to asynchronously reset the D/A output to bipolar zero, a feature useful for power-up reset, recalibration, or for system re-initialization upon system failure. The DAC813 is specified to ±1/2LSB maximum linearity error (J, A grades) and ±1/4LSB (K grade). It is packaged in 28-pin 0.3" wide plastic DIP and 28-lead plastic SOIC. Figure A.13 shows the block diagram of DAC 813 and its pin description listed in the table A.2.

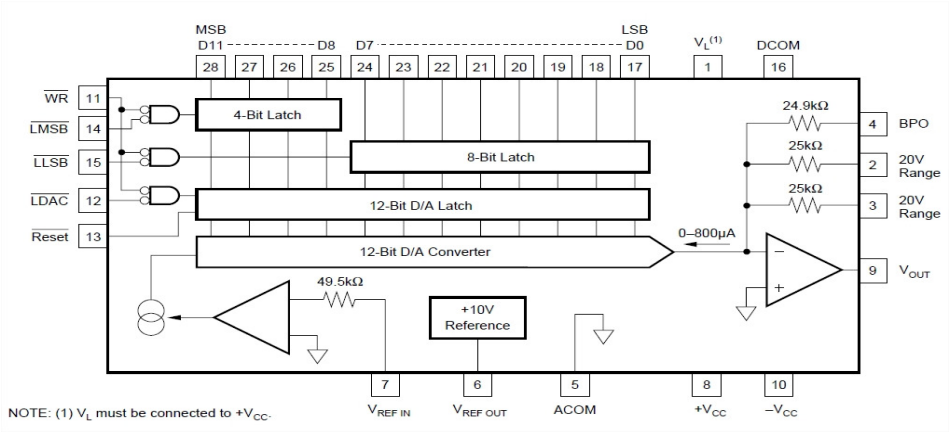

Figure A.13 Block diagram of DAC 813

Table A. 2 Pin description of DAC 813

Pin No	Name	Description
1	+VL	Positive supply pin for logic circuits. Connect to +VCC.
2, 3	20V Range	Connect Pin 2 or Pin 3 to Pin 9 (VOUT) for a 20V FSR. Connect both to Pin 9 for a 10V FSR.
4	BPO	Bipolar offset. Connect to Pin 6 (VREF OUT) through 100W resistor or 200W potentiometer for bipolar operation.
5	ACOM	Analog common, ±VCC supply return.
6	VREF OUT	+10V reference output referred to ACOM.
7	VREF IN	Connected to VREF OUT through a 1kW gain adjustment potentiometer or a 500W resistor.
8	+VCC	Analog supply input, nominally +12V to +15V referred to ACOM.
9	VOUT	D/A converter voltage output.
10	–VCC	Analog supply input, nominally –12V or –15V referred to ACOM.

11	WR	Master enable for LDAC, LLSB, and LMSB. Must be low for data transfer to any latch.
12	LDAC	Load DAC. Must be low with WR for data transfer to the D/A latch and simultaneous update of the D/A converter.
13	Reset	When low, resets the D/A latch such that a Bipolar Zero output is produced. This control overrides all other data input operations.
14	LMSB	Enable for 4-bit input latch of D8-D11 data inputs. NOTE: This logic path is slower than the WR path.
15	LLSB	Enable for 8-bit input latch of D0-D7 data inputs. NOTE: This logic path is slower than the WR path.
16	DCOM	Digital common.
17-28	D0-D11	Data Bit 1(LSB)- data bit 12(MSB)

APPENDIX V

Hall Effect Voltage Transducer LV 25-P

The Hall effect voltage transducer is used for the electronic measurement of voltages like dc, ac, pulsed voltage, with a galvanic isolation between the primary circuit (high voltage) and the secondary circuit (electronic circuit).

Features

- Closed loop (compensated) voltage transducer using the Hall effect
- Insulated plastic case recognized according to UL 94-V0.

Principle

The Hall voltage transducer produces current proportional to the measured voltage in the primary circuit. This current is passed through an external resistance R_1 to generate proportional voltage across HT+ and HT- terminal of the primary circuit. For the voltage generated in primary circuit, proportional current is generated in the measure terminal (M) of the secondary circuit.

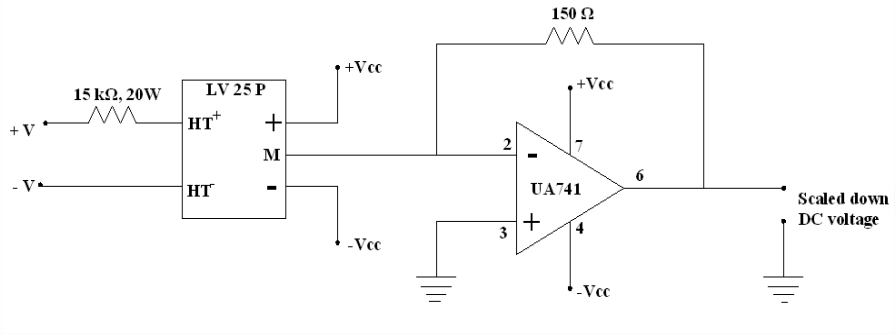

Figure A.14 Hall Effect voltage sensor circuit

The generated secondary current is passed through an external resistance R_2 to obtain the measuring voltage in the secondary circuit. Figure A.14 shows circuit diagram of the Hall Effect voltage sensor card. This particular voltage sensor card is designed for measuring input voltage of peak magnitude 200 V. The value of R_1 and R_2 are 15 kΩ and 150 Ω respectively. The Opamp 741 is used in secondary circuit is acting as current to voltage converting circuit. Electrical specification of the sensor card is given in table A.3.

Table A. 3 Specifications of sensor card

$\mathbf{I}_{PN}$	Primary nominal r.m.s. current	10	mA
$\mathbf{I}_P$	Primary current, measuring range	0 ± 14	mA
$\mathbf{R}_M$	Measuring resistance	$\mathbf{R}_M$ min $\mathbf{R}_M$ max	
	with ± 12 V @ ± 10 mA max	30-190	Ω
	@ ± 14 mA max	30-100	Ω
	with ± 15 V @ ± 10 mA max	100-350	Ω
	@ ± 14 mA max	100-190	Ω
$\mathbf{I}_{SN}$	Secondary nominal r.m.s. current	25	mA
$\mathbf{K}_N$	Conversion ratio 2500 : 1000		
$\mathbf{V}_C$	Supply voltage (± 5 %) ± 12 .. 15 V		
$\mathbf{I}_C$	Current consumption 10 (@ ± 15 V)+ $\mathbf{I}_S$ mA		
$\mathbf{V}_d$	R.m.s. voltage for AC isolation test , 50 Hz, 2.5 kV		

REFERENCES

Adel,M.S and Adel,A.A. (2009). "Optimal self regulating stand alone wave energy conversion scheme." *Proc., IEEE Power and Energy Conference, EPEC,* 1-6.

Ajit, T. and Fergal, H. (2004). "Modeling and scaling of impulse turbine for wave power applications". *Journal of Renewable Energy, Science Direct*, Vol 29, No 3, 305-317.

Ajit, Thakker and Fergal, H. (2003). "Modeling and scaling of the impulse turbine for wave power applications." *Journal of Renewable Energy*, Vol 29, No 3, Elsevier, 305-317.

Anand,S., Jayashankar,V., Nagata,S., Toyota,K., Takko,M., Setoguchi,T.(2006). "Performance estimation of bi directional turbines in wave energy plants." *Journal of Thermal Sciences*, Vol 15, No 4, 1-8.

Amundarain, M., Alberdi, J., Garrido, A.J., Garrido, I. (2010)."Control strategies for owc wave power plants." *Proc., American Control Conference, AACC,* 4319-4324.

Anthony, T.J. and Adam, W. (2005). "Recent progress in offshore renewable energy technology development." *IEEE Power Engineering Society general meeting*, Vol 2, 2017-2022.

Arifujjaman, Md., Iqbal, M.T. and Quaicoe, J.E. (2006). "An isolated small wind turbine emulator". *IEEE CCECE/CCGEL, Proc., Canadian Conference on Electrical and Computer Engineering,* Ottawa, 1854-1857.

Arifujjaman, Md., Iqbal, M.T., John, E.Q. (2008). "Emulation of small wind turbine system with a separately excited dc machine." *Journal of Electrical and Electronics Engineering Mechanics*, Vol 8, No 1, 569-579.

Battaiotto.P.E., Mantz.R.J., Puleston.P.F. (1996)."A wind turbine emulator based on a dual dsp processor system." *Journal of Control Engineering practice* , Vol 4, No 9, 1261-1266.

Bhim, S. and Gaurav, K.K. (2008). "Solid state voltage and frequency controller for a standalone wind power generating system." *IEEE Transactions on Power Electronics,* Vol 23, No 3, 1170-1177.

Bunlung, N., Somporn, S., Somchai, C. (2007). "Development of a wind turbine simulator for wind generator testing." *International Energy Journal*, Thailand, Vol 8, No1, 21-28.

Byoung-Kuk, Lee. and Mehrdad, E. (2001). "A simplified functional simulation model for three phase voltage source inverter using switching function concept." *IEEE Transactions on Industrial Electronics*, Vol 48, No 2, 309-321.

Cancelliere, P., Marignetti, F., Delli, C., Scarano, M. (2005). "A tubular generator for marine energy drives applications."*Proc., IEEE International Conference on Electric Machines and Drives*, 1473-1478.

Chen, Z., Spooner, E. (2001). "Grid power quality with variable speed wind turbines." *IEEE Transactions on Energy Conversion*, Vol 16, No 2, 148-154.

Chen, Z and Spooner, E. (1998). "Grid interface options for variable speed permanent magnet generators."*IEE Proc., on Electrical Power Application,* Vol 145, No8, 273-285.

Childs, J.F. (1996). "The role of converters and their control in the recovery of wave and wind energy."*Proc., IEE conference on Power Electronics and variable speed drives,* Publication No 429, 179-184, Nottingham, UK.

Chinchilla,M., Arnaltes,J.L., Rodriguez,A. (2004). "Laboratory set up for wind turbine emulation." *Proc., IEEE International Conference on Industry Technology, ICIT,* 553-557.

David, G.D., Min, F.H., Chi, C.L. (2010). "A multi chamber oscillating water column using cascaded savonius turbines." *IEEE Transactions on Industrial Electronics*, Vol 46, No 6, 2372-2380.

Dawson, J.M., Din, S., Mytton, M.G., Shore, N.L., Stansfield, H.B. (1980). "System reliability studies for wave energy generation." Physical Science, Measurement and Instrumentation, Management and Education - Reviews, IEE Proceedings A, Vol127, No 5, 296-300.

Duckers, L. (1995). "Water power- wave, tidal and low hydro technologies." Special feature, Power Engineering Journal, Vol 9, No 4, 164-172.

Erika Twinning and Donald Grahame Holmes. (2003). “Grid current regulation of a three phase voltage source inverter with an LCL input filter.” *IEEE Transactions on Power Electronics,* Vol 18, No 3, 888-895.

Evan.A.Amon., Alphonse. A.S., Ted.K.A.(2009). “A novel maximum power tracking algorithm for ocean wave energy devices”. *Proc., Energy Conversion Congress and Exhibition, ECCE,* Vol 127, Part A, No 5, 2635-2641.

Falcao, A.F.de O. (2002). “Control of an OWC based wave power plant for maximum energy production.”*Applied Ocean Research, Elsevier*, Vol 24, 73-82.

Feng,Wu., Xiao-Ping Zhang.,Ping Ju., Michael,J.H.2008). “Modeling and control of AWS based wave energy conversion system integrated into power grid.” *IEEE Transactions on Power Systems*, Vol 23, No 3, 1196-1204.

Fernadez, J.C. and Soerensen, H.C. (2009). “State of art of wave energy in Spain.” *Proc., IEEE International conference on Electrical Power and Energy, EPEC,* 1-6.

Fotios, N.G. and Stavros, A.P. (2006). “Simple control schemes for grid connected three phase voltage source inverters of DG units.”*Proc., ICEM, Hania,* Crete, http://users.ntua.gr/stpapath/paper_2.66.pdf.

Gabriele, M., Anca, D.H. and Thomas, H. (2007). “Control strategy of a variable speed wind turbine with multipole permanent magnet synchronous generator.”*Proc., European Wind Energy Conference and exhibition, Milan.* www.icrepq.com/icrepq’10/317-Cardenas.pdf.

Gareth, P.H and Robin, W.R. (2005). “Sensitivity of wave energy to climate change.” *IEEE Transactions on Energy Conversion*, Vol 20, No 4, 870-877

Glendenning. (1980). “Wave energy.” Proc., IEE, Part A, Vol 127, No5, 301-307.

Hamish, E. (1999). “Integration of wave energy.” *Proc., IEE colloquium on Protection and Connection of Renewable Energy Systems,* 1-7.

Haojie, L., Omer, C., Alireza, K. (2009). “Dynamic modeling and optimum load control of a pm linear generator for ocean wave energy harvesting application.” *Proc., 24th Annual IEEE Applied Power Electronics conference and exhibition*, *APEC,* 739-743.

Henk Poliander and Mattia Scutto. (2005). “Wave Energy Converters and their impact on Power Systems.”*IEEE International Conference on Future Power Systems*, 1-9.

Henk Polinder, Barrie, C.M., Alan, G.J., Phillip, G.D and Markus, A.M. (2005). “Conventional and TFRM linear generators for direct drive wave energy conversion.” *IEEE Transactions on Energy Conversion*, Vol 20, No 2, 260-267.

Hodgins, N., Muller, M.A., Tease, W.K., Staton, D. (2008). “Measurement and modeling of induction generator performance in an oscillating water column wave energy converter.” *Proc., IET conference on Power electronics, Machines and Drives, PEMD,* 76-80.

Hossein, M.K., Liuchen, C., Tobie, B. (2004). “Development of a novel wind turbine simulator for wind energy conversion systems using an inverter controlled induction motor.” *IEEE Transactions on Energy Conversion*, Vol 19, No 3, 547-552.

Indiresan, P.V and Murthy, S.S. (1989). “Generating Electrical Power from Wave Energy.”*Proc., 24th IEEE intersociety Energy Conversion Engineering Conference*, Vol 5, 2121-2126.

Joseph, J., Jayashankar, V., Pratulya, S. and Vinatha, U. (2009). “Measurements for proof of validation of a twin unidirectional turbine wave energy plant.”*Proc., IEEE International conference on Instrumentation and Measurement Technology*, *I2MTC*, Singapore, 1744-1747.

Jayashankar, V., Karthikeyan, B and Manivannan, K. (2000). “Maximizing power output from a wave energy plant.”*Proc., IEEE Power Engineering Society winter meeting*, Vol 3, 1796-1801.

Jennifer, G.V. and Annette, M. (2009). “Economic factors and incentives for ocean wave energy conversion.” *IEEE Transactions on Industrial Applications,* Vol 45, No 2, 547-554.

Jones, A.T and Rowley, W. (2002). “Recent developments and forecasts for renewable ocean energy systems.”*MTS Journal*, Vol 28, No 9, 575-578.

Juan, M.C., Leopoldo, G.F., Jan, T.B., Eduardo, G., Jose, I.L., Roman, C.P., Angeles, M., Narciso, M.A. (2006). “Power electronic systems for the grid

integration of renewable energy sources." *IEEE Transactions on Industrial Electronics*, Vol 53, No 4, 1002-1016.

Krishnan. (2007). "*Electric motor drives: Modeling, analysis, and control*." Prentice Hall of India Private Limited, New Delhi.

Les Duckers. (2000). "Wave power."*Engineering Science and Educational Journal*, Vol 9, No 3, 113-122.

Luiz,A.C.L., Josselien,L., Avishek, M. and Mohammed, F. K. (2005). "A wind turbine emulator that represents the dynamics of the wind turbine rotor and drive train", *Proc., 36th IEEE Power Electronic Specialists Conference, PESC*, 2092-2097.

Mala, K., Badrinath, S.N., Chidanand, S., Kailash, G., Jayashankar, V. (2009). "Analysis of power modules in the Indian wave energy plant." *IEEE Annual India Conference, INDICON*, 1-4.

Mala, K., Jayaraj, J., Jayashankar, V., Santhakumar, S.,Ravindran, R. (2009). "Design of a 60 GWh wave energy plant."*IEEE Annual India Conference, INDICON,* 1-4.

Marian,P.K., Marek,J. (2010)."Power electronics for renewable sea wave energy."*12th IEEE International conference on Optimization of Electrical and Electronic Equipment, OPTIM*, 4-9.

Martha, M., Ottar, S., Anderson, P., Tore, U., Jorgen, H., Torgeir, M., Bernt, S. (2007). "Power electronics as grid interface for actively controlled wave energy converters." *Proc., IEEE International Conference on Clean Electrical Power, ICCEP*, 188-195.

Marta, M., Bjarne, N., William, G., Tore, U. (2005). "Control of wind turbines with induction generators interfaced to the grid with power electronic converters." *Proc., IPEC,* www.elkraft.ntua.no/eno/papers2005/IPEC05-marta.pdf.

Mikel, A., Modesto, A., Aitor, J.G., Izaskun, G., Maseda, F.J. (2010). "Fault ride through capability of OWC based wave power generation plants equipped with doubly fed induction generator and air flow control." *IEEE Transactions on Industrial Electronics*, Vol 25, No 99, 1-13.

Milan Prodanovic., Timothy, C. Green. (2003). "Control and filter design of three phase inverters for high power quality grid connection."*IEEE Transactions on Power Electronics,* Vol 18, No 1, 373-380.

Modesto, A., Mikel, A., Aitor, J.G. and Izakkun, G. (2011). "Modeling and simulation of wave energy generation plants: output power control." *IEEE Transactions on Industrial electronics*, Vol 58, No 1, 105-107.

Mohammad,M., Hossein.M.K., Hasan.R. (2008). "Static and dynamic wind turbine simulator using a converter controlled dc motor." *Journal of Renewable Energy, Science Direct*, Vol 33, No 1, 906-913.

Monica, C., Santiago, A. and Juan, C.B. (2006). "Control of Permanent magnet generators applied to variable speed wind energy systems connected to grid." *IEEE Transactions on Energy Conversion*, Vol 21, No 1, 130-135.

Muetze, A. and Vining, J.G. (2006). "Ocean energy conversion a survey." *Proc., 41st IAS Annual meeting, Industry applications conference*, Vol 3, 1410-1417.

Muller,M.A. (2002)."Electrical generators for direct drive wave energy converters." *Proc., IEE on Generation, Transmission and Distribution,* Vol 149, No 4, 446-456.

Muthukumar, S., Sandeep kakumanu., Sriram, S. and Jayashnkar, V. (2005). "Energy storage considerations for a stand-alone wave energy plant."*Proc., IEEE International Conference on Electric Machines and Drives*, 193-198.

Muthukumar, S., Sandeep kakumanu, Sriram, S., Desai, R., Babar, A.A. and Jayashnkar, V. (2005). "On minimizing the fluctuations in the power generated from a wave energy plant."*Proc., of IEEE Conference IEMDC*, 178-185.

Nie, Z., Clifton, P.C.J and McMohon, R.A. (2008). "Wave energy emulator and ac/dc rectifiers for direct drive wave energy converters."*Proc., 4th IET Conference on Power Electronics, Machines and Drives*, 71-75.

O'Sullivan, D.L. and Lewis, A.W. (2008). "Generator selection for offshore oscillating water column wave energy converters." *Proc., 13th IEEE conference on Power electronics and Motion Control*, *EPE-PEMC*. 1790-1797.

Raftery, M. and Stolkin, R. (2007). "Ocean surface wave energy harnessing development at Steven's institute of technology (sit)." *Proc., IEEE conference on Oceans*, 1-8.

Ravi Kiran, D., Palani, A., Muthukumar, S., Jayashankar, V. (2007). "Steady grid power from wave energy." *IEEE Transactions on Energy Conversion*, Vol 22, No 2, 539-540.

Rabelo, B., Hofmann.W., Gluck.M. (2004). "Emulation of the static and dynamic behavior of a wind turbine with a dc machine." *Proc., 35th annual IEEE Specialist Conference*, 2107-2112.

Rexroth indradrive C drive controllers manual for power section HCS 02.1 and control sections. www.boschrexroth.com.

Setoguchi, T., Santhakumar, S., Takao, M., Kim, T.H., Kaneko, K. (2003). "A modified Wells turbine for wave energy conversion". *Journal of Renewable Energy*, Vol 28, No 1, Science Direct, 79-91.

Subba Rao., Kiran, G.S., Radheshyam, B. and Satyanand. (2006). "Spectral analysis of waves off Mangalore coast."*Proc., 15th Congress of APD-IAHR*, 1003-1013.

Szumko, S. (1989). "Mechanical model for OWC with compressibility."*Journal of Engineering Mechanics*, Vol 115, No 9, 1851-1868.

Tarek Ahmed, Katsumi Nishida, Mutsuo Nakaoka. (2010). "Grid power integration technologies for offshore ocean wave energy." *Proc., IEEE Energy Conversion Congress and Exposition, ECCE-2010*, 2378-2385.

Tarek, A and Zobaa, A.F. (2009). "Offshore power conditioning system connecting arrays of wave energy converters to the electric power grid." *Proc., 8th International conference on Advances in Power system control, Operation and Management, Hong Kong, China,* 1-6.

Tease, W.K. (2002). "Dynamic response of a variable pitch Wells turbine." *Research paper, Voith Hydro Wavegen Limited, Scotland*, www.wavegen.co.uk.

Ted, K .A. and Hai, Y.H. (2009). "Ocean wave energy overview and research at Oregon state university." *Proc., IEEE International conference on Power Electronics, Machines in Wind Application, PEMWA*, 1-7.

Tindal, C.E., Mingzhou, Xu. (1996). "Optimizing a well turbine type wave energy system." *IEEE Transactions on Energy Conversion*, Vol 11, No 3, 631-635.

Thakker, A., Frawley, P., Khaleeq, H.B., Ansari, A.R., Setoguchi, T., Takao, M. (2002). "Performance prediction of an impulse turbine under real sea conditions using numerical simulation techniques."*Proc., International Offshore and Polar Engineering Conference,* Vol 3, 674-681

Thiruvenkatasamy, K., Neelamani, S. and Michio Sato. (2005). "Non breaking wave forces on multi resonant oscillating water column wave power caisson breakwater."*Journal of Waterway, Port and Ocean Engineering, ASCE*, 77-84.

Thorpe, T.W. (1999). "An overview of wave energy technologies: Status, Performance and Costs." *Wave Power: Moving towards Commercial Viability* ,Westminster, London, www.waveberg.com.

Tom, T. (2000). "Harvesting the waves - The emergence of waves as a useful source of energy."*Marine Matters, Ingenia online magazine,* No13, 21-28, UK. www.ingenia.org.uk/issue13/thorpe.pdf.

Vining, J.G. and Muetze, A. (2007). "Government regulation of ocean wave energy converter installations." *Proc., IEEE International conference on Industry Applications,* 749-755.

Wang, Li. and Zan Jia Chen. (2010). "Stability analysis of a wave energy conversion system containing a grid connected induction generator driven by a wells turbine." *IEEE Transactions on Energy Conversion*, Vol 25, No 2, 555-563.

Watterson, J.K., and Raghunathan, S. (1996). "Investigations of wells turbine performance using 3-D CFD." *Proc., 31st IEEE Intersociety Energy conversion engineering conference, IECEC.* 1777-1782.

Whittaker, T.J.T. (1993). "The development of shoreline wave power in the UK." *Proc., IEE Renewable energy*, Vol 385, 117-120.

Wozniak,L., Collier.F., Foster.J. (1991). “Digital simulation of an impulse turbine: the Bradley lake project.” *IEEE Transactions on Energy Conversion*, Vol 6, No 1, 39-44.

Wu, F and Ju, P. (2009). “Application of battery energy storage in wave energy conversion system.” *Proc., IEEE International conference on Sustainable Power Generation and supply, SUPERGEN,* 1-4.

Yagna Narayanan, S.S., Bhagwan Murthy, K. and Sridhara Rao, G. (1996). “Dynamic Analysis of a grid connected induction generator driven by a Wave-Energy Turbine.”*Proc., IEEE International conference on Power electronics, Drives and Energy systems for industrial growth,* Vol 1, 433-438.

Yagna Narayanan, S.S. and Sumit Bose. (1996). “A Dynamometer set up for simulation of a wave energy operated wells turbine.”*Proc., IEEE international conference on Power Electronics, Drives and Energy systems for Industrial growth*, Vol 1, 251-257.

Yagna Narayanan, S.S., Bhagwan Murthy, K. and Sridhara Rao, G. (1999). “Dynamic Analysis of a grid connected induction generator driven by a Wave-Energy Turbine through Hunting Networks.”*IEEE Transactions on Energy Conversion*, Vol 14, No1, 115-121.

Curriculum vatae

NAME : VINATHA U

HIGHEST QUALIFICATION : MTech (Industrial Electronics)

PRESENT DESIGNATION: Associate Professor

ADDRESS Department of Electrical Engineering,
NITK , Surathkal
PO Srinivasnagar
Mangalore
Karnataka state-575025
INDIA

E MAIL : u_vinatha@yahoo.co.in
Vinatha_u@nitk.ac.in

TELEPHONE: +91-(0)824-2474000 EXT 3456 (Office)
+91-(0) 824-9448895389(personal)
+91-(0)824-2474456(Residence)

AREAS OF RESEARCH INTEREST: Power Electronics and Drives
Power converters and control of renewable energy systems

List of publications

1. Vinatha U, Vittal K.P, "Implementation of Turbine Emulator," *International Journal of Electrical Engineering, (JEE)*, Romania, Vol.11, No.2, Article no.11.2.11, pp. 73-79, 2011.

2. Vinatha U, Vittal K.P, " Power control strategy for grid connected permanent magnet synchronous generator for wave energy harnessing," *International Journal of Electrical Engineering, (JEE), Romania,* Vol.11, No.2, Article no.11.2.19, pp. 136-144, 2011.

3. Vinatha U, Dr.K.P.Vittal, "Power Control strategy for grid connected variable speed permanent magnet synchronous generator," *i manager's Journal on Electrical Engineering*, Vol 3, No 1, pp. 40-49, July-September 2009.

4. Vinatha U, Vittal K.P, Divya J, "Isolated Operation of Variable Speed PMSG with Battery Storage System for WECS," *Journal of Electrical and Control Engineering(JECE)*- American V-King Scientific Publishing, Vol. 3, No 4, pp. 47-51, 2013.

5. Vinatha U, Vittal K.P, "Power Control Strategy for Grid Connected Permanent Magnet Synchronous Generator of a Distributed Generation Unit" *International Journal of Electrical Power and Energy Systems, INDERSCIENCE publications*- Accepted.

6. Vinatha U, Vittal K.P, "Design and development of wave turbine emulator in the laboratory environment" *International Journal of Emerging Electric Power Systems– Berkley press publications - Accepted.*

7. Vinatha U, Swetha Pola, Dr.K.P.Vittal, "Recent Developments in Control Schemes of BLDC Motors," in *Proc. of International Conference on Industrial Technology*- IEEE – ICIT, Mumbai, India, December 2006.

8. Jayaraj Joseph, V Jayashankar, Department of Electrical Engineering, Indian Institute of Madras,Chennai,India, Pratulya shivashankar, Vinatha U, Department of electrical engineering, NITK Surathkal. "Measurements for Proof of Concept Validation of a Twin Unidirectional Turbine Wave Energy Plant," in *Proc. of IEEE International Conference on Instrumentation and Measurement Technology*, Suntec, Singapore, May 2009.

9.Vinatha U, Vittal K.P, "Control of dc link voltage of a variable speed permanent magnet synchronous generator driven by Well's turbine" in *Proc. of IEEE International Conference on Power Electronics and Intelligent Transportation System (PEITS 2010)*,Shenzhen, November 2010.

10. Vinatha U, Dr.K.P.Vittal, "Comparison of various generator topologies for Variable speed Wind turbines in *Proc. of National Conference on Advanced Energy Conversion Technologies,* IEEE – AECT, Manipal, India, March 2007.

11. Subbaraju P, Vinatha U, Dr.K.P.Vittal, "Development of numerical frequency relay for protection of distributed generators against islanding condition in *Proc. of National Conference on Advanced Energy Conversion Technologies*, IEEE – AECT Manipal, India, 2007.

12. Vinatha U, Dr.K.P.Vittal, Swetha Pola, "Simulation of Four Quadrant Operation & Speed Control of BLDC Motor on MATLAB / SIMULINK" in *Proc. of IEEE Region 10 conference, TENCON*, Hyderabad, 2008.